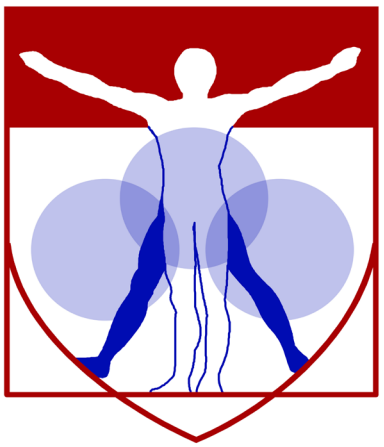

PENN
CENTER for
MUSCULOSKELETAL
DISORDERS

17th Annual Scientific Symposium/Retreat

Wednesday, November 18, 2020
Virtual Symposium
9:00am-12:30pm
www.med.upenn.edu/pcmd/

Table of Contents

Link to Posters on PCMD website https://www.med.upenn.edu/pcmd/2020-annual-symposium-posters.html

We gratefully acknowledge the financial support provided by the National Institute of Arthritis, Musculoskeletal and Skin Diseases of the National Institutes of Health and the University of Pennsylvania, Perelman School of Medicine for our Center.

Penn Center for Musculoskeletal Disorders Virtual Scientific Symposium Agenda

November 18, 2020
University of Pennsylvania

09:00 – 09:15am **Welcome and Overview**
Louis J. Soslowsky, Ph.D.

09:15am – 09:45am **Session I: New Member Session**

- *Jenny T. Bencardino, MD – "Volumetric Muscle Analysis Of The Tensor Fascia Lata In Hip Dysplasia"*
- *Anna M. Massie, DVM - "Bone Biomechanics of Small and Large Animals: Considerations For An Appropriate Model"*

09:50am – 10:20am **Session II: Affiliate Member Session**

- *Ben Binder-Markey, PT, DPT, PhD - "Whole Muscle Passive Mechanics Do Not Simply Scale By Muscle Architecture"*
- *Liyun Wang, PhD - "Physical Activity in Breast Cancer Bone Metastasis".*

10:20am – 10:50pm **Break and Poster Review**

10:50am – 11:05pm **Session III: Pilot Grantee Session**

- *Joel Boerckel, PhD - "Mechanobiology Of Bone Development And Repair"*

11:10am – 12:00pm **Keynote Speaker**

- *Richard L. Lieber, PhD, Chief Scientific Officer and Senior Vice President, Shirley Ryan Ability Lab, Professor of Physiology and Biomedical Engineering, Northwestern University*

"Intraoperative And Laboratory Studies Of Human Muscle Contractures"

12:00pm – 12:15pm **Final Comments**

12:15pm - **Posters**

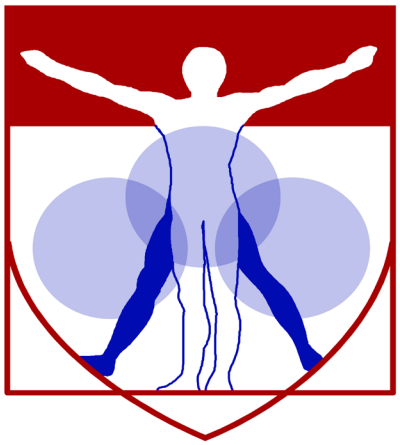

PENN

CENTER for

MUSCULOSKELETAL

DISORDERS

Center

Components

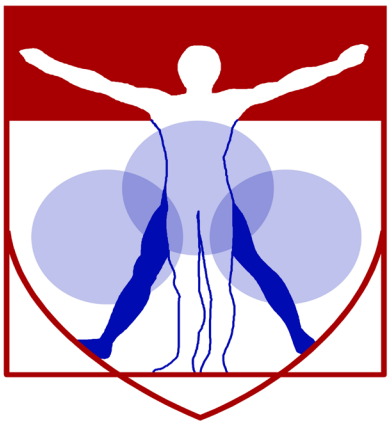

PENN

CENTER for

MUSCULOSKELETAL

DISORDERS

Center Overview

OVERVIEW OF THE PENN CENTER FOR MUSCULOSKELETAL DISORDERS

Director: Louis J. Soslowsky, PhD (soslowsk@upenn.edu)
Associate Director: Maurizio Pacifici, PhD (PacificiM@email.chop.edu)

Musculoskeletal-related conditions in the United States account for 132 million visits to physicians' offices, 29 million visits to emergency rooms, 15 million hospital outpatient visits, and cost over $850 billion each year. Further, musculoskeletal injuries in the United States cause workers to miss more than 440 million days of work annually. In fact, more than one in four Americans has a musculoskeletal impairment. With the widespread increase in athletic and recreational activities, and the increase of the elderly population at large, these numbers are expected to rise substantially. Musculoskeletal injuries represent a critical health concern which must be better understood and better treated. To do so, a dedicated and focused strategic effort is required that optimizes research translation from the bench to the bedside in an efficient and effective manner.

The Penn Center for Musculoskeletal Disorders (PCMD) will continue to enhance the research productivity of, and provide critical resources and programs to, investigators to address multidisciplinary research strategies for musculoskeletal problems. The overall goal of this Center is to promote cooperative interactions among investigators, accelerate and enrich the effectiveness and efficiency of ongoing research, foster new collaborations and new research, and ultimately, translate our research efforts into better and new therapies for musculoskeletal disorders. The central theme of the Center will continue to be "Musculoskeletal Tissue Injury and Repair". This theme is broad (as it includes all musculoskeletal tissue types, such as bone, cartilage, disc, ligament, meniscus, muscle, and tendon), focused (as takes advantage of commonalities in approaches across tissue types), and clinically significant (as it fosters development of assays, procedures and knowledge in preclinical animal and human models of translational relevance). It is important to note that our PCMD is not a "bone center" nor is it a "muscle center". Rather, it is truly a "musculoskeletal center" and has emerged as the recognized home for musculoskeletal research across the Penn campus and as a technical and intellectual resource for the broader Philadelphia musculoskeletal research community.

One focus of our Center is to translate research themes, approaches, and paradigms that are consistent across different tissues. Musculoskeletal tissues have much in common and their similarities are often overlooked when focus is restricted to a single tissue type. For example, the role of inflammatory cytokines is well studied in several tissue injury and repair scenarios; yet specific findings in one tissue-type are not always known and applied in other tissues. Similarly, the availability of technologies for imaging blood vessel formation in vivo to monitor healing in a given tissue is not always known and available to researchers focusing on other tissues. Given that approaches routinely used to evaluate mechanisms in one tissue could aid researchers in other areas, our Center will work to foster this critical cross-talk.

To provide a further focus for our Center, we will continue to develop programs with an emphasis on small animal models utilizing unique and sophisticated methods that can cross length scales to pre-clinical large animal models and human testing. Although large animal models for many human diseases exist and are essential for translational studies, small animals (e.g., mouse and rat) have become more commonly used for fundamental discovery of disease mechanism and initial therapeutic development due to availability of transgenic and knockout approaches and molecular tools, low cost, ease of handling and housing, and other practical issues. However, performing certain assays and experiments in mice and rats can be challenging and these difficulties often cannot be overcome in single investigator laboratories. The PCMD will provide unique expertise and sophisticated analytical tools to investigate musculoskeletal tissues across length scales.

Thus, the primary overall aims of this Center are to enhance and advance the research productivity of investigators in musculoskeletal tissue injury and repair by:

Aim 1: Providing innovation within critical resource core facilities in areas that cross disciplines, length scales, and hierarchies. These core facilities are μCT Imaging, Biomechanics, and Histology.

Aim 2: Developing a pilot and feasibility grant program for investigators, with direct mentorship, whereby new approaches, ideas, and collaborations can be developed prior to seeking extramural funding.

Aim 3: Developing educational and research enrichment programs spanning tissue types, research approaches, and paradigms, through which members can learn from national leaders and from each other.

High quality musculoskeletal research is currently being conducted by many groups at Penn. While many bring sophisticated approaches to bear on musculoskeletal problems, few groups have the required expertise and facilities to perform high quality and specialized assays in their own labs. Furthermore, most investigators are not aware of approaches utilized, and results obtained, in other tissues that may have direct relevance on their research questions. Ultimately, close cooperation, communication, and collaboration among researchers across musculoskeletal tissue types and from a wide variety of disciplines will significantly enhance the research of our members. The Center will provide opportunities to integrate multi-disciplinary techniques to determine mechanisms for tissue function, injury, degeneration, repair, and regeneration, with the ultimate goal of advancing the diagnosis, treatment, and prevention of diseases and injuries of the musculoskeletal system.

In addition to the specific features described in this proposal, there is an intangible feature of our Center that should not be overlooked. Although our musculoskeletal program is strong nationally, the Penn biomedical research community is large and diverse. As such, the Center serves as an essential mechanism to highlight our successes and the importance and excitement of musculoskeletal research across campus, as well as to institutional leadership. Having a strong voice for musculoskeletal researchers is critical to support our collective and individual research goals. In these ways, the Center - with essential support from the P30 - has become and remains an indispensable resource and advocate for our community.

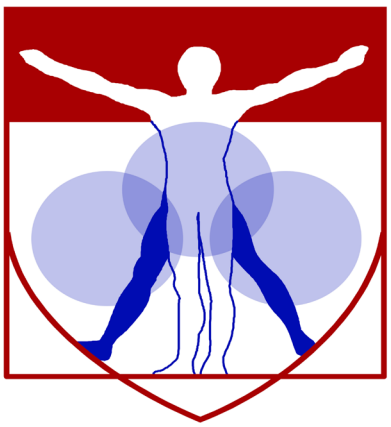

PENN

CENTER for

MUSCULOSKELETAL

DISORDERS

Core I

Biomechanics

Biomechanics Core

Core Director: Robert Mauck, Ph.D. (lemauck@pennmedicine.upenn.edu)
Technical Director: Snehal Shetye, Ph.D. (shetye@upenn.edu)

The overall objective of the Biomechanics Core is to develop and provide a wide range of innovative biomechanical approaches to evaluate musculoskeletal tissue function in the context of damage, repair, and regeneration, and to provide training and funding for new projects and collaborations utilizing these assays. Over the last decade, our Biomechanics Core at the Penn Center for Musculoskeletal Disorders (PCMD) has grown into a thriving resource for the University of Pennsylvania and Philadelphia area musculoskeletal research community. In this submission, we will further expand our services to meet the increased demand for specialized techniques and develop new and innovative methods that address the multi-scale mechanics of musculoskeletal tissues. These developments will provide customized services that enhance the research productivity of our members. The Specific Aims of the Biomechanics Core are:

- To provide guidance and training on the capabilities, advantages, and disadvantages of the various methodologies to assess musculoskeletal tissue biomechanical function through formal educational enrichment programs and one-on-one interactions

- To provide expertise and service for biomechanical assays of musculoskeletal tissues

- To develop innovative biomechanical testing techniques that will be applicable to Musculoskeletal research, and in particular those that provide information across tissue length scales

- To provide funding for the development of new projects and collaborations and to develop preliminary and/or feasibility data for investigators.

Successful completion of these aims will significantly enhance the environment and the capabilities of researchers at the University of Pennsylvania, leading to new approaches to address musculoskeletal disorders and new collaborations between Center faculties who may have not previously included biomechanical function approaches in their musculoskeletal research programs.

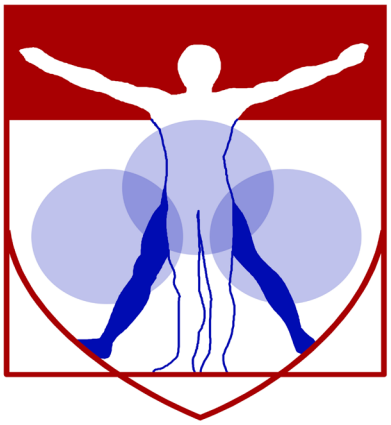

PENN

CENTER for MUSCULOSKELETAL DISORDERS

Core II

Histology

Histology Core

Overview and Mission

The mission of the Penn Center for Musculoskeletal Disorders (PCMD) Histology Core is to provide comprehensive, high quality histology services to musculoskeletal researchers at the University of Pennsylvania and the broader research community.

The Specific Aims of the core are:

- To provide guidance and training on the capabilities, advantages, and disadvantages of the various methodologies to assess musculoskeletal tissue structure and composition through formal educational enrichment programs and one-on-one interactions.
- To provide expertise and service for histological and histomorphometric assays of musculoskeletal tissues.
- To develop new histologically-based techniques that will be applicable to musculoskeletal research.
- To provide funding for development of new projects and collaborations and to develop preliminary and/or feasibility data for investigators.

Services Offered

The core offers a complete spectrum of services from sample preparation and processing, to sectioning, staining and analysis, with capabilities for paraffin, plastic and frozen histology. The core provides state of the art equipment in each of these areas, which can be accessed either on a self-service basis (upon completion of training) or a full-service basis through our full-time histology technician. Service fees are highly competitive, with significant subsidies offered for PCMD members.

- Consultation and protocol development (no charge for first 6 hours)
- Paraffin processing, embedding and sectioning
- Plastic processing and sectioning
- Frozen sectioning, including cryofilm method for undecalcified bone and teeth
- Routine histochemical staining
- Imaging and histoquantitation
- Training in histology techniques

If you are using the core for the first time, we highly recommend scheduling a meeting with one of the core co-directors and the core technician to discuss the scope of your project and specific needs.

We are very happy to provide letters of support for grant applications. To request a letter, please contact the core co-directors and provide the project title, a brief description of the project and core services you propose to use.

Please visit the core website for more information: www.med.upenn.edu/pcmd/histologymain.html

Co-Directors

Ling Qin, Ph.D. (Plastic and Frozen Histology)
Associate Professor of Orthopaedic Surgery
qinling@pennmedicine.upenn.edu
215 898 6697

Lachlan Smith, Ph.D. (Paraffin Histology)
Associate Professor of Neurosurgery
lachlans@pennmedicine.upenn.edu
215 746 2169

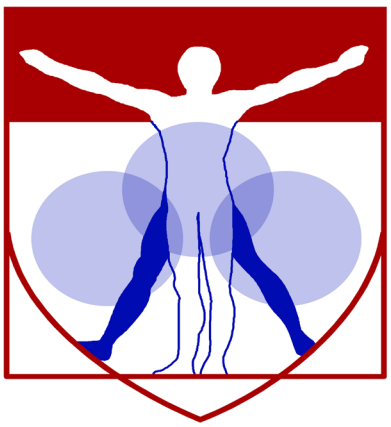

PENN

CENTER for MUSCULOSKELETAL DISORDERS

Core III

MicroCT

MicroCT Core

Director: X. Sherry Liu, Ph.D. (xiaoweil@pennmedicine.upenn.edu)

The development of high-resolution micro-CT (μCT) during the past two decades has revolutionized the quantitative assessment of calcified and X-ray dense tissue morphology. With the capability of non-destructive, three-dimensional (3D) visualization of tissue structure, μCT has largely supplanted traditional histomorphometry and become a gold standard for calcified tissue density and microstructure evaluation for many measures. Due to the low intrinsic X-ray contrast of non-mineralized tissues, traditional applications of μCT in musculoskeletal research have been limited to mineralized tissue. However, the development of contrast-enhanced imaging methods has greatly broadened applications of μCT to include musculoskeletal soft tissues as well. These cutting-edge image-based quantification methods not only enable characterization of soft-tissue morphology, but some also yield insight into tissue composition, such as glycosaminoglycan (GAG) density, which is associated with soft-tissue function and mechanics. Another important advance in the past decade is in vivo μCT imaging of living small animals. Research of musculoskeletal tissue injury and repair has been progressively utilizing animal models of human disease. Unlike many assays that require sacrificing the animal to extract tissues for analysis, in vivo μCT enables longitudinal evaluation of changes in a particular animal non-invasively over time. This new imaging strategy minimizes the number of animals required while enhancing statistical power. With these developments, μCT can now provide a deep and quantitative understanding of the genetic influences on the skeleton, as well as remodeling events in hard and soft tissues during repair, treatment, and with altered loading scenarios. Further, a μCT modality for clinical imaging of calcified tissue microstructure, called high-resolution peripheral quantitative CT (HR-pQCT), has recently been developed. This technology inaugurated a new era of non-invasive quantitative skeletal imaging, and has become a powerful tool for clinical research of musculoskeletal disorders. The overall objective of the μCTIC is to offer a wide range of μCT imaging approaches to evaluate musculoskeletal tissue injury and repair, and to provide training and consultation for new projects and collaborations utilizing these assays.

The Specific Aims for the μCTIC are:

- To provide guidance and expertise on the use of μCT imaging for musculoskeletal research through educational enrichment programs and one-on-one interactions
- To provide a range of μCT imaging resources, expertise, and services for the study of the structure, function and physiology of the musculoskeletal system in laboratory animals and humans
- To develop new μCT imaging-based techniques that will be applicable to musculoskeletal research
- To provide funding for the development of new projects and collaborations and to develop preliminary and/or feasibility data for investigators.

Successful completion of these Aims will significantly enhance the environment and capabilities of researchers at the University of Pennsylvania, leading to novel and innovative approaches to address musculoskeletal disorders and to new collaborations between Core faculty who may not have previously included human and/or animal imaging in their musculoskeletal research programs.

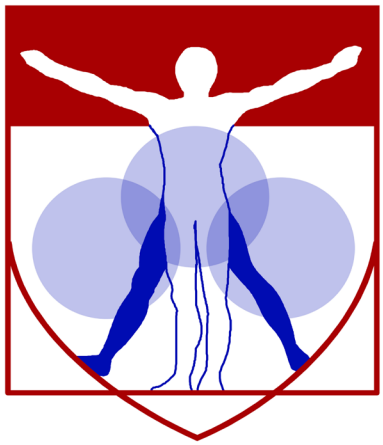

PENN

CENTER for

MUSCULOSKELETAL

DISORDERS

Pilot Grant Program

PENN CENTER FOR MUSCULOSKELETAL DISORDERS
PILOT AND FEASIBILITY GRANT PROGRAM

The Penn Center for Musculoskeletal Disorders has an ongoing Pilot and Feasibility Grant Program. Submissions should be related to musculoskeletal tissue injury and repair which is the broad focus of the Center and Grants are only eligible for Center members (if you are not a member but would like to become one, please contact pcmd@pennmedicine.upenn.edu). For more information on our Cores and Center in general, please see our web site at www.med.upenn.edu/pcmd .

Eligibility

- Only Full Center members are eligible. If you are not currently a member, please go to the link: http://www.med.upenn.edu/pcmd/memberinfo.shtml
- Categories of applicants include: 1) Established investigators with a proposal to test the feasibility of a new or innovative idea in musculoskeletal tissue injury and repair representing a clear and distinct departure from their ongoing research, 2) Established investigators with no previous work in musculoskeletal tissue injury and repair interested in testing the applicability of their expertise on a problem in this area, and 3) New investigators without significant extramural grant support as a Principal Investigator to develop a new project.
- Pilot and Feasibility Grants must use at least one of the Center's Research Cores.
- Pilot project awardees are eligible for one year, with a second year to be considered (budgets will be for $20-50,000 per year and timelines should be for one or two years). The second year of funding, the dollar amount of which would only be for up to half the year one budget, will be considered based on the progress report submitted after the first year of funding and funding availability in the Center. Please note that second year funding will often not be awarded, and when awarded, will be done so primarily to new investigators; second year funding to senior investigators will be quite rare.
- It is expected that these Pilot grants will lead to funding through other independent, extramural mechanisms. Therefore, the likelihood of future extramural funding will enter into the evaluation of these proposals.

Format

- Applications should be formatted loosely in the style of an NIH R03 grant (http://grants.nih.gov/grants/guide/pa-files/PA-18-488.html). The main body of the application (Specific Aims through Research Design and Methods-sections 4-7 below) is limited to five pages. The application should be in a single pdf file. The format should be:

1) Cover Page (not NIH face page) with grant title, PI name (and co-PI name if applicable), affiliation, contact information
2) Budget and brief justification (note that equipment is not allowed) (Please use form PHS398, Page 4)
3) NIH Biosketch of PI (and co-PI if applicable) (in the new NIH format)
4) Specific Aims
5) Significance
6) Innovation
7) Approach
8) Brief Statement of Category of Investigator per guidelines above
9) Brief Statement of How this Funding will lead to other Extramural Funding
10) Human Subjects and/or Vertebrate Animal Subjects (if applicable)
11) Consultants (if applicable)
12) Literature Cited
13) Certification of Patient Oriented Research (if applicable)

The completed proposal are submitted via the PCMD website by going to the uploaded as a single PDF file.

Please do not hesitate to email pcmd@pennmedicine.upenn.edu with any questions or comments.

Penn Center for Musculoskeletal Disorders Pilot & Feasibility Grants
(All grants awarded since inception of Center)

Awarded 2020-2021
Kyu Sang Joeng, Ph.D., Assistant Professor of Orthopaedic Surgery, Perelman School of Medicine: "The function of mTORC1 signaling in the regulation of the provisional matrix during tendon healing"

Patrick Seale, Ph.D., Associate Professor of Cell and Developmental Biology, Institute for Diabetes, Obesity and Metabolism , Perelman School of Medicine: "Fat and synovial tissue development and disease remodeling in joints"

Josh R. Baxter, Ph.D., Research Assistant Professor of Orthopaedic Surgery, Perelman School of Medicine: "Stimulating muscle-tendon healing by prescribing mechanical loading"

Awarded 2019-2020
Jaimo Ahn, M.D., Ph.D., Associate Professor of Orthopaedic Surgery, Perelman School of Medicine: "The Interplay of Notch Suppression and Hypoxia on Bone Regeneration"

Riccardo Gottardi, Ph.D., Assistant Professor of Pediatrics, CHOP Pulmonary Medicine: "Impact of scaffold microporosity in guiding local stem cell differentiation for osteochondral repair"

Lachlan Smith, Ph.D., Assistant Professor of Neurosurgery: "Emergent Nucleus Pulposus Cell Heterogeneity during Intervertebral Disc Development and Growth" *(awarded extramural funding from NIH/NIAMS R21AR077261)*

Awarded 2018-2019
Miltiadis Zgonis, M.D., Assistant Professor of Orthopaedic Surgery, Perelman School of Medicine: "Development, Maturation, and Function of Meniscal Radial Elements"

Joel Boerckel, Ph.D., Assistant Professor of Bioengineering and Orthopaedic Surgery, Perelman School of Medicine: "Role of YAP/TAZ in osteoprogenitor cell-induced angiogenesis for vascularized bone repair" *(awarded extramural funding from NIH/NIAMS R01AR074948 and R01AR073809)*

Awarded 2017-2018
Nathaniel Dyment, Ph.D., Assistant Professor of Orthopaedic Surgery, "Murine anterior cruciate ligament reconstruction model to understand the cellular origins and mechanisms of repair" *(awarded extramural funding from NIH/NIAMS R01 AR076381)*

Yanqing Gong, Ph.D., Research Assistant Professor of Medicine, "Role of plasminogen in mesenchymal stem cell function and post-injury bone regeneration"

Carla Scanzello, M.D., Ph.D., Assistant Professor of Medicine, "Importance of Macrophage Responses in Osteoarthritis"

Susan Volk, V.M.D., Ph.D., D.A.C.V.S., Assistant Professor of Small Animal Surgery, "The Regulatory Roles of Type III Collagen in the Cartilage Collagen Network: Implications for Osteoarthritis Prevention and Treatment"

Awarded 2016-2017
Joseph Baur, Ph.D., Assistant Professor of Physiology Institute for Diabetes, Obesity and Metabolism, "Targeting NAD metabolism in muscular dystrophy" *(awarded extramural funding from Elysium Health)*

Yongwon Choi, Ph.D. Leonard Jarett Professor of Pathology and Lab Medicine, "Cell adhesion regulation of multiple-myeloma induced bone destruction"

X. Sherry Liu, Ph.D., Assistant Professor of Orthopaedic Surgery and Bioengineering, "Mechanical Consequences of Modeling- vs. Remodeling-Based Bone Formation" *(awarded extramural funding from the NSF Award #1661858)*

Hongtao Zhang, Ph.D., Research Assistant Professor, Department of Pathology and Lab Medicine, "Novel cartilage-targeting Fc fusion proteins as novel and effective treatments for osteoarthritis"

Awarded 2015-2016
Yejia Zhang, M.D., Ph.D., Department of Physical Medicine and Rehabilitation, "Inhibition of ADAM-8 to reduce intervertebral disc degeneration" *(Awarded extramural funding from the VA Meri t; VA Competitive Pilot Fund)*

Oren Friedman, M.D., Department of Otorhinolaryngology, "Effect of injury to cartilage and recovery treatment with FGF-18"

Harvey Smith, M.D., Department of Orthopaedic Surgery, "Impact of Pre-Culture and In Vivo Remobilization on Engineered Disc Replacement" *(Awarded extramural funding from the VA RX002274-01A1)*

Tejvir Khurana, M.D., Ph.D., Department of Physiology, "Role of the IL-15 / IL-15Rα axis in modulating muscle-tendon-bone adaptation and repair"

Awarded 2014-2015
Joshua F. Baker, M.D., MSCE, Department of Rheumatology & Epidemiology/Perelman School of Medicine: "Assessment of Intramyocellular Fat Accumulation in Rheumatoid Arthritis Using MR Spectroscopy" *(Awarded extramural funding from American Federation for Aging Research Foundation)*

Russ P. Carstens, M.D., Department of Renal-Electrolyte and Hypertension Division, Perelman School of Medicine: "Roles of Epithelial Splicing Regulatory Proteins in Craniofacial Development" *(awarded extramural funding NIH 1R56DE024749 and awarded R01 NIDCR)*

Foteini Mourkioti, Ph.D., Department of Orthopaedic Surgery/Perelman School of Medicine: "A Novel Molecular Mechanism in Chronic Skeletal Muscle Injury" *(Awarded extramural funding from the NIH R01 AR075914)*

Chamith Rajapakse, Ph.D., Department of Radiology/Perelman School of Medicine: "Biomechanics of Hip Fracture Assessed by MRI" *(Awarded extramural funding from the NIH R01 AR068382)*

Awarded 2013-2014
X. Sherry Liu, Ph.D., Department of Orthopaedic Surgery, Perelman School of Medicine: "Structure and Strength Recovery in Post-Lactation Bone" *(awarded extramural funding from the NIH R01 AR071718, NIH R03 AR065145 and NSF Career Award #1653216)*

Ling Qin, Ph.D., Department of Orthopaedic Surgery, Perelman School of Medicine: "Novel Anabolic Treatment for Radiation-Induced Osteoporosis" *(awarded extramural funding from the NIH R01AR066098)*

Lachlan Smith, Ph.D. Department of Orthopaedic Surgery, Perelman School of Medicine: "Molecular Mechanisms of Failed Vertebral Bone Formation in Mucopolysaccharidosis VII" *(awarded extramural funding from the NIH R03 AR065142 and the MPS Society)*

Hansell H. Stedman, M.D., Department of Surgery, Perelman School of Medicine: "Molecular Pattern Recognition in Acute and Chronic Injury to Muscle and Myotendinous Junction" *(awarded extramural funding from the NIH R01NS094705)*

Awarded 2012-2013
Jason Burdick, Ph.D., Department of Bioengineering, School of Engineering and Applied Science: "Acelluar Fibrous Scaffolds for Stem Cell Recruitment and Cartilage Repair" *(awarded extramural funding from the NIH R01 EB008722)*

James L. Carey, M.D., MPH, Department of Orthopaedic Surgery, Perelman School of Medicine: "Development of a Large Animal Model of Osteochondritis Dissecans" *(awarded extramural funding from the NIH R01 EB008722)*

Andrew Kuntz, M.D., Department of Orthopaedic Surgery, Perelman School of Medicine: "Effects of Intra-Articular Glenohumeral Injection of a Nonsteroidal Anti-Inflammatory Drug on Shoulder Joint Mechanics in a Rat Model"

Arjun Raj, Ph.D., Department of Bioengineering, School of Engineering and Applied Science: "Single Cell Analysis of Molecular and Micromechanical Heterogeneity in Mesenchymal Stem Cells and Engineered Tissues"

Awarded 2011-2012
Struan F.A. Grant, Ph.D., Department of Pediatrics, Children's Hospital of Philadelphia and Perelman School of Medicine: "Utilization of ChIP-seq to Identify Genes Regulated by Osterix"

Motomi Enomoto-Iwamoto, DDS, Ph.D., Department of Orthopaedic Surgery, Children's Hospital of Philadelphia and Perelman School of Medicine: "Tendon Repair by Retinoic Acid Receptor Agonists" *(awarded extramural funding from the NIH R21 AR062193)*

Ian N. Jacobs, M.D., Department of Otorhinolaryngology: Head and Neck Surgery, Children's Hospital of Philadelphia and Perelman School of Medicine: "A Pilot Study for the Development of a Rabbit In-Vivo Tissue- Engineered Cartilage Graft for Pediatric Laryngotracheal Reconstruction" *(awarded extramural funding from The Triological Society)*

Awarded 2010-2011
Susan W. Volk, VM.D., Ph.D., Dipl ACVC, Department of Small Animal Surgery, School of Veterinary Medicine: "The Role of Type III Collagen in Bone Repair and Regeneration"

Jaimo Ahn, M.D., Ph.D., Department of Orthopaedic Surgery, Perelman School of Medicine: "Toward the Identification of Molecular Pathway Alterations in Aged Fracture Healing: A Pilot Study Utilizing a Genetic Model of Senescence" *(awarded extramural funding from the NIH R03 AG040670)*

Shannon Fisher, M.D., Ph.D., Department of Cell and Developmental Biology, Perelman School of Medicine: "Requirement for Osterix in Skull Formation and Maintenance of Adult Bone in Zebrafish" *(awarded extramural funding from the NIH R21 DE021509)*

Awarded 2010-2011 (Jointly with IOA)
Olena Jacenko, Ph.D., Department of Animal Biology, School of Veterinary Medicine: "Aging of the hematopoietic niche" *(awarded extramural funding from the NIH R01 DK088334-01)*

Eileen M. Shore, Ph.D., Departments of Orthopaedic Surgery and Genetics, Perelman School of Medicine: "Modulation of Progenitor Cell Differentiation through BMP Signaling" *(awarded extramural funding from the NIH R01 AR041916-15)*

Kurt D. Hankenson, DVM, Ph.D., Department of Animal Biology, School of Veterinary Medicine: "Notch Signaling in Bone Regeneration" *(awarded extramural funding from the DOD CDMRP)*

Awarded 2009-2010
Ling Qin, Ph.D., Department of Orthopaedic Surgery, School of Medicine: "Mechanisms of EGFR Action on Bone" *(awarded extramural funding from the NIH R01 DK095803)*

Steven Scherer, M.D., Ph.D., Department of Neurology, Perelman School of Medicine: "Are N-cadherin and L1 Adhesion Molecules Required for Recovery of Muscle Strength after Nerve Injury?"

Nader M. Hebela, M.D., Department of Orthopaedic Surgery, Perelman School of Medicine: "A Pre-Clinical Rodent Model of Intervertebral Disc Autograft Transplant" *(awarded extramural funding from the DOD/CDMRP/PROP OR090090)*

Awarded 2008-2009
Sunday O. Akintoye, BDS, DDS, MS, Department of Oral Medicine, School of Dental Medicine: "Orofacial Bone Marrow Stromal Cells Promote Bisphosphonate-Associated Jaw Osteonecrosis" *(awarded extramural funding from the NIDCR R21 DE022826)*

Margaret M. Chou, Ph.D., Departments of Cell and Developmental Biology, Perelman School of Medicine: "Mechanisms of TRE17/USP6 Function in the Etiology of Aneurysmal Bone Cyst" *(awarded extramural funding from the NIH-NCI R01 CA168452 and R21-CA18601)*

Kenneth W. Leichty, M.D., Department of Surgery, Perelman School of Medicine: "The Role of Inflammation in Regenerative Fetal Tendon Wound Healing" *(awarded extramural funding from the NIH DP2 DK083085)*

Kathleen M. Loomes, M.D., Department of Pediatrics, Children's Hospital of Philadelphia: "The Role of Jag1 in Osteogenesis"

Eileen M. Shore, Ph.D., Departments of Orthopaedic Surgery and Genetics, Perelman School of Medicine: "Analysis of an ACVR1 Knock-in Mouse Model for FOP*" (awarded extramural funding from the NIH R01 AR041916-15S1)*

Awarded 2007-2008
Sherrill L. Adams, Ph.D., Department of Biochemistry, School of Dental Medicine: "Collagen III-deficient Mice as a Model for Musculoskeletal Wound Repair"

Kurt D. Hankenson, DVM, Ph.D., Department of Animal Biology, School of Veterinary Medicine: "Regulation of Bone Formation by Novel Activators of Canonical Wnt Signaling"

Awarded 2006-2007
Robert J. Pignolo, M.D., Ph.D., Department of Medicine, Perelman School of Medicine: "Stem Cell Rescue of the Osteoporotic Phenotype in a Mouse Model of Accelerated Aging" *(awarded extramural funding from the NIH R01 AG028873)*

Robert L. Mauck, Ph.D., Department of Orthopaedic Surgery, Perelman School of Medicine "Meniscus Repair with a Novel Aligned Nanofiber Scaffold" *(awarded extramural funding from the NIH R01 AR056624 and the VA RR & D)*

Christopher S. Chen, M.D. Ph.D., Department of Bioengineering, School of Engineering and Applied Science: "Mechanotransduction in Mesenchymal Stem Cells" *(awarded partial funding as Co-Investigator on NIH P41 EB001046)*

Pedro K. Beredjiklian, M.D., Department of Orthopaedic Surgery, Perelman School of Medicine: "Role of Hyaluronic Acid Receptors in Tendon Healing" (*awarded extramural funding from the NIH R21 AR052393*)

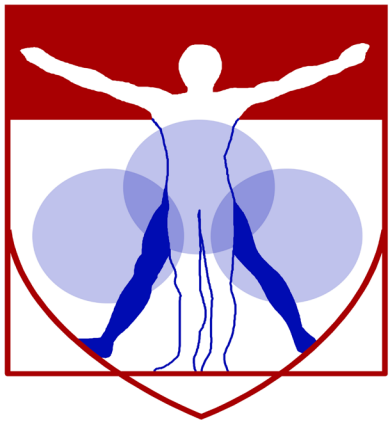

PENN

CENTER for

MUSCULOSKELETAL

DISORDERS

Visiting Professorship Series 2020-2021

Visiting Professorship Series-Academic Year 2020-2021

Tuesday, September 8, 2020, 1:30pm-2:30pm, **Virtual Seminar**
(Co-Sponsored by IRM)
Title: *Regenerative Rehabilitation: Applied biophysics meets stem cell therapeutics*
Fabrisia Ambrosio, Ph.D., MPT
Associate Professor of Physical Medicine & Rehabilitation and Director of Rehabilitation for UPMC International, University of Pittsburgh

Tuesday, October 20, 2020, 1:30pm-2:30pm, **Virtual Seminar**
Title: *Gauging Tendon Mechanics by Observing Tissue Dynamics*
Darryl Thelen, Ph.D.
Professor: Mechanical Engineering and Biomedical Engineering, Affiliate Professor: Orthopedics and Rehabilitation, University of Wisconsin-Madison

ANNUAL SCIENTIFIC SYMPOSIUM
Wednesday, November 18, 2020, 9:00am-12:00pm Virtual Symposium
Title: *Intraoperative and Laboratory Studies of Human Skeletal Muscle Contractures*
Richard L. Lieber, Ph.D., Chief Scientific Officer and Senior Vice President, Shirley Ryan Ability Lab
Professor of Physiology and Biomedical Engineering, Northwestern University

Tuesday, December 8, 2020, 1:30pm-2:30pm, **Virtual Seminar**
Title: *Skeletal Dysplasia in Neurofibromatosis Type 1*
Florent Elefteriou, Ph.D.
Associate Professor of Orthopaedic Surgery and Molecular and Human Genetics
Associate Director, Center for Skeletal Medicine and Biology, Baylor College of Medicine

Tuesday, January 12, 2021, 1:30pm-2:30pm, **Virtual Seminar**
(Co-Sponsored by IRM)
Title: *Biomanufacturing, Biomaterials and Biomechanics for Improved Treatment of Volumetric Muscle Loss Injuries*
George Christ, Ph.D.
Professor of Biomedical Engineering and Orthopaedic Surgery, Mary Muilenburg Stamp Professor of Orthopaedic Research and Director of Basic and Translational Research in Orthopaedic Surgery
University of Virginia

Tuesday, February 23, 2021, 1:30pm-2:30pm, Virtual Seminar
Title: *Pharmacological approaches for manipulating bone quality and mechanics"*
Matthew R. Allen, Ph.D.
Assistant Dean for Faculty Affairs and Professional Development; Associate Professor of Anatomy & Cell Biology, Indiana University School of Medicine

Tuesday, March 16, 2021, 1:30pm-2:30pm, Virtual Seminar
Title: Mechanisms of Human Tendon Plasticity: Links from Molecules to Cells to Athletes to Patients
Professor Jess G. Snedeker
Associate Professor of Orthopaedic Biomechanics, University and ETH Zurich

Tuesday, April 13, 2021, 1:30pm-2:30pm, Virtual Seminar
Title: Targeting the gut to prevent osteoporosis
Laura McCabe, Ph.D.
MSU Foundation Professor, Department of Physiology & Radiology, University of Michigan

Tuesday, May 11, 2021, 1:30pm-2:30pm, Virtual Seminar
"TBD"
Edward Botchwey, Ph.D., Associate Professor, Wallace H. Coulter Department of Biomedical Engineering Georgia Tech

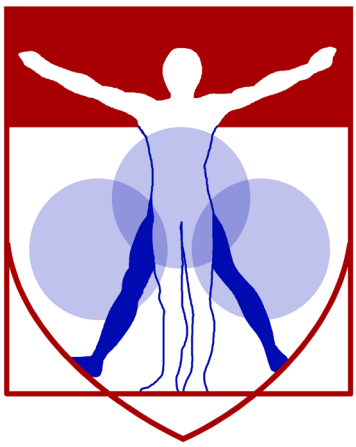

PENN

CENTER for

MUSCULOSKELETAL

DISORDERS

Symposium Participants

First name	Last name	Email	Affiliation
Kimberly	Agnello	kagnello@vet.upenn.edu	UPenn
Saeed	Ahmed	saeed.ahm13@gmail.com	UPenn
Abass	Alavi	janeandabass@yahoo.com	UPenn
Marco	Angelozzi	angelozzim@email.chop.edu	CHOP
Zolt	Arany	zarany@pennmedicine.upenn.edu	UPenn
Tala	Azar	talaazar@seas.upenn.edu	UPenn
Dominique	Barnes	d.barnes@ufl.edu	Univ of Florida
Catherine	Bautista	cbaut@seas.upenn.edu	UPenn
Josh	Baxter	josh.baxter@pennmedicine.upenn.edu	UPenn
Jenny	Bencardino	Jenny.Bencardino@pennmedicine.upenn.edu	UPenn
Benjamin	Binder-Markey	bb983@drexel.edu	Drexel Univ
Joel	Boerckel	boerckel@pennmedicine.upenn.edu	UPenn
Paige	Boneski	pxb083@students.jefferson.edu	Thomas Jefferson Univ
Edward	Bonnevie	edbon@pennmedicine.upenn.edu	UPenn
Niambi	Brewer	nbrewer@pennmedicine.upenn.edu	UPenn
Jason	Burdick	burdick2@seas.upenn.edu	UPenn
James	Carey	James.carey@pennmedicine.upenn.edu	UPenn
Jaclyn	Carlson	jaclynca@upenn.edu	UPenn
Bob	Caron	rcaron@pennmedicine.upenn.edu	UPenn
Sarah	Catheline	cathelines@email.chop.edu	CHOP
Chider	Chen	chenc10@upenn.edu	UPenn
Rebecca	Chung	rebecca.chung@pennmedicine.upenn.edu	UPenn
Sarah	Ciamillo	ciamillo@vet.upenn.edu	UPenn
Alexandra	Ciuciu	axc497@students.jefferson.edu	Thomas Jefferson Univ
Joseph	Collins	jmcollin@seas.upenn.edu	UPenn
Romain	Contentin	contentinr@email.chop.edu	CHOP
Elise	Corbin	Ecorbin@udel.edu	Univ of Delaware
Courtney	Cortese	cortesec@email.chop.edu	CHOP
Christelle	Darrieutort-Laffite	Christelle.darrieutortlaffite@gmail.com	UPenn
Eric	Dai	erkaidai@gmail.com	UPenn
Ryan	Daniels	rydan@pennmedicine.upenn.edu	UPenn
Abhishek	Dhand	adhand@seas.upenn.edu	UPenn
Nikolas	Di Caprio	niko1206@seas.upenn.edu	UPenn
Dennis	Discher	discher@seas.upenn.edu	UPenn
Michael	DiStefano	micdis@seas.upenn.edu	UPenn
John	Drazan	john.drazan2@pennmedicine.upenn.edu	UPenn
Jing	Du	jingdu@psu.edu	Penn State Univ
Nathaniel	Dyment	dyment@pennmedicine.upenn.edu	UPenn
Emily	Eastburn	eae@seas.upenn.edu	UPenn
Yehuda	Elkaim	yehuda.elkaim@pennmedicine.upenn.edu	UPenn
Dawn	Elliott	delliott@udel.edu	Univ of Delaware
Lilith	Elmore	lilith.elmore@students.jefferson.edu	Thomas Jefferson Univ
Mary Kate	Evans	mkevans@seas.upenn.edu	UPenn
Kayla	Even	Evenk@vet.upenn.edu	UPenn

First name	Last name	Email	Affiliation
Matthew	Fainor	mfainor@gmail.com	UPenn
Daniel	Farber	daniel.farber@pennmedicine.upenn.edu	UPenn
Gabriella	Fioravanti	gabriella.fioravanti@jefferson.edu	Thomas Jefferson Univ
Velia	Fowler	vfowler@udel.edu	Univ of Delaware
Theresa	Freeman	theresa.freeman@jefferson.edu	Thomas Jefferson Univ
Chet	Friday	Chet.Friday@Pennmedicine.upenn.edu	UPenn
Ashley	Fung	afung@seas.upenn.edu	UPenn
Angela	Gaesser	agaesser@upenn.edu	UPenn
Jonathan	Galarraga	jgala@seas.upenn.edu	UPenn
Tao	Gui	tao.gui@pennmedicine.upenn.edu	Upenn
Sarah	Gullbrand	sgullb@pennmedicine.upenn.edu	UPenn
Biao	Han	Biao.Han@pennmedicine.upenn.edu	UPenn
Lin	Han	lh535@drexel.edu	Drexel Univ
Abdul	Haseeb	haseeba@email.chop.edu	CHOP
Michael	Hast	hast@pennmedicine.upenn.edu	UPenn
Elizabeth	Henning	ehenning@pennmedicine.upenn.edu	UPenn
Su Chin	Heo	heosc@pennmedicine.upenn.edu	UPenn
Brian	Hercyk	Brian.hercyk@pennmedicine.UPenn.edu	UPenn
Blake	Hernandez	hdzblake@gmail.com	UPenn
Noreen	Hickok	Noreen.Hickok@jefferson.edu	Thomas Jefferson Univ
Todd	Hullfish	todd.hullfish@pennmedicine.upenn.edu	UPenn
Eric	Hume	Eric.hume@pennmedicine.UPenn.edu	UPenn
Lauren	Israel	lxi009@jefferson.edu	Jefferson Univ
Shama	Iyer	siyer@som.umaryland.edu	Univ of Maryland
Olena	Jacenko	jacenko@vet.upenn.edu	UPenn
Natasha	Jaiswal	natasha.jaiswal@pennmedicine.upenn.edu	UPenn
Xi	Jiang	jiangxi@pennmedicine.upenn.edu	UPenn
Zhirui	Jiang	zhirui.jiang@pennmedicine.upenn.edu	UPenn
Stephanie	Jo	stephanie.jo@pennmedicine.upenn.edu	UPenn
Kyu Sang	Joeng	joeng@pennmedicine.upenn.edu	UPenn
Shira	Johnston	shira.johnston@students.jefferson.edu	Thomas Jefferson Univ
Brandon	Jones	bcjones@seas.upenn.edu	UPenn
Dakota	Jones	dakota.jones@pennmedicine.upenn.edu	UPenn
Fadia	Kamal	Fkamal@pennstatehealth.psu.edu	Penn State Univ
Tim	Kamalitdinov	timkam@seas.upenn.edu	UPenn
Fred	Kaplan	Frederick.Kaplan@pennmedicine.upenn.edu	UPenn
Kannan	Karuppaiah	kannan.karuppaiah@pennmedicine.upenn.edu	UPenn
Anirudha	Karvande	karvandea@email.chop.edu	CHOP
Ranjan	Kc	kcr@email.chop.edu	CHOP
Mohd Parvez	Khan	mohdparvez92@gmail.com	UPenn
Dong hwa	Kim	kimd1@pennmail.upenn.edu	UPenn
James	Kim	james.kim@rochester.edu	UPenn
Minwook	Kim	kimm12@email.chop.edu	CHOP
Sharon	Kolasinski	sharon.kolasinski@pennmedicine.upenn.edu	UPenn

First name	Last name	Email	Affiliation
Eiki	Koyama	Koyamae@email.chop.edu	CHOP
Hattanas	Kumchai	hattanas.kumchai@students.jefferson.edu	Jefferson
Meghan	Kupratis	kupratis@udel.edu	Univ of Delaware
Emily	Lambeth	eplambet@udel.edu	Univ of Delaware
Yian	Lau	adrianlau02@gmail.com	UPenn
Thomas	Leahy	thomasleahy.apps@gmail.com	UPenn
Yeonju	Lee	yeonju.lee@pennmedicine.upenn.edu	UPenn
Veronique	Lefebvre	lefebvrev1@email.chop.edu	CHOP
Ryan	Leiphart	rleip@seas.upenn.edu	UPenn
Elisabeth	Lemmon	elemmon@vet.upenn.edu	UPenn
Scott	Levin	Lorna.Muramoto@pennmedicine.upenn.edu	UPenn
Gregory	Lewis	glewis1@pennstatehealth.psu.edu	Penn State
Chenshuang	Li	lichens@upenn.edu	UPenn
Yihan	Li	yihanl@seas.upenn.edu	UPenn
Zizhao	Li	lizizhai@seas.upenn.edu	UPenn
Renata	Linardi	rlinardi@upenn.edu	UPenn
X. Sherry	Liu	xiaoweil@pennmedicine.upenn.edu	UPenn
Ryan	Locke	ryanchrislocke@gmail.com	UPenn
Fanxin	Long	longf1@email.chop.edu	CHOP
Vitali	Lounev	vlounev@pennmedicine.upenn.edu	UPenn
Rich	Lovering	rlovering@som.umaryland.edu	Univ of Maryland
Nuoying	Ma	nuoying@seas.upenn.edu	UPenn
Veda	Madhu	vxm042@jefferson.edu	Thomas Jefferson Univ
Hamd	Mahmood	hamd.mahmood@pennmedicine.upenn.edu	UPenn
Jerahme	Martinez	jerahme.martinez@gmail.com	UPenn
Anna	Massie	amassie@upenn.edu	UPenn
Robert	Mauck	lemauck@pennmedicine.upenn.edu	UPenn
Kendra	Miller	k.g.miller97@gmail.com	UPenn
Clare	Milner	milner@drexel.edu	Drexel Univ
Yasaman	Moharrer	yasamanm@seas.upenn.edu	UPenn
Shreya	Mondal	shrepols@seas.upenn.edu	UPenn
Foteini	Mourkioti	fmour@pennmedicine.upenn.edu	UPenn
Victoria Grace	Muir	vgmuir@seas.upenn.edu	UPenn
Joseph	Newton	josebr@seas.upenn.edu	UPenn
Vu	Nguyen	vunguyen@pennmedicine.upenn.edu	UPenn
Madhura	Nijsure	mnijsure@seas.upenn.edu	UPenn
Courtney	Nuss	cnuss@pennmedicine.upenn.edu	UPenn
Takashi	Ohnishi	takashi.onishi.ortho@gmail.com	Thomas Jefferson Univ
Kyla	Ortved	kortved@vet.upenn.edu	UPenn
Olivia	Ottone	oko002@students.jefferson.edu	Thomas Jefferson Univ
Maurizio	Pacifici	pacificim@email.chop.edu	CHOP
Na Rae	Park	na.park@pennmedicine.upenn.edu	UPenn
Lauren	Paschall	lnp55@psu.edu	Penn State Univ
Liming	Pei	lpei@pennmedicine.upenn.edu	UPenn

First name	Last name	Email	Affiliation
Ana	Peredo	anapperedo@gmail.com	UPenn
Ben	Peterson	bep15@psu.edu	Penn State Univ
Nancy	Pleshko	npleshko@temple.edu	Temple Univ
Annapurna	Pranatharthi-Haran	annapurnap@ncbs.res.in	UPenn
Margaret	Prendergast	prendm@seas.upenn.edu	UPenn
Ling	Qin	qinling@pennmedicine.upenn.edu	UPenn
William	Querido	william.querido@temple.edu	Temple Univ
Harina	Raja	harina@pennmedicine.upenn.edu	UPenn
Pranay	Ramteke	pranay1130@gmail.com	Thomas Jefferson Univ
Dean	Richardson	dwr@vet.upenn.edu	UPenn
Makarand	Risbud	makarand.risbud@jefferson.edu	Thomas Jefferson Univ
Douglas	Roberts	doug.roberts@pennmedicine.upenn.edu	UPenn
Vincent	Ruggieri	ruggieriv@email.chop.edu	CHOP
Danielle	Rux	ruxd@email.chop.edu	CHOP
Kimheak	Sao	Kxs489@students.jefferson.edu	Thomas Jefferson Univ
Ernestina	Schipani	Ernestina.Schipani@Pennmedicine.upenn.edu	UPenn
Ashkan	Sedigh	Ashkan.sedigh@jefferson.edu	Thomas Jefferson Univ
Donna	Seravello	donnaser@upenn.edu	UPenn
Janvi	Shah	Tuh16471@temple.edu	Temple Univ
Snehal	Shetye	snehalshetye@gmail.com	UPenn
Eileen	Shore	shore@pennmedicine.upenn.edu	UPenn
Benjamin	Sinder	sinderb@email.chop.edu	CHOP
Gail	Smith	smithgk@upenn.edu	UPenn
Lachlan	Smith	lachlans@pennmedicine.upenn.edu	UPenn
Chao	Song	songc2@email.chop.edu	CHOP
Hee Kwon	Song	heekwon.song@pennmedicine.upenn.edu	UPenn
Lou	Soslowsky	soslowsk@Upenn.edu	UPenn
Brendan	Stoeckl	bstoeckl@pennmedicine.upenn.edu	UPenn
Michael	Struss	tuf19432@temple.edu	Temple Univ
Jason	Syrcle	SYRCLE@VET.UPENN.EDU	UPenn
Spencer	Szczesny	ses297@psu.edu	Penn State Univ
Margaret	Tamburro	margaret.tamburro@pennmedicine.upenn.edu	UPenn
Sisi	Tang	st240@sas.upenn.edu	UPenn
Waixing	Tang	waixing@pennmedicine.upenn.edu	UPenn
Brittany	Taylor	brtay@pennmedicine.upenn.edu	UPenn
Elisia	Tichy	etichy@pennmedicine.upenn.edu	UPenn
Paul	Titchenell	ptitc@pennmedicine.upenn.edu	UPenn
Ryan	Tomlinson	ryan.tomlinson@jefferson.edu	Thomas Jefferson Univ
Will	Towler	otowler@pennmedicine.upenn.edu	UPenn
Victoria	Tran	vat005@jefferson.edu	Thomas Jefferson Univ
Maria	Tsingas	mxt189@students.jefferson.edu	Thomas Jefferson Univ
Tonia	Tsinman	ttsinman@seas.upenn.edu	UPenn
Ani	Ural	ani.ural@villanova.edu	Villanova Univ

First name	Last name	Email	Affiliation
Susan	Volk	swvolk@vet.upenn.edu	UPenn
Liyun	Wang	lywang@udel.edu	Univ of Delaware
David	Waning	Dwaning@psu.edu	Penn State Univ
Murtaza	Wasi	murtaza@udel.edu	Univ of Delaware
David	Weber	weberd@email.chop.edu	CHOP
Felix	Wehrli	felix.wehrli@pennmedicine.upenn.edu	UPenn
Stephanie	Weiss	weisssn@gmail.com	UPenn
Victoria	Wong	vicwong@sas.upenn.edu	UPenn
Jianing	Xu	jianingx@upenn.edu	UPenn
Karen	Xu	klxu@seas.upenn.edu	UPenn
Meiqi	Xu	mqx@upenn.edu	UPenn
Shuying	Yang	shuyingy@upenn.edu	UPenn
Lutian	Yao	lutian@pennmedicine.upenn.edu	UPenn
Susana	Yassan	syassan@sralab.org	Shirley Ryan AbilityLab
Gongsheng	Yuan	gsyuan@upenn.edu	UPenn
Babette	Zemel	zemel@email.chop.edu	UPenn/CHOP
Chenghao	Zhang	Chenghao.zhang@pennmedicine.upenn.edu	UPenn
Deyu	Zhang	deyuz@pennmedicine.upenn.edu	UPenn
Ellen	Zhang	yzhang98@seas.upenn.edu	UPenn
Qunzhou	Zhang	zqunzhou@upenn.edu	UPenn
Yejia	Zhang	yejiazhang07@gmail.com	UPenn
Leilei	Zhong	zhongleilei8@gmail.com	UPenn
Yilu	Zhou	yiluz@pennmedicine.upenn.edu	UPenn
Hannah	Zlotnick	zlotnick@seas.upenn.edu	UPenn

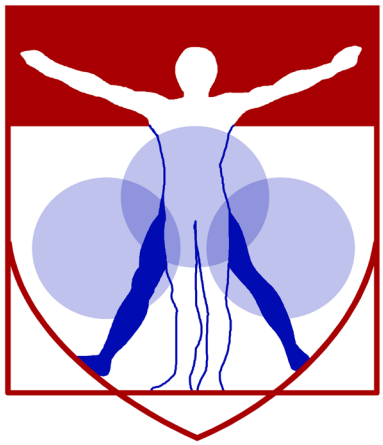

PENN

CENTER for

MUSCULOSKELETAL

DISORDERS

Speaker Abstracts

Asymmetry of the Tensor Fascia Lata Muscle in Hip Dysplasia

Nejadnik H, Selvam N, Bencardino J, Sebro R, Shabshin N, Kase D

Society of Skeletal Radiology

Perelman School of Medicine
University of Pennsylvania

Aim: To determine the association of asymmetric tensor fascia lata (TFL) muscles and hip dysplasia in adults.

Materials and Methods:

- IRB-approved study
- Electronic medical records search using mPower software
- All hip and pelvis MRI studies that included coronal and axial T1 weighted sequences of the pelvis performed 01/01/2010-01/01/2020.
- Inclusion criteria:
  - AP view of the pelvis within 1 year of MR date: proper technique (no rotation)
  - Age >18.
- Exclusion criteria: motion artifact, postoperative hips, neuromuscular disease, inflammatory myopathy, and degraded imaging.

Materials and Methods

- Matched/paired study – each person has a contralateral side for an internal comparison
- The tensor fascia lata (TFL) muscles were classified as symmetric versus asymmetric recording the side of decreased muscle volume.
- Acetabular coverage was assessed by measurements of CEA angles on frontal AP view of the pelvis using SECTRA PACS for measurements.
- The study group was classified as normal CEA >25, borderline 20-25 and dysplastic <20.
- Data was acquired using manual calculations.
- Odds ratio was calculated.

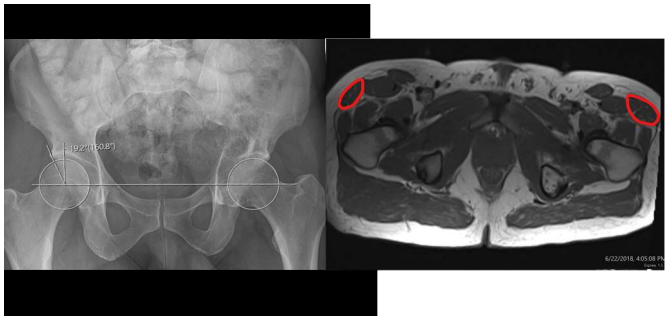

Images from selected patient #3 demonstrate right hip dysplasia on AP radiograph with corresponding mild right sided tensor fascia lata relative atrophy (arrow)

Results

- 99 subjects (63F:36M) were included ranging in age from 21 to 91.
- 91 patients had neither hip dysplasia nor TFL asymmetry (92%).
- 7 patients had TFL asymmetry (7%).
  - 3 of these patients had corresponding hip dysplasia (on the same side as TFL atrophy) (43%)
- 4 patients had hip dysplasia (unilateral or bilateral) (4%)
  - 3 of these patients had TFL asymmetry with atrophy on the same side as hip dysplasia (75%)
- Presence of asymmetry of the TFL is associated with hip dysplasia. The relative risk of having atrophy of the TFL for patients with hip dysplasia is 17.8 resulting in a statistically significant odds-ratio of 68.5 ($p<0.001$, 95%confidence interval [5.7 –815]).

Conclusion

- Our results suggest that asymmetry of the tensor fascia lata muscle can be used as a diagnostic imaging marker of subtle hip dysplasia in adults.

Clinical Significance

- Asymmetry of the tensor fascia lata muscles can be seen in the setting of hip dysplasia. When noticed, decreased muscle bulk of the tensor fascia lata may be used as a secondary sign of hip dysplasia along with decreased CEA angle measurements

Whole Muscle Passive Mechanics Do Not Simply Scale by Architectural Properties

Benjamin I Binder-Markey[1,2,3] and Richard L Lieber[2,3]
[1]Drexel Univeristy, Department of Physical Therapy and Rehabilitation Sciences, Philadelphia, PA , USA
[2]Shirley Ryan AbilityLab & [3]Northwestern University, Department of PM&R, Chicago, IL, USA
Email: bb983@drexel.edu

Introduction

Whole muscle active length-tension properties accurately scale from the sarcomere to the whole muscle level [1], but interestingly, in mammalian muscle, passive mechanical properties do not [1,2]. This is largely because the detailed relationship between the passive mechanical properties of fibers, fascicles, and whole muscles are rarely studied. Only in frog muscle, has uniform passive scaling been demonstrated from the fiber to the whole muscle [3]. We believe that this is because intramuscular connective tissue in frog is very poorly developed compared to mammals [2]. Recent work in rabbit muscle demonstrates that fiber, fiber bundle and fascicle mechanics do not simply scale to whole muscle mechanics [4]. Thus, the purpose of this study was to measure whole muscle passive mechanical properties and use modeling to identify sources that could contribute to non-linear scaling from fascicle to whole muscle.

Methods

Passive mechanical properties from three muscles of varying architecture and function were measured in 12-week C57Bl6 mice: rectus femoris (RF; n=6), semimembranosus (SM; n=6), and tibialis anterior (TA; n=5). Muscles were dissected from origin to insertion, placed in a physiological bath, attached to a 1N force transducer, and lengthened in ~0.5mm increments. Force was recorded after 3-minutes of stress-relaxation. Samples were weighed and physiological cross sectional area (PCSA) was calculated using published architectural properties [5].

Muscle passive force was normalized to PCSA and muscle deformation was converted to fascicle strain using the fiber length-to-muscle length ratio [5], thus creating a passive stress-strain relationship normalized by architectural parameters for each muscle. Each raw and normalized data set was fit to an exponential [3] and all curves were averaged to create a single exponential describing that muscle's passive force-deformation (Fig. 1A) or stress-strain relationship (Fig. 1B). All curve fits were excellent, exceeding r^2 values of 0.96

To investigate potential sources that might lead to the fascicle differences observed in Fig. 1B, we developed three Hill-type models of progressively increasing complexity. **Model 1**: A simple lumped parameter model normalized fascicle property across muscles that has the form $\left(\frac{a}{b}(e^{b\varepsilon}-1)\right)$; **Model 2**: Model 1 plus a muscle-specific parallel element elastic element (c_m) across the whole muscle representing parallel elastic connective tissue differences among muscles; **Model 3**: Model 2 plus a muscle-dependent inter-fascicular shear factor (τ_m) that resists fascicle rotation. For each model, each parameter (a, b, c_m, and τ_m) was optimized in MATLAB by minimizing the sum of the squared error (SSE) between the muscles' modeled force-deformation data and the experimentally collected data (Fig. 1A).

Results and Discussion

Data from all three muscles were well-fit by the exponential stress-strain curve (RF r^2=0.994±0.008 SD, SM r^2=0.991±0.004 SD, RF r^2=0.990±0.012 SD). The RF was the stiffest muscle, followed by the TA (especially at high deformation) and then the SM (Fig. 1A). Accounting for fiber length differences, stress-strain curves became more similar, but not identical (Fig. 1B).

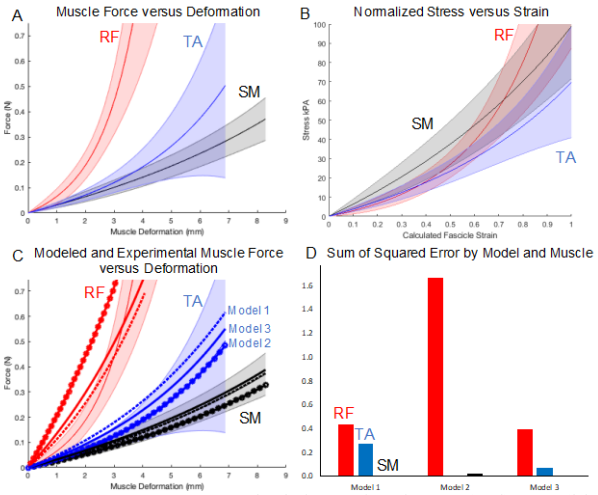

Figure 1: A) Force *vs.* muscle deformation for RF (red), SM (black), and TA (blue). B) Stress-strain relationship for each muscle normalized by architecture. Data shown as average±SD. C) Force *vs.* muscle deformation of the experimental and modeled RF (red), SM (black), and TA (blue) for Model 1 (dashed), Model 2 (circles), and Model 3 (solid). D) SSE for each model and muscle with lower numbers better fit.

The degree to which more complex models explained experimental data were related to the complexity of each muscle (Figs. 1C and 1D). The SM, which is a very simple parallel-fibered muscle with fascicles running from origin to insertion was best fit by the simplest model, Model 1 (SSE=$1.35\text{x}10^{-4}$). The TA, in which fascicles run from a broad proximal tibial origin to a single internal insertion tendon was fit best by the slightly more complex Model 2 (SSE=$3.28\text{x}10^{-3}$). Finally, the RF whose fascicles originate on a central internal tendon and radiate distally to a broad aponeurosis surrounding the muscle was fit best by the most complex model, Model 3. (SSE=0.397).

Significance

These results demonstrate that, to accurately model muscle passive mechanical properties, the model must reflect the complexity of the muscle. To a first approximation, architectural normalization helps (Fig. 1A), but in order to provide high resolution properties, additional terms are needed. The precise structures that represent these mathematical terms are not currently clear and must be the subject of ongoing investigations.

Acknowledgments

The Brinson Fellowship and the Shirley Ryan AbilityLab.

Literature References

[1] Winters *et al.* 2011; [2] Meyer & Lieber 2018; [3] Magid and Law 1985; [4] Ward *et al.* 2020; [5] Burkholder *et al.*1994

Mechanobiology of Bone Development and Repair

Joel Boerckel, PhD
Assistant Professor of Bioengineering and Orthopaedic Surgery

Large bone defects caused by traumatic injury or tumor resection pose a significant clinical challenge as they cannot not heal without intervention, and current bone grafting therapies are limited. Tissue engineering is a promising alternative, but is often limited by poor recruitment or supply of endogenous progenitor cells. Unlike large defects, bone fractures heal readily by recapitulating many steps of bone development. In fracture repair, mechanical cues are essential to determine the pathway by which bone formation occurs, viz. direct bone formation through intramembranous ossification or indirect bone formation through endochondral ossification, in which a cartilage template forms first and is later replaced by bone. The mechanisms by which osteoprogenitor cells are mobilized during bone development and how mechanical cues direct fracture repair are poorly understood. We have found that the mechanosensitive transcriptional regulators, Yes-associated protein (YAP) and Transcriptional co-activator with PDZ-binding motif (TAZ) combinatorially promote both bone development and repair. Specifically, deletion of YAP and TAZ from osterix-expressing cells during development caused skeletal deformities and fragility reminiscent of the human disease osteogenesis imperfecta, resulting in perinatal lethality. Inducible deletion of YAP and TAZ from osterix-expressing cells during bone fracture repair impaired endochondral bone formation through periosteal osteoblast precursor cell proliferation and osteoblastic differentiation. Based on these findings, we developed a mechanotherapeutic approach to regenerate large bone defects by recapitulating bone development. We found that mechanical loading promoted endochondral bone regeneration by engineered mesenchymal condensations, dependent on load timing. Together, these findings provide new insight into the cellular and molecular mechanisms by which mechanical cues direct bone development and repair and identify new approaches for functional bone regeneration.

Intraoperative and Laboratory Studies of Human Skeletal Muscle Contractures

Richard L. Lieber, Ph.D.

Professor and Chief Scientific Officer

Shirley Ryan AbilityLab and

Departments of Physical Medicine and Rehabilitation and Biomedical Engineering

Northwestern University, Chicago, IL 60611

Skeletal muscle is a highly plastic tissue, responding both to level of use and amount of neural input. After cerebral palsy (CP) altered neural input can result in muscle contractures. We have studied the mechanics and biology of muscle from children with wrist flexion contractures secondary to CP. Dramatic architectural changes are observed in these children whereby sarcomere lengths are dramatically altered relative to patients without upper motor neuron lesions. This suggests dramatic alterations in the regulation of muscle growth in these children. Biomechanical studies of isolated single muscle cells reveal an increased passive modulus and decreased resting sarcomere length suggesting alterations in the cellular cytoskeleton. Gene expression profiling reveals a number of "conflicting" biological pathways in spastic muscle. Specifically, this muscle adapts by altering processes related to extracellular matrix production, fiber type determination, fiber hypertrophy and myogenesis. These transcriptional adaptations are not characteristic of muscle adaptations observed in Duchenne muscular dystrophy or limb immobilization. Superimposed upon the dramatic biological and structural adaptations is a loss in the number of satellite cells that are located throughout the muscle. Even the remaining satellite cells have epigenetic changes that can dramatically influence our ability to rehabilitate these muscles. Recently, we have shown that several anti-cancer drugs are able to reverse these epigenetic changes, thus "rescuing" the satellite cells and promoting myogenesis. Taken together, these results support the notion that, while contracture formation is multifactorial and neural in origin, significant structural alterations in muscle also occur. An understanding of the specific changes that occur in the muscle and extracellular matrix may facilitate the development of new conservative or surgical therapies for this devastating problem.

Bone biomechanics of small and large animals: considerations for an appropriate model

Anna Massie, DVM, DACVS-SA
Assistant Professor of Orthopedic Surgery, College of Veterinary Medicine

The use of small and large animals is critical in many aspects of research and development, and the choice of an animal model is multifactorial. Rabbits are extensively used as a model for musculoskeletal research, accounting for ~35% of the animals models published.[1] However, it has been noted clinically that fracture repair is extremely challenging- the fractures are often comminuted; there is an anecdotally high rate of iatrogenic fracture during surgery; and regardless of the original fracture configuration, low-impact catastrophic failure is often noted.[2] In contrast to other domestic species, rabbits carry 70% of their body weight in the pelvic limbs, have a plantigrade stance with a uniquely high-motion gate, and possess thin cortices with a light skeletal weight.[3,4] Rabbits are an appealing specimen due to ease of husbandry, their small size, and an early age of sexual/skeletal maturity.[5]

The first biomechanical principles when applying an implant to bone is what size cortical defect can be iatrogenically created without significantly weakening the bone. A landmark study evaluating sheep bone determined that a defect should not exceed 33% of the bone diameter.[6] This was based on the authors' views that the bone should not be weakened by more than half the original torsional strength of the bone, and has been since applied as a standard orthopedic principle cross-species. Our study aimed to evaluate this torsional strength in rabbit bone to determine what sized defect can be safely created without weakening the bone beyond 50% it's intact strength.

Torsional structural properties of the rabbit femur were evaluated using 18 pairs of New Zealand white rabbit femora.[7] Testing groups included bicortical drill holes of three sizes (1.1 mm-, 1.5mm-, and 2.0 mm-diameter defects) and intact bone. As a percentage of bone diameter, these hole diameters correlated to 15% (1.1 mm hole), 20% (1.5mm hole) and 27% (2.0mm hole). Using these models, the mean torsional strength relative to intact bone was decreased by 37.1% (1.1 mm hole), 53.0% (1.5 mm hole), and 65% (2.0 mm hole). This indicates, based on the previous principle, no hole greater than 15% bone diameter should be created in rabbit bone.

The torque-angle plots were distinctly linear, with a lack of plastic and post-failure behaviors. These properties support the uniquely brittle behavior of rabbit bone. All, and only, the intact bones failed in a severely comminuted pattern, also supporting the strength but ultimate brittleness of these bones.

This study brings up many interesting considerations from the clinical aspect of repairing rabbit fractures, but also unique considerations for the researcher when choosing and animal model. In addition to ease-of-use and housing, considerations in choosing an animal model should be closely correlated with the primary research directive.[8-10] Disparities exist in the macrostructure, microsctructure, composition, and remodeling qualities of bone amongst species, making each uniquely qualified for translational research prior to application of implants or regenerative medicine to human subjects.

References

1. Neyt JG, Buckwalter JA, Carroll NC. Use of animal models in musculoskeletal research. Iowa Orthop J 1998;18:118–23
2. Langley-Hobbs S, Harcourt-Brown N. Fracture management. In: Harcourt-Brown F, Chitty J, eds. BSAVA Manual of Rabbit Surgery, Dentistry and Imaging. British Small Animal Veterinary Association Gloucester, United Kingdom; 2013:283–304
3. Brewer NR, Cruise LJ. Physiology. In: Manning PJ, Ringler DH, Newcomer CE, eds. The Biology of the Laboratory Rabbit. 2nd ed. Orlando, FL: Academic Press; 1994:63–70
4. Cruise LJ, Brewer NR. Anatomy. In Manning PJ, Ringler DH, Newcomer CE, eds. The Biology of the Laboratory Rabbit. 2nd ed. Orlando, FL: Academic Press; 1994:47–61
5. Gilsanz V, Roe TF, Gibbens DT, et al. Effect of sex steroids on peak bone density of growing rabbits. Am J Physiol 1988;255(4 Pt 1): E416–E421
6. Edgerton BC, An KN, Morrey BF. Torsional strength reduction due to cortical defects in bone. J Orthop Res 1990;8(06):851–855
7. Massie A, Kapatkin AS, Garcia-Nolen T, Guzman D S-M, Chou PY, Stover S. The effects of hole diameter on torsional mechanical properties of the rabbit femur. Vet Comp Orthop Traumatol 2019;32:51-58
8. Pearce AI, Richards RG, Milz S, Schneider E, Pearce SG. Animal models for implant biomaterial research in bone: a review. Eur Cell Mater 2007;13:1–10
9. 1 Wang X, Mabrey JD, Agrawal CM. An interspecies comparison of bone fracture properties. Biomed Mater Eng 1998;8(01):1–9
10. Zapata-Cornelio FY, Day GA, Coe RH, Sikora SNF, Wijayathunga VN, Tarsuslugil SM, Mengoni M, Wilcox RK. Methodology to Produce Specimen-Specific Models of Vertebrae: Application to Different Species. Ann Biomed Eng. 2017 Oct;45(10):2451-2460

Physical Activity in Breast Cancer Bone Metastasis

Liyun Wang, Ph.D.
Center for Biomechanical Engineering Research, Department of Mechanical Engineering
University of Delaware. lywang@udel.edu

Physical activity is widely promoted for the well-being of cancer patients because of the reduction in overall mortality [1], and benefits are also shown for patients with bone metastasis [2]. Osteolytic bone lesions—found in most stage IV breast cancer patients and driven by the vicious cancer-bone cycle [3]—weaken the skeleton and result in painful skeletal-related events (SREs) that are difficult to treat or even fatal. Thus, maintaining skeletal structure and strength is of high clinical significance.

It is well established that mechanical loading of the skeleton during physical activity induces bone formation and inhibits bone resorption. In vivo tibial loading of immunocompromised mice showed to delay the destruction of bone due to the promotion of bone formation and inhibition of breast cancer cells [4]. Another study identified that the anti-tumor effect may due to the ATP release from mechanically activated osteocytes [5]. However, this beneficial loading effect was found to be lost with increasing magnitude [6]. In these animal studies, young female mice (<8 weeks) received injection of breast cancer cells, followed by tibial loading under anesthesia. In contrast, breast cancer patients are adults with mature skeleton and running/walking is their popular choice of physical activity.

In this talk, I will share our recent studies, which aimed to test the effects of two different modes of exercise (treadmill running or tibial loading) and exercise intensity (medium 4.5N or high 8N of tibial loading) on bone integrity and tumor growth using adult immunocompetent mice. Our results confirm that there is an optimal window to achieve anti-tumor and skeletal protective effects of tibial loading and accelerated bone destruction was induced by breast cancer when the loading was too much (8.0N) or too little (no loading). Mice underwent treadmill running at 16m/min, 45 min per day, 5 days per week significantly delayed the perforation of bone cortex than non-runners. I will discuss possible factors contributing to our in vivo findings. Overall, our study supports the overall benefits of physical activity and the need of personalized exercise regimen for breast cancer patients with bone metastasis.

1. Ballard-Barbash et al. Physical activity, biomarkers, and disease outcomes in cancer survivors: a systematic review. J Natl Cancer Inst, 2012. 104(11): p. 815-40.
2. Beaton et al. Effects of exercise intervention on persons with metastatic cancer: a systematic review. Physiother Can, 2009. 61(3): p. 141-53.
3. Mundy, G.R., Mechanisms of bone metastasis. Cancer, 1997. 80(8 Suppl): p. 1546-56.
4. Lynch et al. In vivo tibial compression decreases osteolysis and tumor formation in a human metastatic breast cancer model. J Bone Miner Res, 2013. 28(11): p. 2357-67.
5. Zhou et al. Osteocytic connexin hemichannels suppress breast cancer growth and bone metastasis. Oncogene, 2016. 35(43): p. 5597-5607.
6. Fan et al. Skeletal loading regulates breast cancer-associated osteolysis in a loading intensity-dependent fashion. Bone Research, 2020. 8:9

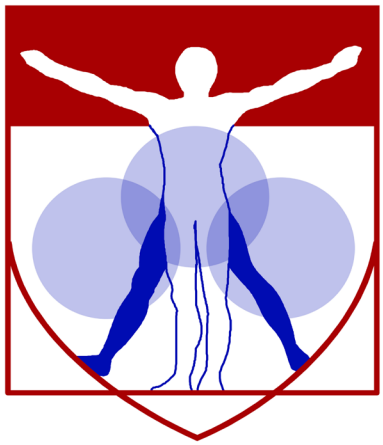

PENN

CENTER for

MUSCULOSKELETAL

DISORDERS

Abstracts

Neural EGFL Like 1, a new dual-functioning disease-modifying osteoarthritis drug

Chenshuang Li[1,2], Pin Ha[2], Wenlu Jiang[2], Emily A. Berthiaume[3], Cymbeline T Culiat[4], Xinli Zhang[2], Kang Ting[2], Chia Soo[3],Zhong Zheng[2,3]

[1]Department of Orthodontics, School of Dental Medicine, University of Pennsylvania; [2]Division of Growth and Development, Section of Orthodontics, School of Dentistry, University of California, Los Angeles; [3]UCLA Division of Plastic Surgery and Department of Orthopaedic Surgery and the Orthopaedic Hospital Research Center, University of California, Los Angeles; [4]NellOne Therapeutics, Inc.

INTRODUCTION: As the leading cause of disability in adults, arthritis appears in over 100 identified diseases. Arthritis can cause inflammation that results in pain, stiffness, swelling, and decreased range of motion in any joint in the body. Currently, arthritis affects over 54.4 million people in the US alone. Moreover, the prevalence of arthritis is expected to increase sharply in the near future due to the increases in life expectancy and aging populations, which equates to a tremendous economic burden. In particular, osteoarthritis (OA) is the most common form of arthritis and affects around 18% of women and 10% of men over the age of 60. Unfortunately, there are no currently approved disease-modifying osteoarthritis drugs (DMOADs) that can prevent, stop, or even restrain the progression of OA.

In order to combat the cartilage destruction seen in OA, recent searches for new OA therapeutics are shifting from synthetic chemicals to biological molecules, with a specific focus on pro-chondrogenic growth factors. For instance, neural EGFL-like 1 (NELL-1) is a novel pro-chondrogenic molecule that enhances the proliferation, chondrogenic differentiation, and maturation of chondrogenic-committed cells and their progenitors *in vitro*. As an extracellular matrix (ECM) molecule expressed in articular cartilage, NELL-1 alone is sufficient to induce cartilage regeneration without osteophyte formation in rabbit knee critical-sized, full-thickness subchondral defects. Moreover, our recent studies identified the novel signaling cascade of NELL-1 → nuclear factor of activated T-cells (NFATc)1 → runt-related transcription factor (RUNX)3 → Indian hedgehog (IHH), which is essential for NELL-1's pro-chondrogenic bioactivities. Inspired by the genome-wide association study that associated single nucleotide polymorphisms (SNPs) within the *NELL-1* gene in ankylosing spondylitis and psoriatic arthritis, the current study is intended to determine the role of NELL-1 in the pathogenesis of OA and its potential therapeutic benefits.

METHODS: All the experiments on live mice were performed under an institutionally approved protocol provided by the Chancellor's Animal Research Committee at UCLA. The importance of NELL-1 in arthritis progression was first determined in a spontaneous model, which is the hallmark of primary OA. Since homozygous *Nell-1*-deficient (*Nell-1*$^{6R/6R}$) mice have a severely reduced expression of *Nell-1* that results in neonatal death, *Nell-1*-haploinsufficient (*Nell-1*$^{+/6R}$) mice were examined in comparison with wildtype (WT) counterparts at 1-month (a prepubescent stage for mice that developmentally approximates 12.5 years of age in humans), 3 months (a mature young adult stage for mice that developmentally approximates 20 years of age in humans), and 18 months (a senescent stage for mice that developmentally approximates >50 years of age in humans). Special focus was directed to the medial tibial plateau area, which is one of the most critical loadbearing areas in the body. Next, a well-documented direct interleukin (IL)1b intra-articular injection strategy was employed to establish an induced OA model. Histological, immunohistological, and gait analyses were used for evaluating OA-like damage, as well as the effect of NELL-1 administration. Next, primary chondrocytes derived from mouse and human articular cartilage were used for gene profiling to revealing the underlying mechanism *in vitro*. Lastly, RNA interference (RNAi) technology was used to identify the transcriptional factors that mediate the anti-arthritic effects of NELL-1. All statistical analyses were conducted with OriginPro 8 (Origin Lab Corp.) in consultation with the UCLA Statistical Biomathematical Consulting Clinic. $P < 0.05$ (*) was considered a suggestive difference, while $P < 0.005$ (**) was recognized as a statistically significant difference.

RESULTS: Encompassing the age spectrum from juvenile, young adult, to elderly, *Nell-1*-haploinsufficiency drastically accelerated and aggravated the arthritis-like cartilage degeneration and was accompanied by significant elevation of proinflammation cytokines in mice. For instance, at 3 months of age, focal wear and tear of hyaline cartilage with early chondrocyte clustering was only observed in *Nell-1*$^{+/6R}$ mice. In comparison with WT mouse cartilage, *Nell-1*$^{+/6R}$ mouse cartilage not only had significant type II collagen reduction and Mmp13 elevation, which represent key events in OA progression, but also had remarkedly pronounced Il1b expression, which indicates elevated inflammation. At 18 months of age, severe loss of hyaline cartilage accompanied by almost completely absent proteoglycan, negligible type II collagen, significantly upregulated expression of inflammatory cytokines and their downstream cartilage catabolic enzymes, and exposure of the underlying calcified cartilage were observed in *Nell-1*$^{+/6R}$ mice knees. All of these findings are similar to those seen in late-stage OA in human patients. In addition, intra-articular IL1b injection induced more severe inflammation and cartilage degradation in the knee joints of *Nell-1*$^{+/6R}$ mice than in WT animals. In particular, 7 days of intra-articular IL1b injection induced severe antalgic gait in *Nell-1*$^{+/6R}$ mice, but not their WT counterparts. NELL-1 significantly reduced IL1b-stimulated inflammation and damage to articular cartilage. Notably, the symptoms of antalgic gait observed in IL1b-challenged *Nell-1*$^{+/6R}$ mice was relieved by NELL-1 administration. Mechanistically, in addition to its pro-chondrogenic potency, NELL-1 also suppressed the expression of inflammatory cytokines and their downstream cartilage catabolic enzymes by upregulating RUNX1 in mouse and human articular cartilage chondrocytes.

DISCUSSION: An ideal OA-combating agent, which has the ability to safely reduce inflammation and promote cartilage regeneration, has long been desired. The traditional use of analgesia, glucocorticoids, and NSAIDs do not effectively control arthritis progression and/or are associated with unfavorable adverse side-effects. Even more disappointing, the efficacy of DMARDs that postpone RA progression by slowing or suppressing inflammation has not been replicated in OA clinical trials *via* systemic or local administration. Additionally, future prospects of using well-known pro-chondrogenic growth factors as treatments for arthritis do not appear to be optimistic due to the lack of anti-inflammatory properties. Our current study demonstrates the pro-chondrogenic, anti-inflammatory dual-functionality of NELL-1 for suppressing OA progression (**Fig. 1**). Future investigations in large animal models are warranted to provide more clinically relevant data for supporting FDA approval of NELL-1 for use in human trials.

SIGNIFICANCE/CLINICAL RELEVANCE: Our current study, for the first time, demonstrates the emerging role of NELL-1 in arthritis pathogenesis and introduces NELL-1 as a promising new-generation DMOAD for preventing and curing arthritis-related cartilage damage due to its pro-chondrogenic and anti-inflammatory dual-potency. These anti-arthritic properties are absent in currently available OA medications.

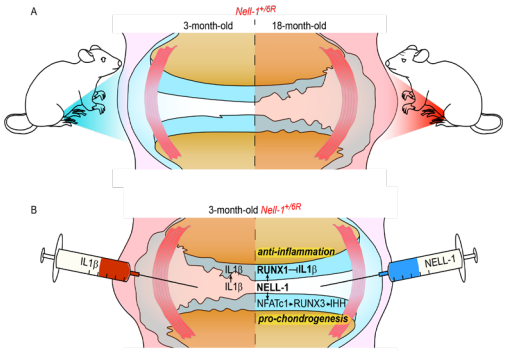

Fig. 1: Schematic of NELL-1's effects in articular cartilage. (A) Focal wear and tear of hyaline cartilage (HC) with early chondrocyte clustering became evident in the tibial plateau cartilage of 3-month old *Nell-1*$^{+/6R}$ mice, while severe loss of HC was observed in the knees of 18-month old *Nell-1*$^{+/6R}$ mice. (B) Our previous studies revealed that the chondrocytic NELL-1 → NFATc1 → RUNX3 → IHH cascade is responsible for NELL-1's pro-chondrogenic bioactivities. Here, we demonstrate that RUNX1, instead of NFATc1, is essential for NELL-1 to exhibit its anti-inflammatory properties in chondrocytes.

Role of Ligamentous Restraints During Anterior-Posterior Drawer Tests of the Murine Knee

Snehal S. Shetye[1], John S. Bova[1], Andrew F. Kuntz[1], Miltiadis H. Zgonis[1], David L. Butler[2], Nathaniel A. Dyment[1]
[1]University of Pennsylvania, Philadelphia, PA; [2]University of Cincinnati, Cincinnati, OH
shetye@pennmedicine.upenn.edu

Disclosures: Snehal S. Shetye (N), John S. Bova (N), Andrew F. Kuntz (N), Miltiadis H. Zgonis (N), David L. Butler (N), Nathaniel A. Dyment (N)

INTRODUCTION: Murine models of altered knee loading are frequently employed to study the pathogenesis of osteoarthritis and more recently, to investigate tendon-bone attachments within the ensuing bone tunnels [1,2]. Human cadaveric and large animal model demonstrated that the anterior cruciate (ACL) and posterior cruciate (PCL) ligaments are the primary restraints to anterior or posterior tibial translation, respectively. Even though murine knee destabilization models are common, the specific contributions of the cruciate ligaments have not been quantified. Further, the role of other murine knee ligaments that provide secondary restraints, such as the medial and lateral collateral ligaments (MCL, LCL) under anterior/posterior loading remains unknown. Therefore, the objective of the study was to investigate the role of ligamentous restraints in the murine knee during anterior-posterior loading. We hypothesized that the ACL and PCL will be the primary restraints to anterior and posterior drawer, respectively. Based on murine knee ligament anatomy, we also hypothesized that the MCL will be the secondary restraint in anterior drawer and the LCL will be the secondary restraint in posterior drawer.

METHODS: *Experimental Design:* All animals and procedures were approved by UPenn's IACUC. CD1 mice (4 male, 3 female, n=7) 16 weeks of age were assessed for anterior-posterior drawer stability in a custom fixture recently described by our group [2]. Briefly, following sacrifice, 7 hindlimbs (6 right, 1 left) were isolated, all extraneous soft tissue removed, and all capsule ligaments, including the cruciates and collaterals, along with the menisci left intact. The patellar tendon was removed based on its previously described role in anterior posterior loading [3]. The distal half of each tibia was potted in an acrylic tube using PMMA. This construct was then loaded onto a material testing machine. The potted tibial end was fixed in a custom fixture that allowed for adjustment of tibial plateau angle. The distal end of the femur was lowered into another acrylic tube affixed to a custom fixture that could control knee flexion by rotating the femur around the joint center of rotation. The knee was set up at 90 degrees of flexion for all tests. The knee joint was tested for anterior and posterior stability by cyclic loading under displacement control between ±0.3mm for 5 cycles and the 5th cycle was used to quantify stability for all cases. *Selective Cutting Procedure:* The intact knee joint loads were evaluated at ±0.3mm (+ve = anterior drawer, -ve = posterior drawer) to establish the baseline conditions. Following this, a 27G needle was used to carefully cut the ACL with an anterior approach. This procedure was performed on the testing machine itself to not lose the initial knee joint zero reference position. The stability test was repeated at ±0.3mm to quantify the contribution of the ACL. Next, the PCL was carefully transected, and the stability test repeated to quantify PCL contribution. After transection of the ACL and PCL, the knee joint was substantially unstable and barely registered any loads at ±0.3mm. Thus, to quantify MCL and LCL contributions, the drawer tests were modified to reach ±1.0mm, as described previously in cadavers [3]. This allowed for quantifying MCL and LCL contributions as secondary restraints. The transection of each ligamentous structure was not randomized since it has been shown previously to not have an effect if tests are conducted under displacement control to a specified peak displacement [3].

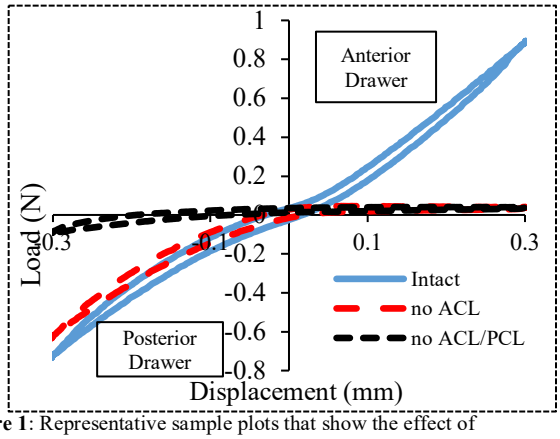

Figure 1: Representative sample plots that show the effect of transecting the ACL and PCL on anterior and posterior drawer

RESULTS: *Primary Restraints:* The peak anterior restraining force for the intact knee was 1.24±0.17N at 0.3mm of displacement. The peak posterior restraining force for the intact knee was 0.82±0.1N at -0.3mm of displacement. Transection of the ACL dropped the peak anterior restraining force at 0.3mm to 0.06±0.04N indicating that ACL contributed to 95.01±3.30% of the restraining force. Interestingly, ACL transection also reduced the peak posterior load by 14.0±9.83%. Transection of the PCL dropped the posterior restraining force at -0.3mm to -0.1±0.07N, which translated to a contribution of 89.55±6.96% of the peak restraining force in the posterior direction at -0.3mm by the PCL. Primary restraint contributions can be seen from a representative sample in Figure 1. *Secondary Restraints:* After ACL and PCL transections, the peak restraining forces at ±1.0mm of displacements were found to be 0.32±0.19N and -0.52±0.31 in the anterior and posterior directions, respectively. Transection of the MCL only influenced the anterior peak force whereby the force dropped by 86.13±8.3%. Transection of the LCL only influenced the posterior peak force whereby the force dropped by 85.12±11.89%.

Table 1: *ACL and PCL force contributions at 0.3mm drawer. Values are reported as Mean (S.D.).*

Anterior Drawer (n=7)			Posterior Drawer (n=5)			
Intact Force	Anterior Cruciate Force	ACL Contribution	Intact Force	Posterior Cruciate Force	PCL Contribution	ACL Contribution
(N)	*(N)*	*(%)*	*(N)*	*(N)*	*(%)*	*(%)*
1.24(0.17)	1.18(0.18)	95.01(3.3)	-0.82(0.1)	-0.58(0.09)	89.55(6.96)	14.0(9.83)

DISCUSSION: To better understand molecular and genetic mechanisms that regulate osteoarthritis pathogenesis in murine models, it is crucial to understand the mechanical stability of the knee joint before and after destabilization and how the joint adapts with time post-injury. The data presented here provide a baseline for studies creating these OA models by transecting supporting ligamentous structure involved in knee stability. We found that, similar to the human knee, the ACL and PCL are the primary structures providing anterior and posterior stability, respectively, in the murine knee. Interestingly, we did see an approximately 14% contribution by the ACL to posterior stability, which has not been observed in humans. Further, at a knee flexion angle of 90 degrees, and in absence of the ACL and PCL, the MCL provides most of the stability in the anterior direction and the LCL provides most of the stability in the posterior direction. While great care was taken to not disrupt other structures such as the menisci during transection of these ligaments, it is possible due to the small size of the murine knee joint. However, future studies will use contrast MicroCT to verify damage to each structure. Our data suggest that the menisci did not play a major role in anterior-posterior knee stability since the peak load were close to 0N after transection of these ligaments. This agrees with a previous study that followed a displacement control protocol as presented here [3]. However, other studies that employed a load-control protocol have shown that the menisci play a role in knee stability at lower flexion angles [4,5]. Furthermore, our study did not apply a compressive load to the knee, which might be necessary for the menisci to be loaded. Alternatively, a case could also be made for the menisci to be more important in varus-valgus knee stability, which was not investigated here. Further studies will investigate the influence of knee flexion angle, compression joint load, and the menisci to anterior-posterior stability of the murine knee.

SIGNIFCANCE/CLINICAL RELEVANCE: This methodology can be applied to murine knee destabilization PTOA models over the time course of OA progression, correlating with biological changes to the joint. In addition, methods to restabilize the knee [2] to attenuate OA progression can be verified.

REFERENCES: [1] Blaker CL et al., *J Orthop Res,* 2017 (35)424–439 [2] Kamalitdinov TB et al., *J Orthop Res,* 2019 [3] Butler DL et al., *JBJS*, 1980 (62)259-270 [4] Markolf KL et al.,*JBJS* 1976 (67)136-146 [5] Shoemaker SC et al., *JBJS* 1986 (68)71-79

ACKNOWLEDGEMENTS: This study was supported by the Penn Center for Musculoskeletal Disorders P30 grant (AR069619), the NIH R00 award (AR067283), and the Thomas B. McCabe and Jeannette E. Laws McCabe Fund at UPenn.

Liquid Poly-N-Acetyl Glucosamine (sNAG) Improves Achilles Tendon Healing in a Rat Model

Nuss CA[1], Huegel J[1], Finkielsztein S[2], Soslowsky LJ[1]
[1]McKay Orthopaedic Research Laboratory, Philadelphia, PA
[2]Marine Polymer Technologies, Inc., Burlington, MA

Disclosures: Nuss CA (N), Huegel J (N), Finkielsztein S (3A- Marine Polymer Technologies, Inc.), Soslowsky LJ (5)

Introduction: The Achilles tendon, while the strongest and largest tendon in the body, is frequently injured. Even after surgical repair, patients risk re-rupture and typically have long-term deficits in function, with a low rate of return to pre-injury levels of activity [1]. Various forms of biological augmentation have been utilized in an attempt to improve tendon repair [2]. Poly-N-acetyl glucosamine (sNAG) polymer has been shown to increase the rate of healing of venous leg ulcers, with an 86% success rate clinically [3]. Additionally, use of this material improved tendon-to-bone healing in a rat model of rotator cuff injury and repair [4]. However, whether this nanofiber material, in an injectable liquid formulation, could improve soft tissue tendon healing after Achilles injury is unknown. Therefore, the purpose of this study was to investigate the healing properties of sNAG containing membranes in a rat partial Achilles tear model. We hypothesized that sNAG would improve tendon healing as measured by improved mechanical properties and cellular morphology.

Methods: *Study Design*: 32 adult male Sprague-Dawley rats (400-450g) were used in this IACUC-approved study. All animals underwent a partial-width, full thickness injury using a 1.5 mm biopsy punch through the right Achilles tendon as described [5]. After injury, animals were randomized into two groups, receiving either 10 µl of 0.9% saline (control group) or 10 µl of 20 mg/ml sNAG polymer gel (sNAG group). Animals were allowed normal cage activity after surgery, without immobilization. Animals received repeat saline or sNAG injections at the site of the injury through the skin at one and two weeks post-surgery. All animals were sacrificed three weeks after injury. *Ex Vivo Assessments*: The Achilles-calcaneus complex was immediately harvested and processed for histological analysis including quantitative collagen fiber organization analysis (n=6/group). All other animals (n=10 per group per time point) were frozen at -20°C and later thawed for dissection and mechanical testing. For testing, the Achilles tendon and foot complex were dissected and the calcaneus was potted in poly(methyl methacrylate). While immersed in 37°C phosphate-buffered saline and in a physiologic orientation, the Achilles tendons were gripped and subjected to a mechanical loading protocol consisting of: preloading, stress relaxation at 6% strain, dynamic frequency sweeps, and fatigue cycling under load control until specimen failure. *Statistics:* Mechanical testing and collagen fiber organization data were evaluated using two-tailed t-tests after confirming data normality. Semi-quantitative histological comparisons were made using Mann-Whitney U tests. Significance was set at $p<0.05$ for all comparisons.

Results: *Mechanical properties*: At three weeks after injury, there was no difference in tendon cross-sectional area (not shown). Tendon stiffness was improved with sNAG treatment (Fig 1A), but modulus was not different between groups (Fig 1B). Frequency sweeps demonstrated an increase in dynamic modulus across tested frequencies (Fig 1C), but tanδ, a measure of force dissipation, was not different (not shown). Fatigue testing demonstrated increases in tendon secant stiffness (Fig. 1D) and tangent stiffness (Fig. 1E) throughout fatigue life for sNAG-treated tendons compared to controls. There was no difference in cycles to failure (Fig. 1F), or other properties measured (not shown). *Histologic observations*: Semi-quantitative grading did not demonstrate differences in cell density (Fig. 2A) or cell shape (Fig. 2B) at the injury region. Collagen alignment in this region was also not different between groups (Fig. 2C). Representative images of the injury region for both groups are shown in Figure 2D.

Discussion: This study investigated the effects of repeated sNAG polymer application on tendon healing after partial Achilles injury. Although several parameters did not exhibit differences between treatment groups, other results demonstrate that sNAG has a positive effect on rat Achilles tendon healing at three weeks after a full thickness, partial width injury. Quasistatic testing demonstrated increased tendon stiffness with sNAG treatment, which continued during fatigue cycling, as shown in increased tangent and secant stiffness across fatigue life. Increased dynamic modulus also suggests improved viscoelastic properties with sNAG treatment. Importantly, use of this material did not have any negative effects on any measured parameter. Previous studies suggest that this material may mitigate pain after rotator cuff injury [4]. Functional testing such as gait assessment might be valuable, potentially expanding the use of this material as a less invasive treatment for painful Achilles tendonitis [6]. Additionally, dosage studies and number of repeated sNAG injections may optimize the use of sNAG for soft tissue tendon healing. Finally, studies to elucidate the mechanism of action for the changes identified are important.

Significance: Repeated injections of sNAG polymer improve Achilles tendon properties after partial tear. These results support further study of this material as a minimally invasive treatment modality for tendon healing.

References: [1] Barfod KW et al. J Bone Joint Surg, 2014. [2] Shapiro E et al. Curr Rev Musculoskelet Med, 2015. [3] Kelechi, TJ et al. J Am Acad Derm, 2011. [4] Nuss CA et al. Ann Biomed Eng, 2017. [5] Huegel J et al. J Biomech, 2019. [6] Barg A & Ludwig T. Foot Ankle Clin, 2019.

Acknowledgements: We thank Stephanie Weiss and Peter Chan for assistance.

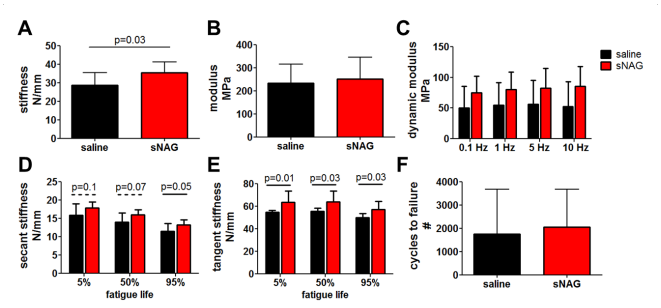

Figure 1. Mechanical Properties. Three weeks after injury, sNAG treated tendons had (A) increased stiffness, (B) no change in modulus, (C) increased dynamic modulus across testing frequencies, (D) increased secant stiffness, and (E) increased tangent stiffness. There were no changes in (F) cycles to failure between groups. Data shown as mean+SD.

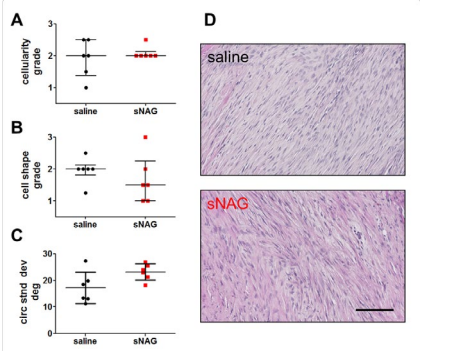

Figure 2. Histological Properties. There were no differences between groups for (A) cellularity, (B) cell shape, or (C) collagen alignment. Representative images of the injury region are shown in (D). Data represented as median±IQR in A and B, and as mean±SD in C. Scale bar in D: 100 µm.

Injury and Healing Effect on Fatigue Properties of Collagen V Haploinsufficient Female Murine Tendons

Carlson JA[1], Beach ZM[1], Weiss SN[1], Birk DE[2], Soslowsky LJ[1]
[1]McKay Orthopaedic Research Laboratory, University of Pennsylvania, Philadelphia, PA, [2] University of South Florida, Tampa, FL

Disclosures: Carlson JA(N), Beach ZM(N), Weiss SN(N), Birk DE(N), Soslowsky LJ(N)

INTRODUCTION: Patients with Classic Ehlers-Danlos Syndrome (*c*EDS), a disorder characterized by mutation in the *COL5* genes with *COL5a1* haploinsufficiency being the most common, suffer from articular hypermobility, skin hyperextensibility, tendon/ligament fragility and abnormal wound healing[1,2]. Furthermore, human studies have shown that females have decreased collagen synthesis and fibroblast activity[3-5] as well as altered gene expression during repair[6], potentially exacerbating detrimental changes present in *c*EDS tendons. Quasi-static loading of the mouse patellar tendon[7-9] demonstrates decreases in modulus, failure stress, failure load, and stiffness due to reduced collagen V throughout healing. Although the hierarchical structure of the tendon has been implicated in changes following cyclic fatigue loading, and collagen V is essential in regulating collagen fibrillogenesis, fatigue properties have not been examined in *c*EDS tendons[7,10]. Therefore, the objective of this study was to define the fatigue properties of female patellar tendons following injury, as well as the effect of a reduction in collagen V on these properties. We hypothesized that reduction in collagen V following injury will delay improvements in the fatigue properties compared to wild-type tendons.

METHODS: Adult female wild-type (WT) C57/BL6 and heterozygous ***Col5a1***$^{+/-}$ mice, a model for *c*EDS, at 120 days of age (n=60) were used (IACUC approved). Mice were randomly divided into uninjured and injured groups, with injured mice undergoing bilateral patellar tendon injury surgery as described[11]. Injured mice were sacrificed early in the remodeling healing phase (3w) or later in remodeling (6w) and uninjured age-matched mice were sacrificed. *Mechanics.* The patella-patellar tendon-tibia complexes of all mice were dissected and prepared for mechanical testing[12]. Cross-sectional area was measured using a custom laser device[13]. Tendons underwent a fatigue protocol, consisting of pre-conditioning and 1 Hz cyclic loading until failure. Cyclic loads corresponded to 20% and 55% maximum stress (previously determined from quasi-static testing). Fatigue parameters were analyzed at the end of the primary phase (BP1) and secondary phase (BP2) of fatigue life, capturing changes in material parameters that occur with fatigue damage, including peak cyclic strain, tangent modulus, secant modulus, tangent stiffness, secant stiffness, hysteresis, and laxity. Secant modulus and stiffness are calculated in reference to the zero displacement point and tangent modulus and stiffness are calculated from a specific loading cycle. *Statistics.* Two-way ANOVAs with post-hoc Bonferroni tests were used to assess the effects of genotype (collagen V expression), injury time-point, and their interaction on fatigue mechanical properties. Significance was set at $p \leq 0.05$ and trends at $p \leq 0.1$.

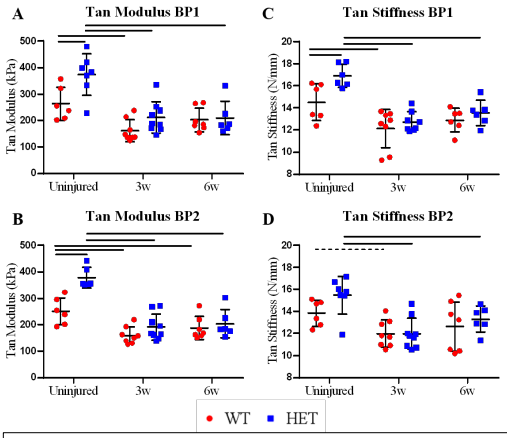

Figure 1: Tangent Modulus BP1 (A) and BP2 (B). Tangent Stiffness BP1 (C) and BP2 (D). ***Col5a1***$^{+/-}$ tendons had persistent decreases in tangent modulus and tangent stiffness 3 and 6w PI at BP1 and BP2. WT tendon decreases in tangent modulus and tangent stiffness seen 3w PI were only persistent to 6w PI in tangent modulus at BP2. Solid lines denote significance and dashed lines denote trends.

RESULTS: WT patellar tendons 3w post-injury (PI) showed a significant decrease in tangent modulus (BP1 and BP2) (Fig.1A,B), tangent stiffness (BP1 and BP2 [trend]) (Fig.1C,D), and secant modulus (BP1 and BP2) (not shown) when compared to uninjured controls. The decrease in tangent modulus at BP2 persisted to 6w PI. However, no other parameters had differences at 6w PI. ***Col5a1***$^{+/-}$ patellar tendons 3 and 6w PI exhibited reduced tangent modulus (Fig.1A,B), tangent stiffness (Fig.1C,D), and secant modulus at both BP1 and BP2 when compared to uninjured controls. There were no differences in ***Col5a1***$^{+/-}$ tendons compared to uninjured tendons in peak strain (Fig.2C) or secant stiffness (not shown) at BP1. However, 3w PI at BP2, there was an increase in peak strain (Fig.2D) and a trending decrease in secant stiffness (not shown), with no differences 6w PI. Hysteresis was significantly higher in WT tendons 3w PI when compared to uninjured and 6w tendons at BP1. However only a trending difference was seen at BP2 between uninjured and 3w PI (Fig.2A,B). ***Col5a1***$^{+/-}$ tendons showed no differences in hysteresis at BP1, but had significantly higher hysteresis 3 and 6w PI compared to uninjured tendons at BP2, and a trending increase between 3 and 6w PI (Fig.2A,B). Differences between genotypes, were primarily seen in the uninjured groups, with WT tendons having a significantly lower tangent modulus (BP1 and BP2) (Fig.1A,B), tangent stiffness (BP1) (Fig.1C), and secant modulus (BP1 and BP2) (not shown), and a significantly higher laxity (BP1) (not shown). When compared to WT tendons, ***Col5a1***$^{+/-}$ tendons at 6w PI had a decreased peak strain (BP2) (Fig.2D) and increased secant stiffness (BP1 [trend] and BP2) (not shown).

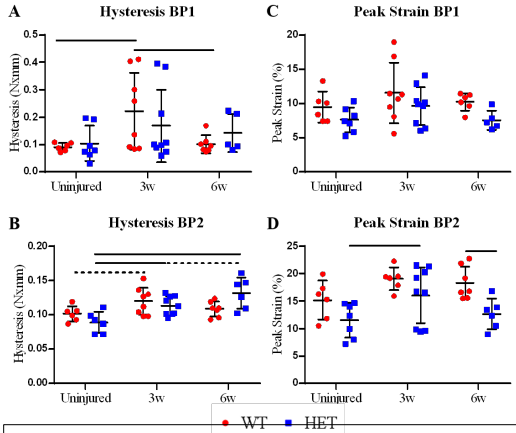

Figure 2: Hysteresis BP1 (A) and BP2 (B). WT tendons had increased hysteresis at BP1 3w PI, while ***Col5a1***$^{+/-}$ tendons had increased hysteresis 3 and 6w PI at BP2. **Peak Strain BP1 (C) and BP2 (D).** Peak strain was increased 3w PI in ***Col5a1***$^{+/-}$ tendons at BP2. Solid lines denote significance and dashed lines denote trends.

DISCUSSION: This study evaluated the fatigue properties of the patellar tendon in uninjured and injured mice as well as the role of collagen V. Cyclic fatigue loading mimics the *in vivo* loading pattern of the patellar tendon, and therefore is a relevant approach to study mechanic properties. Overall, fatigue properties of ***Col5a1***$^{+/-}$ tendons were persistently affected to a later time-point post-injury, while the fatigue properties of WT tendons showed minimal differences later in healing. Therefore, as hypothesized, collagen V deficient mice have a delayed healing response, with changes persisting to 6w PI, while WT tendon fatigue properties recover by 6w PI. Additionally, genotypic differences in uninjured tendons indicate that collagen V plays a role in the tendon response to cyclic loading. However, these differences are not consistently present PI. This shows that WT and ***Col5a1***$^{+/-}$ tendon fatigue properties are affected to different degrees following injury, and the diminished healing of ***Col5a1***$^{+/-}$ tendons could be obscuring genotypic differences post-injury. Lastly, hysteresis analysis indicates that energy loss is different throughout fatigue life between WT and ***Col5a1***$^{+/-}$ tendons following injury, as WT tendons show increased hysteresis at the end of the primary phase, while ***Col5a1***$^{+/-}$ tendons show increased hysteresis at the end of the secondary phase. More energy is lost at the end of fatigue life in ***Col5a1***$^{+/-}$ tendons, while the opposite is true for WT tendons. This indicates that collagen V affects the ability of the tendon to heal in a manner that resists microstructural damage associated with cyclic use. Therefore, this study demonstrates that collagen V plays a role in the tendon's ability to respond to fatigue loading, and following injury, collagen V plays a crucial role in the tendon healing process.

SIGNIFICANCE: This study demonstrates that WT tendon fatigue properties recover following injury while a decrease in collagen V results in a delayed healing response, highlighting the importance of evaluating the effect of collagen V in the tendon healing process.

REFERENCES: [1] Steinmann B et al. *Connective Tissue and Its Heritable Disorders.* Wiley-Liss; 2002. [2] Wenstrup RJ et al. *J Biol Chem.* 2006. [3] Ainsworth SR et al. *CORR.* 1993. [4] Yu WD et al. *CORR.* 2001. [5] Kjaer M et al. *J. Anat.* 2006. [6] Hart DA et al. *CORR.* 1998. [7] Johnston JM et al. *J. Orthop Res.* 2017. [8] Carlson JA et al. ORS 2018. [9] Carlson JA et al. ORS 2019. [10] Freedman BR et al. *Orthop. Res.* 2015. [11] Beason DP et al. *J. Biomech*, 2012. [12] Dunkman AA et al. *Matrix Biol.* 2013. [13] Favata M, PhD Thesis: University of Pennsylvania. 2006.

ACKNOWLEDGEMENTS: *This study was supported by NIH/NIAMS AR065995 and the Penn Center for Musculoskeletal Disorders (AR069619).*

Differential Role of Skeletal Muscle AKT Signaling in the Regulation of Glucose Metabolism and Muscle Growth

Natasha Jaiswal[1], Matthew Gavin[1], William Quinn [1,] Emanuele Loro[2], Timothy luongo[1], Rebecca Gefler[1], Joseph Baur[1], Tejvir S. Khurana[2] and Paul M. Titchenell[1,2]

[1]Institute for Diabetes, Obesity, and Metabolism and [2]Department of Physiology, Perelman School of Medicine at the University of Pennsylvania

Insulin resistance is considered to be the principal factor underlying several metabolic diseases including type II diabetes mellitus. Since, skeletal muscle is the predominant site of insulin-mediated glucose uptake in the postprandial state, a reduction in the insulin signaling pathway of diabetic skeletal muscle is widely considered to be the primary cause of postprandial hyperglycemia. The serine/threonine kinase AKT is a central regulator of insulin action and a decrease in AKT activity is observed in muscle from insulin-resistant mice and humans. This has understandably led to the dogma that impaired AKT activity in skeletal muscle causes insulin resistance and defects in glucose homeostasis and muscle function. To test the direct requirement of skeletal muscle AKT signaling on systemic glucose metabolism and muscle physiology, we generated several mouse models of skeletal muscle AKT deficiency. Unexpectedly, mice lacking AKT2 alone, exhibited normal insulin signaling, insulin sensitivity and muscle mass despite a dramatic reduction in phosphorylated muscle AKT. In contrast, deletion of both muscle AKT isoforms (M-AKTDKO) resulted in a complete loss of AKT-mediated insulin signaling. Despite the lack of AKT activity, M-AKTDKO mice were insulin sensitive and displayed normal rates of glucose uptake in response to insulin. This chronic loss of AKT was associated with mitochondrial dysfunction and subsequent AMPK activation, which we identified to be an important regulator of muscle insulin sensitivity. Unlike glucose metabolism, loss of muscle AKT resulted in muscle atrophy and defective muscle performance. Mechanistically, activation of mTORC1 and inhibition FOXO1 were both required and sufficient to induce muscle hypertrophy in the absence of AKT. Collectively, these data define the cellular pathways responsible for AKT's control of muscle growth and function. Moreover, we made the surprising discovery that AKT is not an obligate intermediate for insulin-stimulated glucose uptake in all conditions, which suggests the existence of additional insulin-dependent, AKT-independent signaling pathways for the regulation of glucose homeostasis.

Determining the Roles of Decorin and Biglycan in Tendon Healing Using Inducible Knockdown at Time of Injury

Ashley K. Fung[1], Stephanie N. Weiss[1], David E. Birk[2], Louis J. Soslowsky[1]
[1]McKay Orthopaedic Research Laboratory, University of Pennsylvania, Philadelphia, PA
[2]Department of Molecular Pharmacology and Physiology, University of South Florida, Tampa, FL

Disclosures: Ashley K. Fung (N), Stephanie N. Weiss (N), David E. Birk (N), Louis J. Soslowsky (N)

INTRODUCTION: Tendon injury leads to a healing cascade of inflammatory, proliferative, and remodeling phases, but the mechanisms underlying these processes remain unclear. Small leucine-rich proteoglycans (SLRPs) such as decorin (Dcn) and biglycan (Bgn) are regulators of fibrillogenesis and matrix assembly and play important roles throughout tendon healing. Previous studies using conventional *Bgn*$^{-/-}$ and *Dcn*$^{-/-}$ mice showed that absence of Dcn impaired the healing response with no improvement in dynamic modulus between 3- and 6-weeks post-injury, while absence of Bgn had a moderate effect on early tendon healing, together suggesting differential roles of these SLRPs throughout the injury response [1]. However, these results are confounded by the cumulative effects of SLRP deficiency on altered development and growth, and the isolated roles of Dcn and Bgn on tendon healing are unknown. Therefore, the objective of this study was to determine the regulatory role(s) of Dcn and Bgn on the mechanical properties of healing tendons in mature mice using conditional deletion at the time of tendon injury resulting in an isolation of Dcn, Bgn, and both Dcn/Bgn knockdown. We hypothesized that induced deletion of Dcn, Bgn, and both Dcn and Bgn expression would impair the healing response compared to wild type mice leading to reduced improvement in tendon mechanical properties post-injury. Because Dcn has been shown to mediate all stages of healing while Bgn is primarily important in the inflammatory phase, we hypothesized that deletion of Dcn would result in greater impairment.

METHODS: Female *Dcn*$^{+/+}$/*Bgn*$^{+/+}$ control (WT, n=48), *Dcn*$^{flox/flox}$ (I-*Dcn*$^{-/-}$, n=32), *Bgn*$^{flox/flox}$ (I-*Bgn*$^{-/-}$, n=32), and compound *Dcn*$^{flox/flox}$/*Bgn*$^{flox/flox}$ (I-*Dcn*$^{-/-}$/*Bgn*$^{-/-}$, n=32) mice with a tamoxifen inducible Cre (B6.129-Gt(ROSA)26Sortm1(cre/ERT2)Tyj/J, Jackson Labs) were utilized [2] (IACUC approved). At 120 days old, Cre excision of conditional alleles was induced in all mice via two (injured mice) or three (uninjured mice) consecutive daily IP injections of tamoxifen. WT mice also received tamoxifen to account for any potential side effects. WT mice (n=16) were designated as uninjured controls, and remaining mice were divided into 3- or 6-week post-injury groups to represent the early and later remodeling phases of healing (n=16/genotype/time point). At time of induction, mice in injury groups underwent bilateral patellar tendon injury surgery as described [3] and were sacrificed 3- or 6-weeks later. Uninjured groups were sacrificed at 150 days old. The patellar tendon-bone complex from one limb of each animal was dissected and prepared for mechanical testing to assess potential differential effects in both the midsubstance and insertion regions of the tendon [4]. Tendons were subjected to a testing protocol consisting of preconditioning and a quasi-static ramp to failure. Dynamic collagen fiber realignment was measured throughout the ramp-to-failure using a crossed polarizer setup. Images were used to optically measure moduli in the insertion site and midsubstance regions. To evaluate the effect of genotype on tendon healing, one-way ANOVAs with Bonferroni corrections were conducted for 3- and 6-week post-injury groups. Significance was set at $p \leq 0.05$; trends at $p \leq 0.1$.

RESULTS: WT, I-*Dcn*$^{-/-}$, and I-*Bgn*$^{-/-}$ mice had significantly reduced insertion site modulus compared to uninjured controls at both 3- and 6-weeks post-injury, while insertion site modulus was reduced in I-*Dcn*$^{-/-}$/*Bgn*$^{-/-}$ mice only at 6-weeks (Fig. 1A,B). Midsubstance modulus in I-*Dcn*$^{-/-}$ mice was significantly lower than uninjured and I-*Dcn*$^{-/-}$/*Bgn*$^{-/-}$ groups and trended lower compared to I-*Bgn*$^{-/-}$ mice 3-weeks post-injury (Fig 1C). Similarly, midsubstance modulus was significantly lower in I-*Dcn*$^{-/-}$ mice compared to uninjured and I-*Bgn*$^{-/-}$ groups 6-weeks post-injury (Fig 1D). Midsubstance modulus in I-*Dcn*$^{-/-}$/*Bgn*$^{-/-}$ mice also trended lower compared to I-*Bgn*$^{-/-}$ mice (Fig 1D). For failure properties, maximum stress trended lower in I-*Dcn*$^{-/-}$ and I-*Dcn*$^{-/-}$/*Bgn*$^{-/-}$ groups compared to uninjured mice 3-weeks post-injury (Fig 1E), while maximum stress trended lower in I-*Dcn*$^{-/-}$/*Bgn*$^{-/-}$ mice compared to I-*Bgn*$^{-/-}$ mice at 6-weeks (Fig 1F). Finally, normalized circular variance in the midsubstance at 3-weeks was higher (indicating less collagen fiber alignment) in I-*Bgn*$^{-/-}$ and I-*Dcn*$^{-/-}$/*Bgn*$^{-/-}$ groups at strains between 1 and 4%. (Fig 2C). Few differences were observed at the insertion site or at 6-weeks (Fig 2A,B,D).

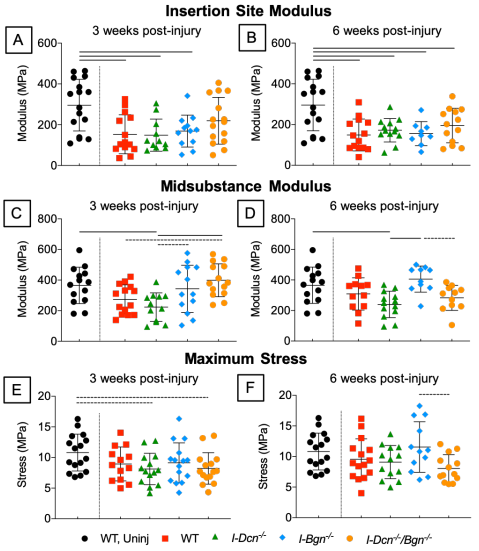

Figure 1: Quasi-static mechanical properties. Insertion site modulus was lower in injured tendons at (A) 3- and (B) 6-weeks post-injury. Only I-*Dcn*$^{-/-}$ groups exhibited reduced midsubstance modulus compared to uninjured at both (C) 3- and (D) 6-weeks post-injury. Maximum stress trended lower in I-*Dcn*$^{-/-}$ and I-*Dcn*$^{-/-}$/*Bgn*$^{-/-}$ compared to uninjured 3-weeks post-injury but (F) not at 6-weeks post-injury. Solid lines denote significance for $p<0.05$ while dashed lines denote trends for $p<0.1$.

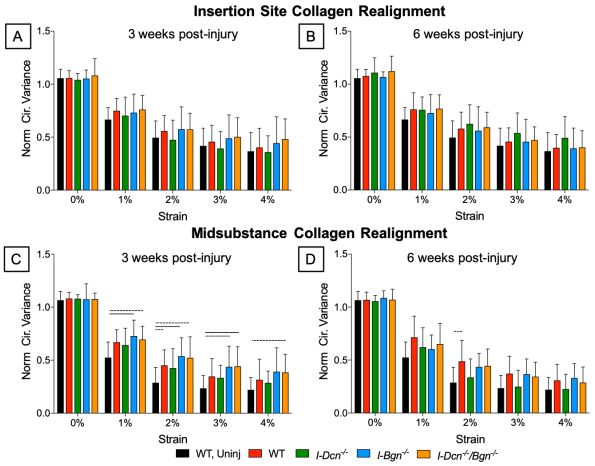

Figure 2: Collagen fiber realignment. There were no differences in collagen fiber realignment at (A) 3- or (B) 6-weeks post-injury within the insertion site region. However, (C) normalized circular variance was higher in I-Bgn$^{-/-}$ and I-Dcn$^{-/-}$/Bgn$^{-/-}$ groups at values of strain between 1 and 4%, and these differences were not sustained to (D) 6-weeks post-injury. Solid lines denote significance for $p<0.05$ while dashed lines denote trends for $p<0.1$.

DISCUSSION: This study investigated the roles for Dcn and Bgn in determining tendon mechanics after injury using conditional deletion of Dcn, Bgn, and both Dcn and Bgn at the time of injury. As hypothesized, results revealed that absence of Dcn negatively impacts tendon healing. Modulus within the midsubstance region, the location where the injury is introduced, was only significantly lower in I-*Dcn*$^{-/-}$ mice at both 3- and 6- weeks post-injury compared to uninjured controls. This healing response is consistent with our previous studies using conventional *Dcn*$^{-/-}$ mice [1], further highlighting the critical role of Dcn in all stages of tendon healing. However, contrary to our hypothesis, induced knockout of Bgn did not impair the healing response compared to WT control animals. These findings contrast those observed in the conventional *Bgn*$^{-/-}$ model suggesting that altered growth, especially considering the important role of Bgn in tendon development and fibrillogenesis, may impair the tendon healing response. Interestingly, midsubstance modulus in I-*Dcn*$^{-/-}$/*Bgn*$^{-/-}$ mice was significantly greater than I-*Dcn*$^{-/-}$ mice 3-weeks post-injury, indicating there may be a compensatory or protective effect for Bgn against detrimental changes due to deletion of Dcn. However, these differences were not evident in the insertion site, suggesting the regulatory roles of decorin and biglycan are regionally dependent. Additionally, increased circular variance in both I-*Bgn*$^{-/-}$ and I-*Dcn*$^{-/-}$/*Bgn*$^{-/-}$ groups in the midsubstance at 3-weeks reveal that deletion of Bgn may alter how fibers in healing tendons respond to changes in load. However, the mechanisms driving differences in tendon modulus during healing remain unknown, and ongoing work to assess changes in gene expression, matrix composition, and fibril structure will further elucidate how Dcn and Bgn impact tendon healing.

SIGNIFICANCE: In contrast to biglycan, induced deletion of decorin at time of injury has a detrimental effect on mechanics of healing tendons. Elucidating the isolated roles of decorin and biglycan in the response to tendon injury will contribute largely to understanding mechanisms that drive poor tendon healing.

REFERENCES: [1] Dunkman AA et al., Ann Biomed Eng, 2014. [2] Robinson et al., Matrix Biology, 2017. [3] Lin et al., J Biomech, 2006. [4] Dunkman AA et al., Matrix Biology, 2013.

ACKNOWLEDGEMENTS: This study was funded by NIH/NIAMS R01AR068057, T32AR007132, and the Penn Center for Musculoskeletal Disorders (P30AR0696919).

Microdialysis as a Longitudinal, *In Vivo* Assessment of Achilles Tendon Healing in a Rat Model

Joseph B. Newton, Snehal S. Shetye, Courtney A. Nuss, Matthew M. Counihan Daniel C. Farber, Louis J. Soslowsky
McKay Orthopaedic Research Laboratory, University of Pennsylvania, Philadelphia, PA
DISCLOSURES: Joseph B. Newton (N), Snehal S. Shetye (N), Courtney A. Nuss (N), Matthew M. Counihan (N), Daniel C. Farber (N), Louis J. Soslowsky (N).
Josebr@seas.upenn.edu

INTRODUCTION: The Achilles tendon is the most frequently ruptured tendon, leading to significant pain, loss of function, and healthcare costs [1]. *In vivo* assessment of healing after an Achilles tendon rupture can provide valuable metrics not only to monitor healing, but also to guide treatment options [2,3]. Specifically, *in vivo* assays such as ultrasound imaging, passive joint mobility assessments, and functional gait analysis can provide longitudinal measures of structural and functional properties of the healing tendon. However, these assays do not provide insight into the biologic changes in the healing tendon [4-6]. While microdialysis has been used to assess tendon healing in humans, it has not been used in an animal model of Achilles tendon injury [7,8]. Therefore, the objective of this study was to develop and pilot a novel use of microdialysis *in vivo* to directly measure key biologic markers of tendon healing and matrix deposition in the rat Achilles tendon. We hypothesized that, following Achilles injury, metabolite and procollagen concentrations would significantly increase indicating higher metabolic activity and collagen synthesis, respectively.

METHODS: *Experimental Design:* After facility acclimation, six, 4-month male Sprague Dawley rats underwent unilateral blunt transection of the right Achilles tendon without repair (IACUC approved). The right hind limb was immobilized for 7 days. Microdialysis measurements were taken before injury and 7, 14, and 21 days post injury. *Dialysate Collection and Analysis:* Under isofluorane anesthesia and ultrasound guidance, a microdialysis catheter (CMA 71; CMA Microdialysis AB; 100kDa molecular cutoff, 0.5mm outer diameter; 4mm in length) was introduced from the proximal aspect of the tendon towards the calcaneus. The active part of the membrane was placed in the rupture site and a perfusion fluid of artificial CSF with 3% 500kDa dextran (Sigma Aldrich) was used. The fluid was pumped through the inner tube of the catheter into the space between the inner tube and the semipermeable catheter membrane, where the exchange between the interstitial and perfusion fluid takes place. The resultant dialysate solution was transmitted from the catheter and collected in a 1.5mL vial (Microvial, CMA Microanalysis AV). With a perfusion speed of 1.0 µL/min, samples were collected for 2.5 hours. Due to fluid pump adjustment during the first few minutes, trauma from the probe insertion, and to remain conservative, the first 30 minutes of dialysate was discarded. Lactate, pyruvate, glucose, glutamate, glycerol, and procollagen type I N propeptide (PINP), concentrations were quantified via ELISAs. *Statistics*: All comparisons were made using the nonparametric Kruskal-Wallis ANOVA followed by Dunn's post hoc tests, which compared values at 7, 14, and 21 days post injury to preinjury values.

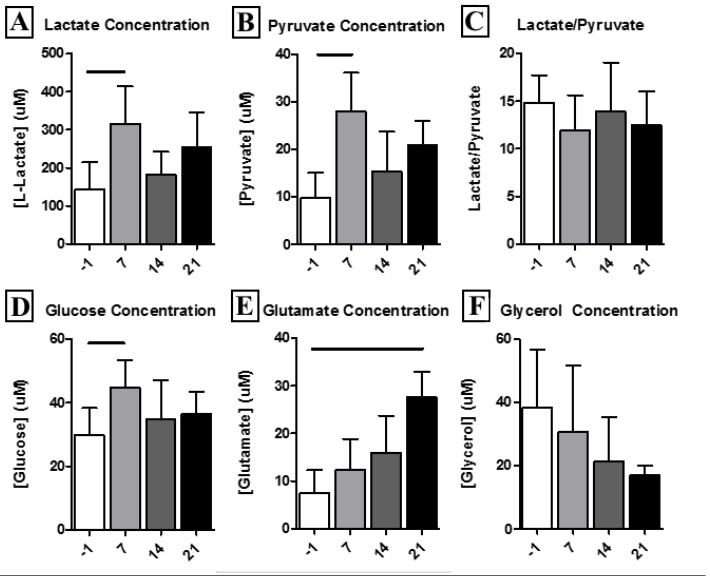

Figure 1. ELISA results from dialysate prior to injury (-1) and 7, 14, and 21 days post injury. Lactate (A) and pyruvate (B) concentrations peaked at 7 days post-injury while their relative ratio (C) was maintained. Glucose (D) peaked at day 7. Glutamate (E) was significantly increased at day 21. No changes were found in glycerol (F). Data as mean +/- standard deviations; bar indicates significance.

RESULTS: Lactate (Fig.1A) and pyruvate (Fig.1B) concentrations significantly increased 7 days post-injury, with no changes in lactate:pyruvate ratio at any time points (Fig.1C). Glucose concentration 7 days post-injury showed significant increases (Fig.1D). Glutamate was elevated 21 days following injury (Fig.1E). No changes were found in glycerol concentration following injury (Fig.1F). PINP concentrations were decreased at each post-injury time point compared to pre-injury measures (Fig.2).

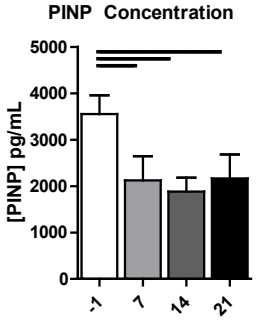

Figure 2. ELISA results showed a decrease in PINP concentration throughout healing compared to pre-injury levels. Data as mean +/- standard deviations; bar indicates significance.

DISCUSSION: Results indicate an early increase in overall metabolic activity and simultaneous decrease in collagen I production following Achilles injury. Increases in lactate and pyruvate 7 days post-injury indicate increased anaerobic and aerobic metabolic activity, respectively, as the resident cell population begins tissue repair. No changes in the lactate:pyruvate ratio demonstrate that the local environment is sufficiently oxygenated, as aerobic and anaerobic activity levels are maintained throughout healing [7]. Under normal healing conditions, angiogenesis peaks around day 7 in a healing tendon [9], which is supported by the early increase in glucose concentration. This increase in glucose concentration may also indicate increased metabolic activity immediately following injury, concurrent with the lactate and pyruvate changes shown. Glutamate concentration peaks at 21 days post-injury in congruence with nerve ingrowth [7]. Glycerol is a marker for cellular damage, and results show no changes in the metabolite's concentration, thus the severity of cellular damage remains unclear in our injury model [7,8]. PINP decreased immediately following injury, demonstrating a reduction in collagen I production. The study timeline was likely not long enough to see the expected increase in collagen I production as the tendon begins the remodeling phase of healing in which collagen III in the fibrotic scar tissue is replaced by more aligned collagen I [2]. Future studies will investigate changes in the biological environment of a healing Achilles tendon in response to exercise and new modalities to improve healing outcomes.

SIGNIFICANCE: This study demonstrates that microdialysis is a viable *in vivo*, longitudinal measure of Achilles tendon healing in a rat model. This technique will provide valuable metrics to monitor the biological environment in healing Achilles tendons.

REFERENCES: [1] Holm C et al., 2014. *Scand J Med Sci Sports*, 25:e1-10. [2] Auijla R et al., 2018. *Foot Ankle Surg*, 24:336-341. [3] Jandali Z et al., 2018. *J Reconstr Microsurg*, 34:632-641. [4] Riggin CN et al., 2019. *Ultrasound Med Biol*, 45:1841-1849. [5] Pardes A et al., 2016. *J Biomech*, 49:376-381. [6] Freedman BR et al., 2017. *J Biomech*, 56:55-60. [7] Greve K et al., 2012. *Scan J Med Sci Sports*, 22:e55-63. [8] Alim A et al., 2016. *BMJ Open Sport Exerc Med*, 2:e000114. [9] Gelberman R et al., 1991. *J Bone Joint Surg Am*, 73:868-881. [10] Neilsen M et al., 2013. *Am J Transl Res*, 5:303-315

ACKNOWLEDGEMENTS: The authors acknowledge the contributions of the Dani Lab at the University of Pennsylvania, specifically Dr. William Doyon for his assistance with microdialysis. This study was supported by the Penn Center for Musculoskeletal Disorders (P30 AR069619) and the NIH (R01AR064216).

A subset of FAP cells expressing Gli1 promote muscle regeneration with less fat accumulation

Lutian Yao[1] (Lutian.yao@pennmedicine.upenn.edu), Elisia D. Tichy[1], Leilei Zhong[1], Sarthak Mohanty[1], Luqiang Wang[1], Emily Ai[1], Shuying Yang[2], Foteini Mourkioti[1,3,4], Ling Qin[1]

[1]Department of Orthopaedic Surgery, Perelman School of Medicine, [2]Department of Basic & Translational Sciences, School of Dental Medicine
[3]Department of Cell and Developmental Biology, [4]Penn Institute for Regenerative Medicine, Musculoskeletal Program, Perelman School of Medicine, University of Pennsylvania, Philadelphia, PA 19104, USA

Disclosures: None

INTRODUCTION: Skeletal muscle has a remarkable capacity for regeneration after injury. Recently, a new type of muscle-resident progenitor cell, referred to as fibro-adipogenic progenitors (FAPs), was identified to be critical in supporting the process of injured muscle regeneration. To date, FAPs remains a poorly defined, heterogeneous population without any specific genetic markers. Using a lineage tracing mouse model (*Gli1-CreER Tomato, Gli1ER/Td*), we recently discovered that Gli1 marks a small subset of muscle-resident FAPs (17%) that preferentially expand upon muscle injury (40% of FAPs at day 3 after injury). Here, we performed cell ablation, pharmacologic manipulation, and single cell transcriptomics to further investigate the role of Gli1$^+$ FAPs in muscle regeneration and fat deposition after injury.

METHODS: *Animals-* All animal work was approved by the Institutional Animal Care and Use Committee (IACUC) at the University of Pennsylvania. *Gli1-CreER Rosa-tdTomato* (*Gli1ER/Td*) mice and *Gli1-CreER Rosa-tdTomato DTA* (*Gli1ER/Td/DTA*) mice were generated. To induce *CreER* activity, 2-month-old male mice received tamoxifen (Tam) injections (75 mg/kg/day) for 5 days. Acute muscle injury was induced by injection of 10 µl Notexin (NTX, 10 µg/mL) or 50 µl glycerol (50% vol/vol) into Tibialis Anterior (TA) muscle. *Histology-* TA muscles were processed for cryosections followed by H&E, WGA, or Perilipin antibodies staining. *Single cell RNA sequencing (scRNA-seq) analysis-* Prealigned and filtered single-cell RNA-seq matrix files of mouse muscle cells were acquired from GEO: GSE110878. Unsupervised clustering was conducted by Seurat and GO/KEGG term enrichment were analyzed by Clusterprofiler. *Statistics-* Data are expressed as means ± standard error of the mean and analyzed by t-tests or one-way ANOVA.

RESULTS: In the TA muscle of *Gli1ER/Td* mice, Td$^+$ cells were exclusively FAPs located in the interstitial area of myofibers (Fig. 1A). Though initially presented at a low level in freshly digested muscle cells, Td$^+$ cells constituted 40% of confluent cells after culturing. Sorted Td+ FAPs formed 6.2-fold more CFU-Fs than Td$^-$ FAPs. They had fibroblastic and adipogenic differentiation abilities, but generated much fewer adipocytes than Td$^-$ FAPs (Fig. 1B). Both Td$^+$ and Td$^-$ cells had no osteogenic differentiation ability (Fig. 1B). To investigate their in vivo function, we generated *Gli1ER/Td/DTA* mice. At 2-month of age, Tam injections quickly reduced Td$^+$ cells by 80% and eliminated Td$^+$ CFU-F colonies from muscle (n=3/group), indicating successful cell ablation. Interestingly, myofibers regenerated at d7 and d28 in *Gli1ER/Td/DTA* mice after Notexin injury were 34.1% and 22.7%, respectively, smaller than those in *Gli1ER/Td* mice (Fig. 2A, n=5/group), suggesting an impairment of myogenesis. Gli1 is an effector of Hedgehog (Hh) signaling. Intramuscular injection of purmorphamine (PUR), an Hh agonist, expanded Td$^+$ cells at d4 and increased myofiber size by 1.6-fold at d30 after Notexin injury (Fig. 2B, C, n=4/group). Local glycerol injection causes muscle degeneration with fat infiltration. Strikingly, Td$^+$ FAPs were less likely to become adipocytes compared to Td$^-$ FAPs and ablation of Td$^+$ cells led to 39.9% more adipocytes in muscle (Fig. 3A-D, n=4/group). Hh signaling inhibitor, GANT61, induced 78.3% more adipocytes, while PUR almost completely depleted adipocyte infiltration (n=5/group). ScRNA-seq analysis of mouse muscle mononucleated cells showed that FAPs can be subclustered into Gli1$^+$ and Gli1$^-$ FAPs (Fig. 3E, F). Pathway analysis suggested that Gli1$^+$ FAPs are more metabolic active and more related to tissue regeneration than Gli1$^-$ FAPs. For example, they have higher Interleukin-6 (Il6) production and TGF-beta signaling, two known positive regulators of myoblast proliferation and tissue regeneration. Furthermore, Gli1$^+$ FAPs express higher levels of known muscle regulators, such as *Tgfb1, Wisp1, Malat1, Igf1*, *Il15* and *Il33* (Fig. 3G), compared with Gli1$^-$ FAPs, which was further validated by qRT-PCR (Fig. 3H). *Il15* and *Wisp1*, are also involved in inhibiting FAPs differentiation into adipocytes. Further analysis revealed increased expression of anti-adipogenic regulators, such as *Tsc22d3*, *Dlk1*, *Ddit3* and *Nr4a1* (Fig. 3I), and reduced expression of pro-adipogenic regulator, such as *Zfp423* and *Ebf1* (Fig. 3J).

DISCUSSION: Our study found that *Gli1-CreER* labels a subpopulation of FAP cells. Compared to Gli1$^-$ FAPs, Gli1$^+$ FAPs are more metabolically active for muscle repair and less likely to contribute to muscle adiposity. Our studies demonstrated that Hh/Gli1 signaling pathway is critical for regulating muscle regeneration and fat accumulation, indicating that pharmacological activation of this pathway could be a therapeutic approach to boost muscle regeneration.

SIGNIFICANCE: Our study revealed a subpopulation of FAPs that preferentially promotes muscle regeneration with less fat accumulation and implied a potential therapeutic effect of Hedgehog signaling in muscle diseases.

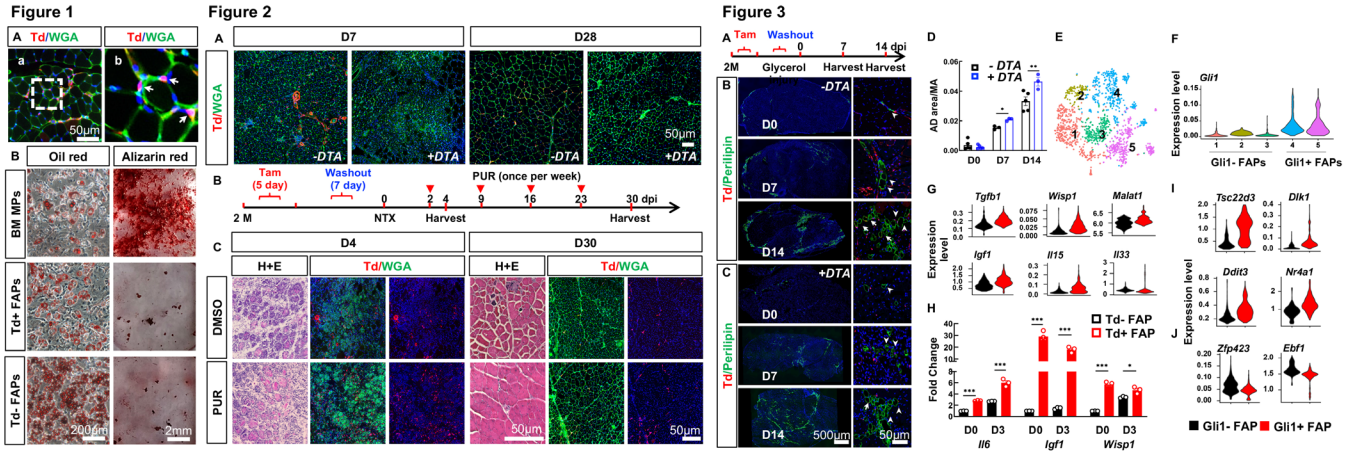

Figure 1. Td in the muscle of *Gli1ER/Td* mice labels a subpopulation of FAPs with less adipogenicity. (A) Td$^+$ cells located in the interstitial area of TA muscle in *Gli1ER/Td* mice. (B) Representative images of osteogenic and adipogenic differentiation of BM MPs (Bone marrow mesenchymal progenitors), Td$^+$ FAPs and Td$^-$ FAPs. **Figure 2. Ablation of Gli1$^+$ cells causes delayed muscle regeneration and activation of Hh signaling accelerates muscle healing.** (A) Representative immunofluorescence imaging of *Gli1ER/Td* and *Gli1ER/Td/DTA* muscle at day 7 and 28 post NTX injury. (B) Schematic plot of mouse muscle NTX injury model with PUR treatment. (C) Representative H&E staining and immunofluorescence images of TA muscles with DMSO or PUR treatment group at day 4 and day 30 post NTX injury. **Figure 3. Gli1$^+$ FAPs suppress intramuscular adipogenesis and Single cell RNA-seq analysis of FAPs.** (A) Schematic plot of mouse muscle glycerol injury model. (B, C) Representative immunofluorescence images of TA muscle from *Gli1ER/Td* or *Gli1ER/Td/DTA* mice at day 0, 7, and 14 post glycerol injury with perilipin staining. Arrows point to Perilipin$^+$Td$^+$ cells and arrowheads point to Perilipin$^+$Td$^-$ cells. (D) Quantification of muscle adipocyte area revealed that muscle adiposity is increased in *Gli1ER/Td/DTA* mice. (E) Further subclustering of FAPs generates 5 subclusters. (F) Violin plots show clusters 4 and 5 express Gli1 at a higher level compared to clusters 1, 2 and 3. (G) Violin plot of myogenic factors expression. (H) qPCR of *Il6*, *Igf1* and *Wisp1* expression at D0 and D3 after injury of sorted Td$^-$ and Td$^+$ FAPs. (I) Violin plot of anti-adipogenic factors expression. (J) Violin plot of pro-adipogenic factors expression.

Limited Scar Resection for Chronic Achilles Repair: Use of a Rat Model

Matthew Counihan MD, Courtney Nuss AS, Joseph Newton BS, Louis Soslowsky PhD, Daniel Farber MD
McKay Orthopaedic Research Laboratory, University of Pennsylvania, Philadelphia, PA
Disclosures: Matthew Counihan MD (N), Courtney Nuss AS (N), Joseph Newton BS (N), Louis Soslowsky PhD (N), Daniel Farber MD (N)

INTRODUCTION: Acute rupture of the Achilles tendon is misdiagnosed in up to 24% of patients [1]. Without acute intervention, the tendon ends retract, the injury gap fills with scar tissue, and treatment becomes more difficult [2]. Current treatment of chronic Achilles tendon ruptures involves debridement of scar tissue back to normal tendon ends, followed by interposition of healthy graft tissue to fill the gap, such as in the gastrocnemius fascia turndown (GFT) technique [3]. Direct repair with the limited scar resection (LSR) technique offers a less invasive alternative, allowing for primary repair of the tendon without a graft, avoiding donor site morbidity [4]. However, LSR has not been adopted as a common surgical alternative due to concern that scar tissue does not heal as well as healthy donor graft tissue. Therefore, the objective of this study was to define and compare the healing properties of the Achilles tendon after chronic injury reconstruction with GFT or LSR, utilizing an animal model to control the injury and treatment strategies. We hypothesized that LSR would have superior healing properties to the GFT and non-repair control groups in a chronic Achilles injury model.
METHODS: *Study Design:* After facility acclimation, 90 male Sprague Dawley rats (400-450g) were used (IACUC approved). Animals were randomized equally into three groups: non-repair (NR), gastrocnemius fascia turndown (GFT), and limited scar resection (LSR). Chronic Achilles injury was generated via unilateral blunt transection of the right Achilles tendon in each rat, followed by 1 week of immobilization of the injured limb in a maximally dorsiflexed position and 5 weeks of cage-activity without immobilization. 6 weeks after the index surgery, GFT and LSR groups underwent chronic Achilles reconstruction. In the GFT technique, all interposed scar tissue was debrided, then the gastrocnemius fascia was flipped on a distal hinge to bridge the gap, reconstructing the tendon. In the LSR technique, a small midsection of the scar tissue was removed to restore the tendon to pre-injury length, followed by end-to-end primary repair of the remaining scar tissue ends. A modified Kessler repair was used in both techniques. The hind limb was immobilized in plantarflexion after the index surgery. Animals were sacrificed at 3 and 6 weeks after repair. The NR group was sacrificed at 9 and 12 weeks from the index procedure to match sacrifice points for all three groups. All rats underwent biweekly in vivo assessments including ambulatory kinetics and kinematics, passive ankle joint mechanics, and ultrasound. Ex vivo assessments included mechanical testing and histology. Cycles to failure comparisons were made using a nonparametric Kruskal-Wallis ANOVA. Other ex-vivo comparisons were made using 1-way ANOVAs. In-vivo assessment comparisons were made using a 2-way ANOVA with repeated measures on time with follow-up t-tests between groups at each time point. Significance was set at $p<0.05$ for all tests.
RESULTS: *Ultrasound*: Ultrasound assessment showed successful post-injury elongation of the Achilles tendon in all groups which is critical to the chronic Achilles injury model. The cross-sectional area of each of the repaired tendons was significantly increased compared to the NR tendons at both time points. The LSR repair had increased vascularity compared to NR in the post-repair period, with increased contrast wash-in rate and decreased contrast time to peak at the 9 week time point. *Mechanical Testing*: Stiffness of LSR and GFT repairs was significantly lower compared to NR at 3 weeks. At 6 weeks, LSR and GFT tendon stiffness improved, such that there was no longer a difference between the three groups. Modulus was significantly lower in both LSR and GFT groups at both 3 and 6 weeks. Cycles to failure (CTF) was significantly higher in NR at 3 weeks as compared to both LSR and GFT. CTF improved in both repair groups at 6 weeks such that there was no longer a difference between the three groups. *Passive Joint Mechanics*: Passive joint mechanics revealed significantly increased dorsiflexion stiffness in the GFT repair group at the first post-repair time point at 8 weeks when compared to NR. LSR repair had increased dorsiflexion stiffness that trended toward significance at the 8 week time point compared to NR. Both LSR and GFT groups had significantly decreased range of motion at the 8 week post-repair time point as compared to NR. *Ambulatory Assessment*: Gait analysis of the GFT and LSR repair groups had significantly decreased ground reaction forces (peak vertical force, peak propulsion forces) as compared to the NR group at the first post-repair assessment 8 week time point. Ground reaction forces were recovered quickly in the LSR group, with no significant difference from the NR group at 10 and 12 weeks. Ground reactive forces for the GFT group remained significantly decreased from the NR group at both 10 and 12 weeks without recovery.
DISCUSSION: The present study supports that both LSR and GFT reconstruction techniques are viable options for treatment of the chronic Achilles tendon injury in a rat model. We established that the injury surgery successfully recreated the elongated Achilles tendon typical of the chronic Achilles injury. Both reconstruction techniques established increased dorsiflexion stiffness and decreased range of motion across the ankle joint. This is representative of the re-establishment of normal length and tension of the Achilles complex in both of the repair groups, which is critical to the success of operative management of a chronic Achilles injury. Ground reaction forces were expectedly decreased after surgery, but quickly recovered in the LSR group, while the GFT group remained significantly decreased through the study. This is reflective of the decreased morbidity incurred by the LSR technique, allowing for a significantly shorter recovery time. Vascular analysis provided evidence of adequate microcirculation and vascularization of this tissue, contesting the notion that a lack of circulation in scar tissue would be a barrier to healing in this technique. Mechanical testing results raise the question of whether these tendons fared better with non-operative management compared to either reconstruction technique. However, it must be noted that at the 3 week and 6 week post-repair sacrifice points, the NR tendons are actually matured to 9 and 12 weeks, respectively. The difference in the relative maturity of the tendon in NR vs GFT/LSR groups inherently introduces a difference in stiffness and strength between the groups. Importantly, the repair groups were able to match the stiffness and strength of the NR group at the 6 week time point, when they have had relatively half the time for healing and scar maturation as the NR group. A limitation of the rat model is that the gastrocnemius muscle of the rat is relatively thinner with a larger soleus as compared to humans, and as such the GFT procedure may cause relatively larger morbidity to the gastrocnemius muscle in the rat.
SIGNIFICANCE: This study supports that the limited scar resection technique is a viable surgical alternative, particularly when minimizing postoperative morbidity and surgical time are paramount. The study also suggests the non-operative management of chronic Achilles injuries may yield similar results as compared to operative management, which necessitates further research into conservative treatment modalities for this condition.
ACKNOWLEDGEMENTS: Funding was provided by the Orthopaedic Research and Education Foundation and the NIH/NIAMS supported Penn Center for Musculoskeletal Disorders (P30AR069619). The authors thank Snehal Shetye, Thomas Leahy, and Harina Raja for their assistance.
REFERENCES: [1] Raikin et al., 2013. Foot Ankle Int. 34:475-80. [2] Bevilacqua et al., 2012. Clin Podiatr Med Surg. 29:291-9. [3] Maffulli et al., 2007. Foot Ankle Clin. 12:583-96. [4] Yasuda et al., 2016. J Bone Joint Surg Am. 98:1168-75.

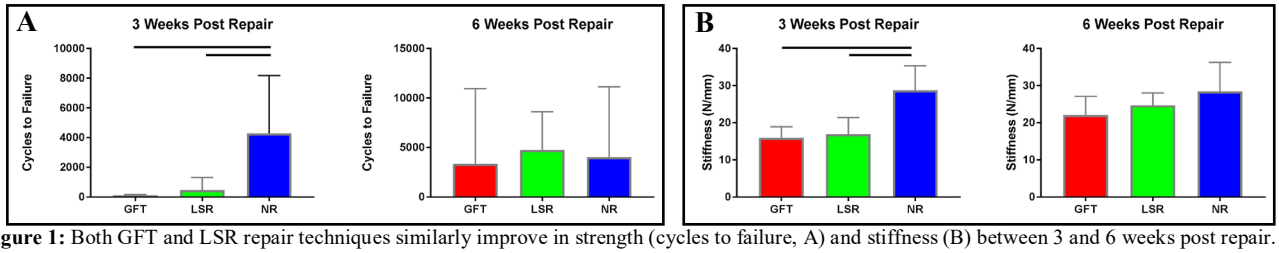

Figure 1: Both GFT and LSR repair techniques similarly improve in strength (cycles to failure, A) and stiffness (B) between 3 and 6 weeks post repair.

Identification of a novel adipose lineage cell population that regulates bone marrow environment

Leilei Zhong[1] (leileiz@pennmedicine.upenn.edu), Lutian Yao[1], Robert J. Tower[1], Yulong Wei[1], Luqiang Wang[1], Wei Yu[1], Yejia Zhang[1], Yanqing Gong[2], Fanxin Long[1], Patrick Seale[3], Chider Chen[4], Jaimo Ahn[1], and Ling Qin[1]

[1]Department of Orthopaedic Surgery, [2]Division of Transnational Medicine and Human Genetics, [3]Cell and Developmental Biology, Perelman School of Medicine, [4]Department of Oral and Maxillofacial Surgery/Pharmacology, University of Pennsylvania, Philadelphia, PA 19104, USA.

Disclosures: None

Introduction: Bone marrow adipocytes are conventionally viewed as large cells containing unilocular lipid droplets. Originally considered as space fillers, they are now thought to be a negative regulator of osteogenesis because both adipocytes and osteoblasts are derived from bone marrow mesenchymal stem cells (MSCs). We recently applied single cell RNA-sequencing (scRNA-seq) on sorted bone marrow mesenchymal lineage cells from 1-mo-old mice that has very few marrow adipocytes. Unexpectedly, we identified a large mesenchymal subpopulation that expresses many mature adipocyte markers (*Pparg, Cebpa, Adipoq, Apoe*, and *Lpl*) but not liqid droplet-associated genes (*Perilipin* and *Fabp4*). Here, we constructed mature adipocyte-specific *Adipoq-Cre(ER) Rosa-tdTomato (Adipoq(ER)/Td)* mice to validate this novel cell population and study their actions in bone.

Methods: *Animals-* All animal work performed was approved by the Institutional Animal Care and Use Committee (IACUC) at the University of Pennsylvania. *Col2/Td*, *Adipoq/Td, AdipoqER/Td* mice were obtained by crossing *Rosa-tdTomato* mice with *Col2-Cre*, *Adipoq-Cre, Adipoq-CreER* mice, respectively. *Adipoq/Td/DTR* mice were generated by breeding *Adipoq/Td* mice with *Rosa-DTR* mice. *AdipoqER/Td* mice received Tamoxifen (Tam) injections (75 mg/kg/day) at P6 and P7 and euthanized at 1 mo of age. *Adipoq/Td/DTR* mice received vehicle or diphtheria toxin (DT, 50 µg/kg) every other day for 2 wk. For focal radiation, mouse right femur received a clinically relevant radiation dose of 5 Gy using small animal radiation research platform (SARRP). *Immunofluorescence-* Bones were processed for 50 µm-thick whole mount cryosections and stained with indicated antibodies. *Transplantation-* Freshly FACS-sorted Td^+ cells ($5x10^4$/transplant) were mixed with Gelfoam and placed under the kidney capsule of 2-mo-old *C57Bl/6* mice. 4 wk later, mice received calcein injection (15 mg/kg) 1 day before harvesting grafts. *Statistics*- All analyses were conducted using t-tests.

Results: Td labeled all $Perilipin^+$ adipocytes, many $CD45^-$ stromal cells, and pericytes, but not osteoblasts, osteocytes, and chondrocytes in 1-mo-old *Adipoq/Td* mice (Fig.1A). The majority of Td^+ cells (99.8%) did not harbor lipid droplets and none of them incorporated EdU (Fig.1B,C). Td^+ cells constituted ~18% of $CD45^-Ter119^-$ bone marrow cells. After isolation, they attached to the culture dish but did not form CFU-F colonies (Fig. 1D). While Td^+ cells from *Col2/Td* mice (in which Td labels mesenchymal progenitors) formed bony structure after transplantation, freshly sorted Td^+ cells from *Adipoq/Td* mice did not (Fig.1E), indicating that they are not mesenchymal progenitors. Upon adipogenic differentiation, Td^- mesenchymal progenitors from *Adipoq/Td* mice first became Td^+ cells with no lipid droplets and then evolved into Td^+ cells with lipid (Fig. 1F). Similar cell culture results were also obtained with *AdipoqER/Td* mice. Fate mapping in postnatal *AdipoqER/Td* mice confirmed that $Perilipin^+$ lipid-laden adipocytes are derived from non-lipid-laden Td^+ adipocytes (Fig. 1G). In the bone marrow of young *Adipoq/Td* mice, all pericytes identified by PDGFRβ or Laminin staining in a peri-capillary location were Td^+ (Fig. 2A). Strikingly, using whole mount sectioning and confocal scanning, we found that bone marrow Td^+ stromal cells and pericytes form a 3D network made of cell processes to communicate amongst themselves and other components of bone, including vessel walls (Fig 2B). Ablating those cells in 1-mo-old *Adipoq/Td/DTR* mice after 2 wk of DT injections disrupted bone marrow vasculature and caused drastic *de novo* bone formation in the diaphyseal bone marrow (Fig. 3), suggesting that those cells function in maintaining vessel integrity and inhibiting osteogenesis. Focal radiation on long bones rapidly expanded the non-lipid-laden Td^+ cells at d3, accompanied with vessel dilation and a loss of Td^+ pericytes (Fig. 4). By d7, both vessel structure and Td^+ pericyte density returned to relatively normal levels. These data implied a role of Td^+ adipocytes in the repair and stabilization of marrow vessels after radiation injury.

Discussion: Our study demonstrate that bone marrow contains a large number of non-proliferative, mature adipocytes with no significant lipid stores. Those cells represent a stable transitional cell type situated after mesenchymal progenitors and before classic lipid-laden adipocytes along the adipogenic differentiate route. They are morphologically and functionally distinct from traditional adipocytes. Existing as stromal cells or pericytes, they possess numerous cell processes to form a vast 3D network structure in bone marrow. Our scRNA-seq data suggest that they express many secretory factors, including angiogenic factors. Most likely through secreting these factors into marrow environment, they play pivotal roles in maintaining marrow vasculature, suppressing osteogenic differentiation of mesenchymal progenitors, and participating into vessel repair after radiation injury. Therefore, we name them marrow environment regulating adipose cells (MERAs).

Significance: We discovered a novel type of adipose lineage cell population that regulates bone marrow environment.

Fig. 1

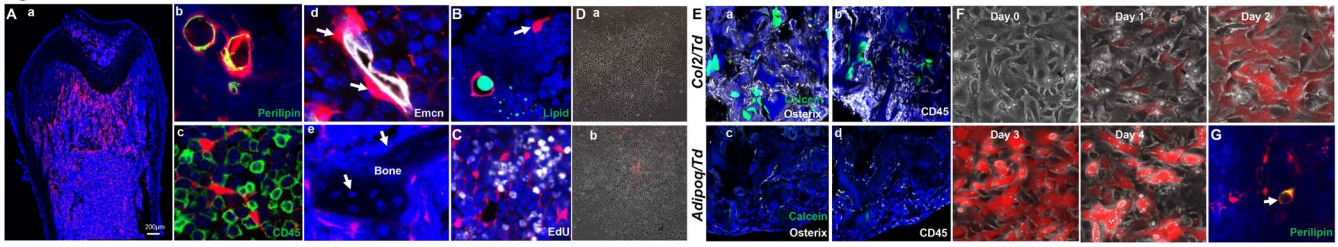

Fig. 2

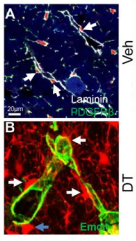

Fig. 3

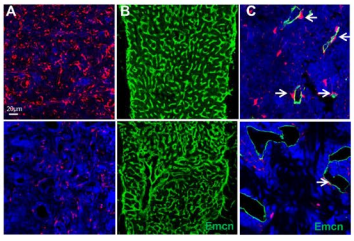

Fig. 4

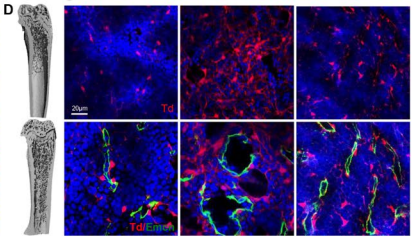

Figure 1. Mouse bone marrow contains abundant non-lipid-laden adipocytes. (A) In a 1-mo-old *Adipoq/Td* femur (a), Td labels $Perilipin^+$ adipocytes (b), $CD45^-$ stromal cells (c), pericytes (d), but not osteoblasts and osteocytes (e). (B) BODIPY lipid staining shows a Td^+ stromal cell (arrow) with no lipid. (C) Td^+ cells do not incorporate EdU. (D) all CFU-F colonies are made of Td^- cells (a) while some Td^+ cells do attach to the dish (b). (E) Td^+ cells from *Col2/Td* mice, but not *Adipoq-Td* mice, form bone-like structure. (F) In vitro adipogenic differentiation assay of Td^- mesenchymal progenitors from *Adipoq/Td* mice. The same area was imaged daily. (G) Bone marrow $Perilipin^+$ adipocytes are derived from non-lipid-laden Td^+ adipocytes in 1-mo-old *AdipoqER/Td* mice (Tam injections at P6, 7 when no $Perilipin^+$ cells can be detected in the bone marrow). **Figure 2. Non-lipid-laden Td^+ cells are stromal cells and pericytes forming a 3D network inside the bone marrow.** (A) All $PDGFR\beta^+$ and $Laminin^+$ cells with a pericyte morphology are Td^+ (arrows). (B) Td^+ stromal and pericytes are morphologically similar with many cell processes. **Figure 3. Ablation of adipocytes reveals their roles in maintaining vasculature and bone.** (A) Bone marrow Td^+ cells in *Adipoq/Td/DTR* mice were ablated by DT. (B) DT altered bone marrow vessel structure. (C) High magnified image showed that vessels were dilated coinciding with a depletion of Td^+ pericytes. (D) 3D µCT images show drastic *de novo* bone formation in femoral midshaft after DT injections. **Figure 4. Adipocytes are required for the recovery of bone marrow vasculature after radiation injury.** Fluorescent images of total Td^+ cells (top) and pericytic Td^+ cells (bottom) in the bone marrow of 1-mo-old *Adipoq/Td* femurs before (NR) and after (R) focal radiation (3 and 7 days).

Structural and Cellular Responses of Supraspinatus Tendon Enthesis and Subchondral Bone to Pregnancy, Lactation, and Post-Weaning Recovery

Yilu Zhou, Yihan Li, Zachary Davis, Wenzheng Wang, Ashley K. Fung, Snehal S. Shetye, Xi Jiang, Andrew F. Kuntz, Nathaniel Dyment, Louis J. Soslowsky, X. Sherry Liu

Department of Orthopaedic Surgery, University of Pennsylvania, Philadelphia, PA, USA. yiluz@pennmedicine.upenn.edu

Disclosures: All authors have nothing to disclose.

INTRODUCTION: The maternal skeleton undergoes dramatic bone loss during pregnancy and lactation [1], and fluctuating hormones levels increase the risk of musculoskeletal joint disorders such as shoulder pain [2-3]. Previously, we discovered transient changes in mechanical properties of the supraspinatus tendon during pregnancy [4]. However, the cellular mechanisms behind such effects in a reproductive cycle remain unknown. Since, the supraspinatus tendon transfers force from the muscle to the bone of the humerus through the enthesis, the objective of this study was to track the structural and cellular responses in specific regions of the supraspinatus tendon enthesis and underlying humeral bone. We hypothesized that differential effects of pregnancy, lactation, and post-weaning on cellular activities would alter the dynamic change of microstructure in the enthesis and subchondral bone.

METHODS: (IACUC approved) *In vivo μCT study*: Thirteen female SD rats (7 virgins and 6 rats with a complete reproductive cycle) received *in vivo* μCT scans of the right proximal humeri at mating (baseline), end of 3-week pregnancy, 3-week lactation, and 6-week post-weaning recovery using VivaCT 80 (Scanco Medical AG, voxel size 21μm). The humerus was divided into 3 regions of interests (3 ROI: the region below supraspinatus tendon enthesis, the epiphysis, and the metaphysis, Fig 1A) and each region was subjected to trabecular bone microstructure analysis. *Histomorphometry Study*: Twenty four rats (aged 7 month at euthanasia) were assigned to 4 groups (n=6/group): virgin, pregnancy (euthanized at parturition), lactation (euthanized after 2-week lactation), and recovery group (euthanized 2-week post weaning). All rats were injected with calcein green, alizarin red, and tetracycline at 16, 9, 2 days before euthanasia. The left shoulder was harvested and cryo-embedded. Cryo-sections were first imaged to identify fluorochrome mineralization labels, followed by tartrate-resistant acid phosphatase (TRAP) staining to visualize catabolic enzyme activities; and a subsequent toluidine blue staining for identifying cell population and different zones in the tendon enthesis site: unmineralized fibrocartilage (UF), tidemark (TM), mineralized fibrocartilage (MF), and bone (B). *Statistics*: Longitudinal comparisons were made using 2-way, repeated-measures ANOVA with baseline adjustment and Bonferroni corrections for post hoc tests. All cross-sectional comparisons were made using 1-way ANOVA and Tukey's HSD for post hoc tests.

RESULTS: All differences and changes reported here are statistically significant ($p<0.05$). Across a reproductive cycle, similar changes were seen in trabecular bone microstructure at the epiphysis (data not shown) and the region adjacent to the enthesis (Fig 1D-F), with the changes being more striking at the latter (data not shown). Specifically, at the enthesis region, no change in bone microstructure was observed during pregnancy. In contrast, lactation resulted in 41%, 12%, and 7% reduction in BV/TV, Tb.N, and Tb.Th, respectively (Fig 1B, D-F). Weaning triggered a substantial anabolic response (Fig 1C), resulting in complete recovery in Tb.N and Tb.Th, and greater BV/TV in post-weaning rats than virgins (Fig 1D-F). Different from the epiphysis and enthesis region, the metaphsysis underwent greater bone loss during pregnancy. By the end of lactation, there were 69%, 42%, and 18% decreases in BV/TV, Tb.N, and Tb.Th than baseline, respectively (Fig 1G-I). Even 6 weeks after weaning, Tb.N still remained 25% lower than the baseline (Fig 1H). Histomorphometry images showed TRAP activities on bone surface in all groups and the expression level reached the peak during lactation (Fig 2A-F). Furthermore, the fraction of TRAP-expressing osteocytes (Fig 2G) in bone at the base of the enthesis rapidly increased from 8% (baseline) to 30% (lactation). Multicolor mineralizing labels were found in the subchondral bone near the enthesis in all groups, with the strongest activities observed in the recovery group (Fig 2D), which was consistent with μCT data showing substantial trabecular bone recovery after weaning. However, flurochrome labels at the enthesis tidemark were only found in the pregnancy group (Fig 2B&E). Within the mineralized zones of the enthesis, we found that bone fraction (Fig 2H) and osteocyte/fibrochondrocyte number ratio (Fig 2I) in recovery group were 21% and 40% greater than that of lactation group, respectively.

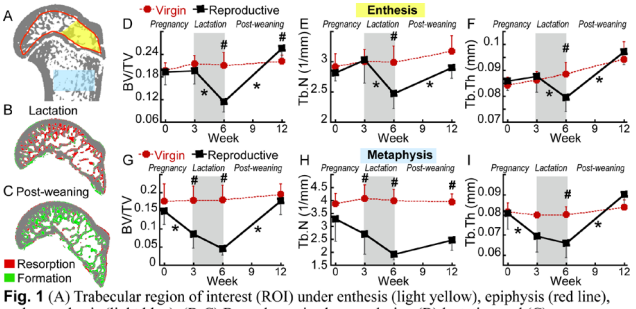

Fig. 1 (A) Trabecular region of interest (ROI) under enthesis (light yellow), epiphysis (red line), and metaphysis (light blue). (B-C) Bone dynamic changes during (B) lactation and (C) post-weaning recovery. Red indicates bone resorption and Green indicates bone formation. (D-I) Changes of trabecular bone microstructure at the (D-F) enthesis and (G-I) metaphysis. $p<0.05$: # Virgin ≠ Reproductive; * difference between two time points in Reproductive group.

DISCUSSION: Pregnancy, lactation, and weaning cause substantial fluctuations and complex interactions of circulating calciotropic and sex hormones. These changes result in upregulated TRAP expression in both osteoclasts and osteocytes during lactation and subsequent increases in bone formation adjacent to the enthesis. In the humeral epiphysis, substantial bone loss was observed during lactation followed by a complete recovery after weaning, unlike the metaphysis which did not fully recover. Moreover, striking changes were perceived specifically at the location adjacent to enthesis, where tensile force from tendon is transmitted to underlying bone. In contrast to the metaphysis, the epiphysis and the location adjacent to enthesis are resistant to pregnancy-induced bone loss. Interestingly, we found an activation of mineral deposition from enthesis fibrochondrocytes at the tidemark (Fig 2E) during pregnancy, but did not detect structural changes in the enthesis fibrocartilage. Furthermore, tidemark mineral deposition was also observed in pseudopregnancy rats (data not shown), potentially due to fibrochondrocytes activated by elevated progesterone level during pregnancy and pseudopregnancy [5]. Our results also demonstrated osteocyte peri-lacunar/canalicular remodeling (PLR) [6] at the subchondral bone during lactation. Future studies are required to gain more insights into the regulatory role of osteocyte PLR in balancing calcium homeostasis and tissue mechano-sensitivity at the tendon enthesis.

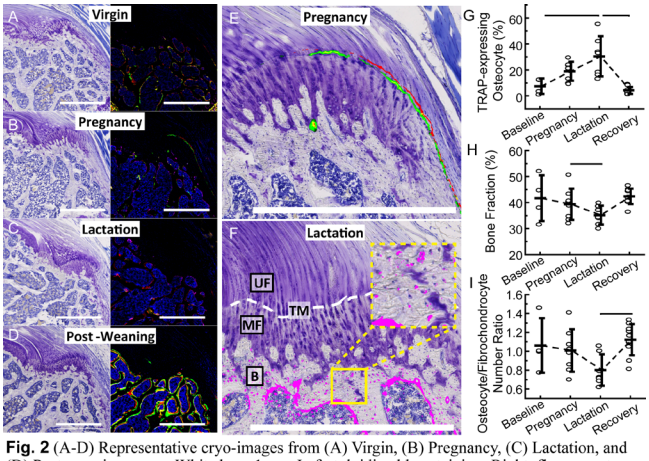

Fig. 2 (A-D) Representative cryo-images from (A) Virgin, (B) Pregnancy, (C) Lactation, and (D) Post-weaning group. White bar =1mm. Left: toluidine blue staining; Right: fluorescent images; Green, Red, Yellow indicate flurochrome mineralizing labels; blue: nucleus; pink: TRAP staining. (E) A representative Toluidine blue image overlapped with flurochrome mineralizing labels from Pregnancy group. (F) Representative Toluidine blue image overlapped with TRAP staining (pink) from Lactation group. Tendon enthesis zones: unmineralized fibrocartilage (UF),tidemark (TM), mineralized fibrocartilage (MF), and bone (B). (G-I) Quantifications in mineralizd enthesis:(G) TRAP expressing fraction of osteocyte, (H) bone fraction, (I) osteocyte/fibrochondrocyte ratio. Solid line indicates $p<0.05$ between two groups.

SIGNIFICANCE: This study demonstrated that the adaptive responses in cellular activities during female reproduction optimize the balance between calcium homeostasis and the structural and mechanical integrity of tendon enthesis and underlying bone.

REFERENCES: [1] Kovacs, *Physiol Rev.,* 2015; [2] Watt *et al., Post Reprod Health*, 2018; [3] Cucchi *et al., Joints*, 2017; [4] Fung *et al., SB3C,* 2019; [5] Bowman *et al., JBMR*, 1996; [6] Qing *et al*., *JBMR*, 2012.

ACKNOWLEDGEMENTS: NIH/NIAMS R01-AR071718, NSF #1653216, and Penn Center for Musculoskeletal Disorders (P30-AR069619).

Knockout of Collagen V during the Inflammatory Healing Phase Significantly Affects Quasi-Static Tendon Mechanics

Brittany L. Taylor[1], Ryan J. Leiphart[1], Stephanie N. Weiss[1], David E. Birk[2], Louis J. Soslowsky[1]
[1]McKay Orthopaedic Research Laboratory, University of Pennsylvania, Philadelphia, PA
[2]Department of Molecular Pharmacology and Physiology, University of South Florida, Tampa, FL
brtay@pennmedicine.upenn.edu

Disclosures: Brittany L. Taylor (N), Ryan J. Leiphart (N), Stephanie N. Weiss (N), David E. Birk (N), Louis J. Soslowsky (N)

INTRODUCTION: Collagen V is a quantitatively minor component of collagen fibrils with major regulatory roles throughout tendon healing. Our established murine model of collagen V haploinsufficiency demonstrated diminished recovery of mechanical properties and altered fibril morphology following tendon injury; which supports the important modulatory role of collagen V in tendon injury repair [1]. However, these studies utilized conventional mouse models of collagen V deletion and therefore the lack of collagen V during development and maturation *and* the effect on the injury response is confounding. Thus, the isolated role of collagen V at defined phases of tendon healing following injury remains unknown. Therefore, the objective of this study was to elucidate the specific mechanistic regulatory role(s) of collagen V in the late inflammatory and remodeling responses of tendon healing in a normal matrix using inducible collagen V null and heterozygous models. We hypothesize that decreased collagen V during the inflammatory and remodeling phases will result in significantly decreased dose-dependent tendon mechanical properties during both phases.

METHODS: Animal Surgery: Adult male wild-type (WT) (n=15), Col5a1$^{flox/+}$ (n=45), and Col5a1$^{flox/flox}$ (n=45) mice with a tamoxifen (TM) inducible Cre were utilized for this study (IACUC approved). Bilateral partial width, full thickness patellar tendon injury was performed on the Col5a1$^{flox/+}$ and Col5a1$^{flox/flox}$ mice at maturity (120 days) under sterile conditions as described [2]. Cre-induced excision of the conditional alleles of the transgenic mice was performed at 5 days following surgery during the late inflammatory phase (TM5) and 21 days following surgery during the remodeling phase (TM21) via two consecutive daily IP injections of tamoxifen (2mg/40g body weight). The TM5 mice were sacrificed at 3 and 6 weeks post-injury and the TM21 mice were sacrificed 6 weeks post injury (n =15/genotype/timepoint). The WT uninjured control mice were administered TM doses (3 days of 4mg/40g body weight) at 120 days old and were sacrificed 30 days later. The patellar-tendon-tibia complexes were harvested and prepared for uniaxial mechanical testing. Mechanical Testing: The tendons were subjected to viscoelastic mechanical testing, which consisted of 10 cycles of preconditioning and stress relaxations at 3%, 4%, and 5% strain. Each stress relaxation was followed by 10 cycles of frequency sweeps, quasi-static ramp to failure, and 5% stress relaxation. The ramp to failure data was used to determine stiffness, modulus, maximum load, and maximum stress. Percent relaxation was quantified for each percent strain level. Statistics: One-way ANOVAs with Bonferroni correction post-hoc tests were performed to compare the WT uninjured and injured controls to the injured Col5a1$^{flox/+}$ (HET) and Col5a1$^{flox/flox}$ (NULL) tendons at each Cre-induction and healing time point (TM5 at 3 weeks, TM5 at 6 weeks, TM21 at 6 weeks) to define the specific effect of collagen V at each healing phase. Significance was set at $p \leq 0.05$ and trends were set at $p \leq 0.1$.

RESULTS: Cross-sectional area and stiffness of the injured tendons were significantly increased compared to the uninjured WT tendons at both induction and healing time points. The injured WT tendons trended towards increased cross-sectional area compared to HET tendons at TM5 induction after 3 weeks of healing, but the opposite trend was observed between the injured WT and HET at TM5 and TM21 induction after 6wks (data not shown). The injured WT tendons were significantly stiffer than the injured HET and NULL tendons at TM5 after 3 and 6 weeks of healing (Fig. 1A & 1B), but these differences were not seen with TM21 at 6 weeks (data not shown). Max load of the uninjured WT was significantly greater than the injured WT tendons at TM5 after 3 weeks of healing, injured NULL tendons at TM5 after 3 and 6 weeks of healing, and injured HET tendons at TM5 and TM21 after 6 weeks of healing (Fig. 2). Injured WT tendons also had increased max load compared to injured HET tendons at TM5 after 3 (Fig. 2A) and 6 weeks of healing (Fig. 2B). Decreasing trends in max load were observed between injured WT and NULL at TM5 after 3 weeks of healing (Fig. 2A), and at TM21 after 6 weeks of healing between uninjured WT and injured NULL, and injured WT and HET tendons (Fig. 2C). The injured tendons had decreased modulus compared to the uninjured WT tendons (data not shown). Significant differences in max stress were observed between the uninjured WT tendons and injured tendons at TM 5 after 3 weeks, injured HET and NULL tendons after TM 5 after 6 weeks, and injured WT (trend) and NULL tendons at TM21 after 6 weeks (Fig. 2D-F). The injured WT tendons also exhibited increased max stress compared to the injured NULL at TM5 after 6 weeks and injured TM5-induced HET tendons at both healing time points (Fig. 2D & 3E). Stress relaxation of the injured tendons at 3 and 4% strain was increased compared to the uninjured WT tendons at both induction and healing time points (data not shown). Statistical differences in stress relaxation were observed with TM5 after 3 weeks of healing between injured WT and HET tendons at 4% (trend), injured WT and NULL tendons at 3% and 4% (data not shown). Stress relaxation at 5% strain was increased for the injured HET and NULL tendons compared to the uninjured WT at TM 5 and TM21 (trend) independent of healing time, and decreased for the injured WT tendons compared to the injured HET and NULL tendon at TM5 after 3 weeks (data not shown). No differences were observed between the injured HET and NULL tendons across all parameters, induction, and healing time points.

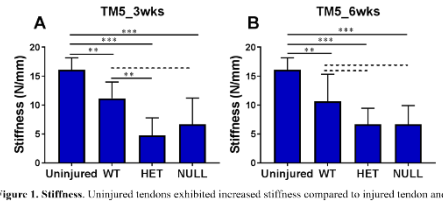

Figure 1. Stiffness. Uninjured tendons exhibited increased stiffness compared to injured tendon and injured WT tendons were stiffer than the HET and NULL tendons when collagen V was knocked out at 5 days post-surgery (TM5) after **(A)** 3 and **(B)** 6 weeks of healing.***: $p \leq 0.001$, **: $p \leq 0.01$, *: $p \leq 0.05$, ---: $p < 0.1$.

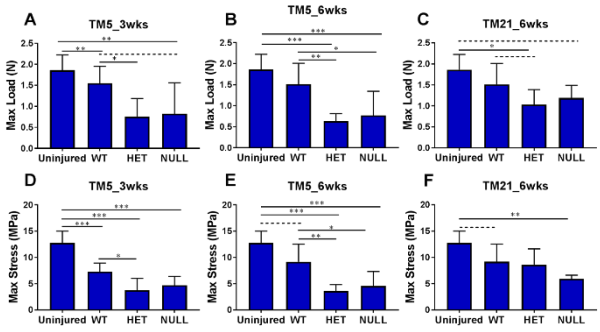

Figure 2. Max Load and Max Stress. Injured tendons exhibited decreased **(A-C)** max load and **(D-F)** max stress compared to uninjured WT when collagen V was knocked out at 5 days post- surgery after **(A&D)** 3 and **(B&E)** 6 weeks of healing. These differences were lessened at the 21 day induction time point and 6 weeks of healing **(C &F)**. ***: $p \leq 0.001$, **: $p \leq 0.01$, *: $p \leq 0.05$, ---: $p < 0.1$.

DISCUSSION: This study investigates the mechanistic regulatory role(s) of collagen V in the late inflammatory and remodeling phases of tendon healing in a normal matrix using inducible collagen V null and heterozygous models. Overall, the injured tendons exhibited significantly altered material and structural properties independent of genotype. Contrary to our hypothesis, these differences were not allele dose-dependent as no differences were observed between the HET and NULL tendons. This is contrary to the dose-dependent response observed in a previous study where collagen V knockout induced at the time of surgery resulted in trending differences in cross-sectional area and max stress between injured HET and NULL tendons. This demonstrates that the degree of collagen V deficiency does not have a significant effect on the healing response in the late inflammatory and remodeling phases. Interestingly, knocking out collagen V during the late inflammatory phase resulted in substantial deficits in tendon mechanics, and this effect was not as pronounced when collagen V was altered during the remodeling phase. This observation confirms the direct correlation between collagen V production and tendon inflammation as concluded in a study where collagen V was substantially increased in chronically inflamed connective tissue [3]. This finding supports the unique binding and connecting role of collagen V during the inflammatory process. Further investigation is required to elucidate the mechanistic role of collagen V at the gene and protein level and to define the pathologic and functional significance of collagen V.

SIGNIFICANCE: This study demonstrates the role collagen V on tendon repair at defined healing phases and provides mechanistic insights toward understanding the healing response of a normally developed tendon in a collagen deficient healing environment.

REFERENCES: [1] Johnston et al, *J Orthop Res*, 35(12), [2] Dunkman et al., *Ann. Biomed Eng,* 42(3), [3] Harayanan et al., *Collagen Rel Res,* 3(4)

ACKNOWLEDGEMENTS: Thank you to Mary-Kate Evans for her assistance on this project. This work was supported by the NIH/NIAMS (R01AR065995 and P30AR069619).

Greater Activation of Modeling-Based Bone Formation and Improvement in Bone Microarchitecture by Intermittent PTHrP *vs.* PTH in Ovariectomized (OVX) Rats

Tala Azar, Wenzheng Wang, Wei-Ju Tseng, Hongbo Zhao, Nathaniel Dyment, X. Sherry Liu
[1]McKay Orthopaedic Research Laboratory, Department of Orthopaedic Surgery, University of Pennsylvania, Philadelphia, PA; talaazar@seas.upenn.edu

Similar to parathyroid hormone (PTH), PTH-related protein analog (PTHrP), an FDA approved treatment for postmenopausal osteoporosis, exhibits anabolic effect when administered intermittently. However, the effects of PTH and PTHrP at the trabecular level, including microarchitecture and types of bone formation (BF) induced, have not been compared. Modeling-based BF (MBF - BF on quiescent surfaces) and remodeling-based BF (RBF - BF coupled with resorption by osteoclasts), are important mechanisms by which anabolic agents improve bone mass. We hypothesized that different levels of MBF and RBF induced by PTHrP *vs.* PTH may lead to different degrees of improvement in bone microarchitecture.

We injected calcein (green, G), alizarin complexone (red, R), and tetracycline (yellow, Y) fluorochrome labels in a G-R-Y-G sequence on days -2, 5, 12, and 19 (treatment initiated on day 0) with euthanasia on day 21 in 5-mo-old OVX rats. In VEH-, PTH- (20 μg/kg), and PTHrP-treated (20 μg/kg) samples (n=6/group, Fig A-C), fluorochrome labels and cement lines on cryo-sections of tibial trabecular bone were used to identify MBF (smooth cement line, Fig D) or RBF (scalloped cement line, Fig E) sites. Compared to VEH, both PTH and PTHrP groups had significantly greater MBF- and RBF-induced mineralizing surface (MS/BS), mineral apposition rate (MAR), and bone formation rate (BFR/BS, Fig F-H). Compared to PTH, PTHrP activated 55% and 50% greater MBF-induced MS/BS and BFR/BS, respectively. MAR did not differ between PTH and PTHrP, indicating similar rates of mineral deposition at each BF site. Conversely, there were similar increases of RBF-induced MS/BS, MAR, and BFR/BS in response to PTH *vs.* PTHrP.

In vivo μCT at wks 0 and 3 (Fig I) demonstrated that PTH and PTHrP (40 μg/kg, n=7-9/group) improved bone volume fraction (BV/TV), thickness (Tb.Th), and number (Tb.N) of tibial trabecular bone, and yielded more plate-like trabeculae indicated by reduced structure model index (SMI, Figs J-M). Compared to PTH, PTHrP led to greater improvement in BV/TV (78% *vs.* 54%), more plate-like trabeculae (-0.8 *vs.* -0.6 in SMI), and less reduction in Tb.N (-1% *vs.* -14%). Increases in Tb.Th did not differ between PTH and PTHrP.

In conclusion, compared to PTH, PTHrP treatment better improved trabecular bone volume and microarchitecture in estrogen deficient rats. This may be due to greater activation of new MBF sites that most efficiently enhance structural integrity of the trabecular network.

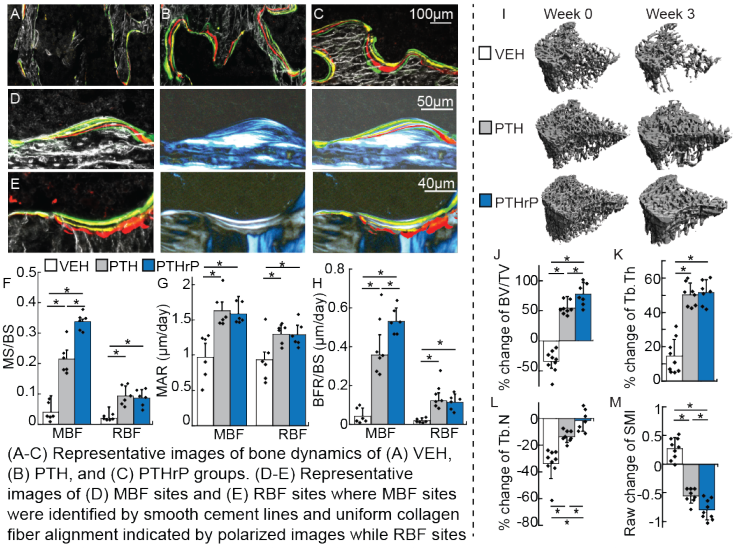

(A-C) Representative images of bone dynamics of (A) VEH, (B) PTH, and (C) PTHrP groups. (D-E) Representative images of (D) MBF sites and (E) RBF sites where MBF sites were identified by smooth cement lines and uniform collagen fiber alignment indicated by polarized images while RBF sites were identified by scalloped cement lines with interrupted collagen fiber alignment. (F) MS/BS, (G) MAR, and (H) BFR/BS of MBF and RBF. (I) Representative trabecular bone images at weeks 0 and 3. (J-M) % change in (J) BV/TV, (K) Tb.Th, (L) Tb.N, and (M) raw change in SMI from registered scans. *p< 0.05 by one-way ANOVA.

Mechanically-Activated Microcapsules Deliver Chondroprotective Agents and Prevent Degeneration in an Inflammatory Microenvironment

Ana P. Peredo[1,2,3], Yun Kee Jo[4], Daeyeon Lee[4], George R. Dodge[2,3], Robert L. Mauck[1,2,3]
[1]Department of Bioengineering, University of Pennsylvania, Philadelphia, PA, [2]McKay Orthopaedic Research Lab, Department of Orthopaedic Surgery, University of Pennsylvania, Philadelphia, PA, [3]Translational Musculoskeletal Research Center, Corporal Michael J. Crescenz Veterans Affairs Medical Center, Philadelphia, PA, [4]Department of Chemical and Biomolecular Engineering, University of Pennsylvania, Philadelphia, PA
anapperedo@gmail.com

DISCLOSURES: GR Dodge (4, 6, 8, 9), RL Mauck (8, *JOR Spine*).

INTRODUCTION: More than 5 million Americans suffer from post-traumatic osteoarthritis (PTOA) – a progressive degenerative condition that arises from an acute joint injury that causes chondrocyte death and persistent inflammation[1]. PTOA mainly affects younger, more active individuals compared to other forms of osteoarthritis, and so requires surgical intervention earlier in life. To treat focal cartilage lesions that occur with PTOA, a number of cell-based repair methods have emerged[2]. After surgery, patients follow a strict rehabilitation protocol that slowly re-introduces weight bearing to stimulate cartilage healing and homeostasis, with return to full activity taking as long as one year[3]. To accelerate tissue healing, bolus injections of pro-chondrogenic and/or anti-inflammatory factors into the synovial space can be used, yet these have limited benefits as they are rapidly cleared out of the joint[3]. To prolong biomolecule activity and promote cartilage repair, we developed mechanically-activated microcapsules (MAMCs) that can be combined with existing surgical repair methods and deliver molecules in response to the loading present during recovery[4]. We previously demonstrated that MAMCs remain stable and retain their mechano-activation potential *in vivo*[5]. Here, we demonstrate the ability of MAMCs to deliver a bioactive anti-inflammatory agent that blocks the loss of extracellular matrix (ECM) molecules in engineered cartilage exposed to inflammatory conditions. Utilizing this drug delivery approach, simultaneous delivery of anti-inflammatory and anabolic factors may accelerate cartilage healing and provide a faster return to full physical activity.

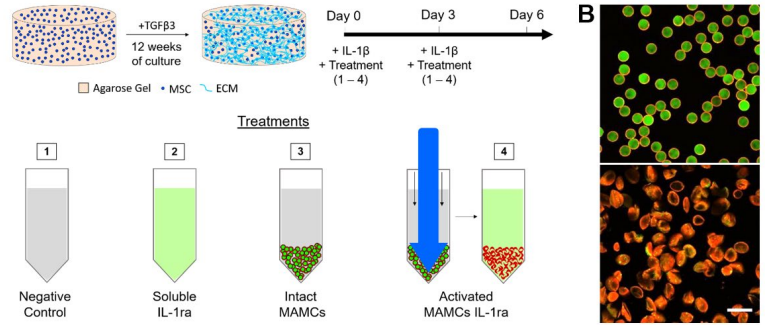

Figure 1. (A) Schematic of experimental groups of cartilage constructs treated with IL-1β. (B) Intact (left) and activated (right) MAMCs (red = PLGA shell, green = IL-1ra solution; scale bar = 100μm).

METHODS: Recombinant IL-1ra was derived from the clinical formulation of Anakinra (Kineret®, Sobi). IL-1ra was purified from its stabilizing agents using a 10kDa-pore-size filter and was resuspended at 350 μg/mL in 0.1% bovine serum albumin PBS solution for encapsulation. MAMCs containing this solution were generated using a glass capillary microfluidic device[6]. Agarose hydrogels (2.25mm thick) were cast between parallel plates and contained bovine mesenchymal stem cells (MSCs) at 60x10^6 cells/mL. Individual constructs were cored using a 4-mm biopsy punch and cultured in chondrogenic media (+TGF-β3) for 12 weeks to generate mature constructs. To create an inflammatory environment, IL-1β (0, 10, or 50 ng/mL) was added to the media with every media change for a total of 6 days after constructs had matured (**Fig. 1A**). With each media change, soluble IL-1ra (unfiltered Anakinra), intact MAMCs, or the contents from activated IL-1ra-containing MAMCs were added to achieve an actual/theoretical concentration of 500 ng/mL (**Fig. 1B**). Gels exposed to IL-1β only (with no treatment) served as negative controls. Media was sampled for nitrite and released glycosaminoglycan (GAG). Gels were mechanically tested (n=4/group), digested for GAG analysis (n=4/group), and histologically sectioned and stained with Safranin O (n=4/group). Normally distributed data was analyzed by one-way ANOVA followed by Tukey's post-hoc; non-normally distributed data was analyzed via Kruskal-Wallis test with Bonferroni post-hoc.

RESULTS: Untreated controls and constructs treated with intact MAMCs showed increasing nitrite levels with increasing IL-1β concentration, while treatment with soluble IL-1ra or the contents of activated MAMCs maintained nitrite at baseline levels (**Fig. 2A**). Exposure to IL-1β also resulted in a marked loss of GAGs from untreated and intact MAMC-treated constructs. Conversely, both soluble IL-1ra and activated MAMCs protected against this loss of ECM with inflammatory challenge (**Fig. 2B, D**). ECM loss from untreated constructs and those treated with intact MAMCs resulted in decreased mechanical properties. Conversely, treatment with soluble IL-1ra and the contents of activated MAMCs preserved the mechanical integrity of constructs, even with inflammatory challenge (**Fig. 2C**).

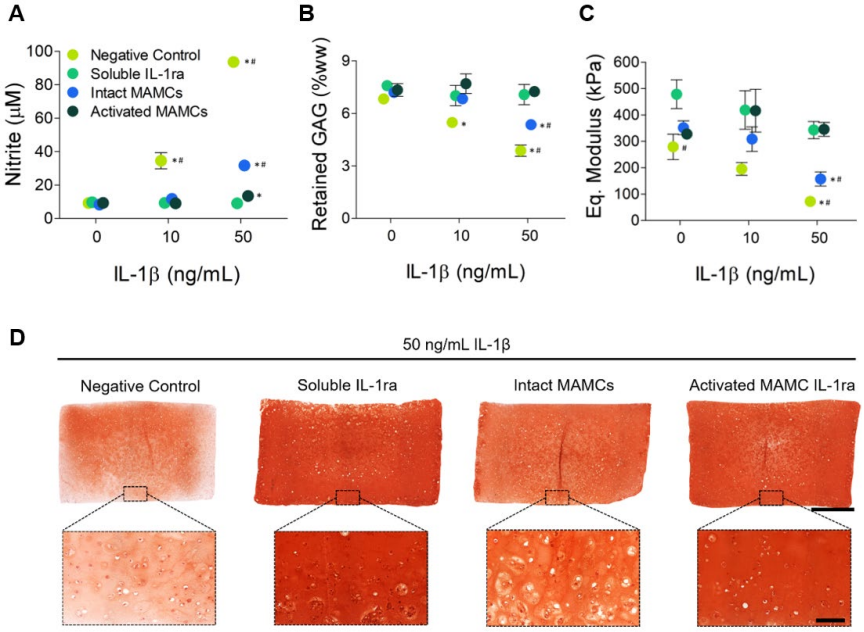

Figure 2. (A) Media nitrate concentration, and (B) GAG content and (C) equilibrium moduli for cartilage-like tissue constructs after 6 days of treatment (*p≤0.05 vs. 0ng/mL; #p≤0.05 vs. Soluble IL-1ra). (D) Safranin O staining of constructs after treatment (scale bar = 1mm, inset scale bar = 100μm).

DISCUSSION: This study demonstrates that MAMCs retain bioactivity post-fabrication and can provide the same benefits as drug injections upon activation. IL-1ra delivered via MAMC activation resulted in similar effects as delivery of the soluble drug formulation. These data support that MAMCs may provide prolonged delivery to attenuate the inflammatory conditions present in the PTOA joint, and may be further tuned, via changes in fabrication, to mechano-activate and deliver therapeutically-relevant molecules on-demand in a sequential manner.

SIGNIFICANCE: Current approaches for the treatment of focal cartilage defects do not recapitulate native cartilage structure and function[7]. This novel drug delivery system has the potential to sequentially deliver therapeutic agents in response to the physiologic loading environment to improve neocartilage quality and ultimately develop functional cartilage.

REFERENCES: [1] Thomas + 2017; [2] Macmull + 2010; [3] Ebert+ 2004; [4] Mohanraj + 2019; [5] Peredo + 2019; [6] Tu + 2012; [7] Dhinsa + 2012.

ACKNOWLEDGEMENTS: This work was supported by the National Institutes of Health (R01 AR071340).

YAP and TAZ coordinate endochondral bone development

Joseph M Collins[1], Nathaniel A. Dyment[1], and Joel D. Boerckel[1]
[1]Departments of Orthopaedic Surgery and Bioengineering, University of Pennsylvania, Philadelphia, PA.

Disclosures: Joseph M Collins (N), Nathaniel A. Dyment (N), Joel D. Boerckel (N)

Introduction: In development, bone formation occurs through two distinct modes: intramembranous and endochondral ossification. Intramembranous ossification involves the direct osteogenic differentiation of local progenitors. In contrast, endochondral ossification initiates from a cartilage anlage, which is replaced by bone through chondrocyte hypertrophy, co-mobilization of osteoprogenitors and blood vessels, and matrix remodeling, culminating in bone formation. The molecular mechanisms which differentially contribute to intramembranous vs. endochondral ossification during embryonic development are poorly understood. We recently reported that YAP and TAZ combinatorially promote skeletal development in vivo[1] with homozygous deletion of both genes causing perinatal lethality. At the 2019 ORS meeting, we reported that YAP and TAZ play key roles in limb development *in utero*. Deletion of YAP and TAZ from Osterix1-expressing cells delayed and impaired development of the primary ossification center (POC), where bone formation occurs through endochondral ossification, but only moderately affected the bone collar, where bone formation occurs through intramembranous ossification[2]. Here, we sought to determine the underlying cellular mechanisms.

Materials and Methods: We conditionally deleted YAP and TAZ from Osx1-expressing cells ($YAP^{fl/fl}$;$TAZ^{fl/fl}$;Osx1-GFP::Cre, hereafter KO^{osx}) and evaluated embryonic humeral bone development in comparison to littermate wild type ($YAP^{fl/fl}$;$TAZ^{fl/fl}$, hereafter WT) and Osx1-GFP::Cre wild type ($YAP^{WT/WT}$;$TAZ^{WT/WT}$;Osx1-GFP::Cre, hereafter WT^{osx}) controls.[1,2,3] Embryos were harvested at 15.5 days (E15.5) and 17.5 days (E17.5) post-conception. Embryonic forelimbs were processed by cryohistology. Protein and GFP fluorophore localization were performed by immunofluorescent staining and quantified in ImageJ using defined regions of interest. Comparisons were made using Student's t-test. A p-value less than 0.05 was considered significant. Each embryo was considered an independent sample. All procedures were performed with IACUC approval.

Results: Previously, we found that Osx-conditional YAP/TAZ deletion significantly reduced the cell density of the POC, but only modestly reduced cell density in the bone collar. To determine whether YAP/TAZ deletion specifically altered the mobilization of the targeted osteoprogenitors, we evaluated Osx1-GFP-labeled cells in both WT^{osx} and KO^{osx} mice. YAP/TAZ deletion reduced GFP^+ osteoprogenitors in the POC but only moderately reduced the GFP^+ cell density in the bone collar (Fig. 1, green). Next, to determine the effects of YAP/TAZ deletion on osteogenesis in these regions of interest, we evaluated alkaline phosphatase (ALP) activity and mineralized matrix deposition. YAP/TAZ deletion significantly reduced ALP activity in the POC, but did not alter ALP activity or mineralization in the bone collar (Fig. 2).

In addition to osteoblast-lineage cells, Osx1-GFP::Cre is also expressed in hypertrophic chondrocytes. Therefore, we next evaluated chondrocyte hypertrophy and cartilage matrix remodeling in WT and cKO mice at E17.5 (Fig. 3A,B). Using WT mice, we identified three distinct subzones of the hypertrophic cartilage, based on morphology and Collagen-10 immunolocalization, which we term the hypertrophic initiation, maturation, and remodeling zones. YAP/TAZ deletion had no effect on hypertrophic initiation, but significantly lengthened the hypertrophic maturation zone. Most notably, YAP/TAZ deletion caused hypertrophic chondrocyte persistence and failure to resorb, leading to an extended, cone-shaped hypertrophic remodeling zone, characterized by Collagen 10-rich extracellular matrix and high intracellular immunolocalization of the vascular permeability factor, VEGF-A.

It was recently reported that invading neovascular capillaries are primarily responsible for hypertrophic matrix resorption.[4] Therefore, we next immunostained for the endothelial cell marker, endomucin, and found that YAP/TAZ deletion from $Osx1^+$ cells disorganized and reduced the number of cartilage-resorbing capillaries, which localized only near the outer base of the cone-shaped hypertrophic remodeling zone (Fig. 3C,D). Consistent with excess VEGF-A expression by the hypertrophic chondrocytes, the vasculature within the POC was also disorganized and leaky, as evidenced by extravascular red blood cell accumulation. Finally, vessels that did successfully migrate into the POC of the KO^{osx} limbs were substantially less associated with GFP^+ osteoprogenitors (Fig. 1B).

Discussion: Together, these data suggest that YAP and TAZ in Osx1-expressing cells are critical for endochondral primary bone formation, but are dispensable for intramembranous ossification in the bone collar, raising questions about the physiological roles of YAP and TAZ in osteogenic differentiation, per se. These data further identify crucial roles of YAP and TAZ in cartilage maturation, hypertrophic matrix remodeling by cartilage-resorbing capillaries, neovascular integrity, and osteoprogenitor mobilization. YAP/TAZ-dependent osteoprogenitor mobilization may occur by cell non-autonomous recruitment and/or cell-autonomous migration and/or proliferation. Collectively, these data underscore the importance of endothelial-chondrocyte and endothelial-osteoprogenitor cell crosstalk during limb morphogenesis.

References

1. Kegelman+ FASEB J 2018. 2. Collins+ ORS 2019. 3. Rodda+ Development 2006. 4. Romeo+ Nature Cell Biology 2019.

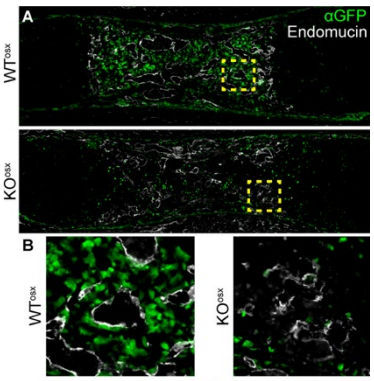

Figure 1. E17.5 Humeri immunostained for Endomucin and GFP

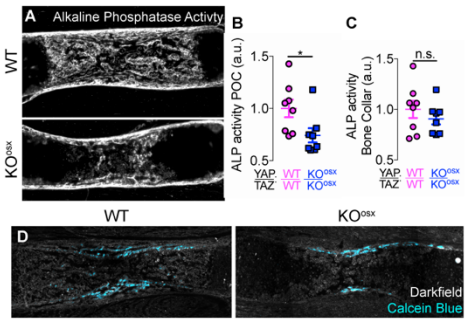

Figure 2. **(A)** Representative E17.5 WT and KOosx humeri stained for Alkaline Phosphatase Activity (ALP). **(B,C)** Region of interest quantification of E17.5 ALP activity. **(D)** Representative E17.5 WT and KOosx humeri stained for Calcein blue.

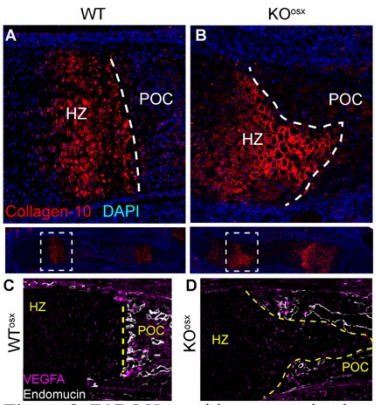

Figure 3. E17.5 Humeri immunostained for **(A,B)** Collagen-10 and DAPI and **(C,D)** VEGFA and Endomucin.

Leveraging Hedgehog Signaling to Improve Tendon-to-Bone Repair

Timur B. Kamalitdinov[1], Keitaro Fujino[1,2], Xi Jiang[1], Mary Kate Evans[1], Miltiadis H. Zgonis[1], Andrew F. Kuntz[1], Nathaniel A. Dyment[1]
[1]University of Pennsylvania, Philadelphia, PA, [2]Osaka Medical College, Osaka Prefecture, Japan.
timkam@seas.upenn.edu

Disclosures: None

INTRODUCTION: Growth and development studies have defined a critical role for Hedgehog (Hh) signaling in promoting the formation and maturation of fibrocartilage in zonal tendon-to-bone insertions (i.e. entheses) [1]. Despite this important developmental role, it is not known whether the Hh pathway plays a similar function in adult tendon-to-bone repair, representing a significant gap in knowledge. Unfortunately, traditional tendon-to-bone repair surgeries do not recreate a zonal insertion. However, ligament injuries reconstructed with a tendon graft passed through a bone tunnel can result in zonal insertions [2,3]. In this setting, amplifying α-smooth muscle actin (αSMA)-expressing bone marrow progenitor cells (BMPCs) contribute to tunnel integration by forming zonal fibrocartilaginous attachments [2]. Using our established murine anterior cruciate ligament (ACL) reconstruction model, our objective is to genetically and pharmacologically modulate the Hh pathway in these αSMA-expressing cells to determine the effect of Hh signaling on tunnel integration in adult repair. Our hypothesis is that the Hh pathway promotes tendon-to-bone integration in the adult, similar to growth and development.

METHODS: All animals and procedures were approved by UPenn's IACUC. Experimental Design. ACL reconstructions (ACLR) were performed on 51 transgenic mice. *Genetic Hh Inhibition Study*. αSMACreERT2 mice [4] that target the amplifying progenitor pool that gives rise to zonal attachments [2] were crossed with Smoothened flox ($Smo^{flox/flox}$) mice [5] (Smo^{tm2Amc}/J) to yield SMACre;$Smo^{flox/flox}$ (SmoKO) experimental mice to decrease Hh signaling and $Smo^{flox/flox}$ control genotypes. Mice were sacrificed at 28 days post-surgery and assigned to cryohistology (n = 5/group). *Genetic Hh Activation Study*: αSMACreERT2 mice were crossed with constitutively active SmoM2 mice [6] (Gt(ROSA)26$Sor^{tm1(Smo/EYFP)Amc}$/J) to yield SMACre;SmoM2 (SmoCA) mice with increased Hh signaling and Cre-negative control genotypes. Mice were sacrificed at 28 days post-surgery and assigned to cryohistology (n = 4-6/group). Tamoxifen injections (80 mg/kg) were given on the day of surgery then every other day for a total of five injections to ablate Smo or constitutively activate Smo in αSMA-expressing cells. *Pharmacologic Hh Activation Study*: Mice received either Hh agonist (20mg/kg Hh-Ag1.5) or PBS injections 5X per week. Mice were assigned to cryohistology (n = 4-6/group) at 7- or 28-days post-surgery and biomechanics (n = 5-6/group) at 28 days post-surgery. Demeclocycline and EdU were given 1 day before sacrifice to help define mineralized fibrocartilage (MFC) zones of attachments and label proliferating cells, respectively. ACL Reconstruction. The ACL was excised near the femoral insertion. The tibial and femoral tunnels were drilled with 27G needles. A tail tendon autograft was passed through the tunnels and anchored to outer cortices with stainless steel washers [2,3]. Mineralized Cryohistology. Knees were fixed in formalin, embedded, sectioned undecalcified with cryofilm, and imaged on the Zeiss Axio Scan.Z1. Tunnel Pullout Test. Femurs were potted in PMMA and gripped such that the tunnel was parallel to the linear actuator. A suture was passed through the washer and loaded to failure. Image Quantification. MFC area/total length and MFC interface length/total interface length were measured to assess the extent of zonal integration while EdU+ cells in expanding marrow were measured to assess amplification of the progenitor pool. Statistics. Experimental and control groups were compared via Student's t-tests ($p < 0.05$). Data presented as Mean ± SD.

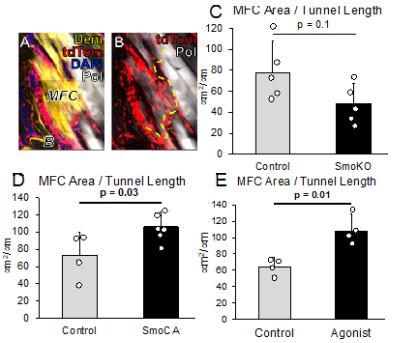

Fig. 1: Hh promoted tendon to bone integration.

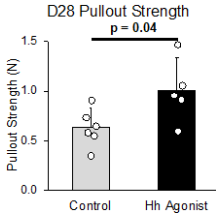

Fig. 2: Hh agonist improved tunnel integration strength.

RESULTS: SmoKO, SmoCA, and Hh agonist-treated groups did not display any adverse systemic effects throughout the duration of the study. Hh Pathway Positively Regulated Tunnel Integration and Strength. When targeting the SMA-expressing amplifying progenitor pool, SmoKO mice had a 40% decrease in MFC area in the bone tunnels compared to controls at day 28 ($p = 0.1$) (Fig. 1C). SmoCA mice had 45% greater MFC compared to controls at day 28 ($p < 0.05$) (Fig. 1D). Mice that received Hh agonist for four weeks had 70% more MFC at the tunnel interface ($p < 0.05$) (Fig. 1E) resulting in 60% greater pullout strength ($p < 0.05$) (Fig. 2). Hh Pathway Activation Increased Attachment Sites Partially Through Proliferation of the Progenitor Pool. Since agonist-treated mice showed greater MFC formation at 28 days, we next sought to identify the mechanism that led to this improved integration. MFC area can be dictated by an increased number of attachments in the tunnel or increased mineral apposition within each attachment. We found that 34% more of the tunnel interface contained MFC (i.e., MFC interface length/total interface length) than controls after 28 days ($p = 0.1$) (Fig. 3A). Additionally, there were 50% greater EdU+ cells in the expanding bone marrow adjacent to the graft in agonist treated mice after 7 days ($p = 0.1$) (Fig. 3B).

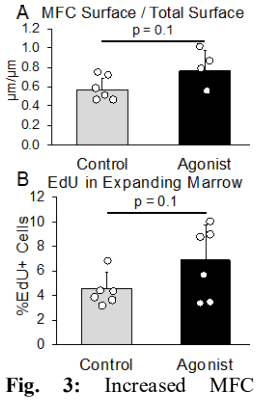

Fig. 3: Increased MFC surface (A, Day 28) partially due to expansion of the progenitor pool (B, Day 7).

DISCUSSION: Following ACL reconstruction, BMPCs must expand and infiltrate the periphery of the tendon graft, then assemble collagen and proteoglycan-rich fibrocartilage to properly anchor tendon to adjacent bone. In the present study, we demonstrated that Hh signaling positively regulated mineralized fibrocartilage formation (Fig. 1) leading to greater pullout strength (Fig. 2) and a higher percentage of the tunnel interface being mineralized (Fig. 3A), which can partially be explained by increased proliferation of the progenitor pool (Fig. 3B). While Hh signaling improves fracture repair via improved osteogenesis and angiogenesis [7], here we found that Hh improves fibrocartilage formation similar to enthesis development. Our results indicate that the increased MFC formation may, at least partially, be due to increased proliferation of the BMPCs. However, Hh could also promote fibrocartilage differentiation. Different agonist delivery timing windows will need to be investigated to assess this important proliferation vs. differentiation question.

SIGNIFICANCE/CLINICAL RELEVANCE: An improved understanding of the signaling pathways that regulate zonal insertion formation in the adult will be crucial to developing new therapies to improve repair outcome. If the Hh pathway is harnessed therapeutically, it could result in a paradigm shift in the clinical treatment of these debilitating injuries, especially in more challenging scenarios that require reformation of the enthesis, such as rotator cuff repair.

REFERENCES: 1. Dyment et al., *Dev Biol*, 2015; 2. Kamalitdinov et al., *JOR*, 2019; 3. Hagiwara et al., *Ann N Y Acad Sci*, 2019; 4. Grcevic et al., *Stem Cells*, 2012; 5. Long et al., *Development*, 2001; 6. Liu, et al., *PLoS ONE*, 2013; 7. McKenzie et al., *JOR*, 2019.
ACKNOWLEDGEMENTS: Work supported by NIH R00AR067283, NIH P30AR069619, NIH R01AR076381, the Thomas B. McCabe and Jeannette E. Laws McCabe Fund at UPenn, and startup funds from the Department of Orthopaedic Surgery at UPenn.

The developmental phenotype of the great toe in fibrodysplasia ossificans progressiva

O Will Towler[1,4], Frederick S Kaplan[1,2,4], Eileen M Shore[1,3,4]

Departments of [1]Orthopaedic Surgery, [2]Medicine, and [3]Genetics, and [4]The Center for Research in FOP & Related Disorders, Perelman School of Medicine, University of Pennsylvania, 3450 Hamilton Walk, 309A Stemmler Hall, Philadelphia, PA 19104, USA.

Abstract

Fibrodysplasia ossificans progressiva (FOP) is a rare genetic disorder in which extensive heterotopic ossification (HO) begins to form during early childhood and progresses throughout life. Although HO does not occur during embryonic development, children who carry the *ACVR1*^{R206H} mutation that causes most cases of FOP characteristically exhibit malformation of their great toes at birth, indicating that the mutation acts during embryonic development to alter skeletal formation. Despite the high prevalence of the great toe malformation in the FOP population, it has received relatively little attention due to its clinically benign nature. In this study, we examined radiographs from a cohort of 41 FOP patients ranging from 2 months to 48 years of age to provide a detailed analysis of the developmental features, progression, and variability of the great toe malformation of FOP, which include absent skeletal structures, malformed epiphyses, ectopic ossification centers, malformed first metatarsals and phalangeal fusion.

Effects of chondrogenic priming duration on mechanoregulation of engineered cartilage anlagen

Emily A. Eastburn[1,4*], Anna M. McDermott[1,2,3*], Daniel J. Kelly[3†], Joel D. Boerckel[1,2,4†]
[1]McKay Orthopaedic Research Laboratory, Department of Orthopaedic Surgery, University of Pennsylvania, Philadelphia, PA.
[2]Department of Aerospace and Mechanical Engineering, University of Notre Dame, Notre Dame, IN.
[3]Trinity Centre for Biomedical Engineering, Trinity College Dublin, Dublin, Ireland.
[4]Department of Bioengineering, University of Pennsylvania, Philadelphia, PA.

Disclosures: Emily A. Eastburn (N), Anna M. McDermott (N), Daniel J. Kelly (N), Joel D. Boerckel (N)

Introduction: Bone formation during development and repair occurs through endochondral ossification[1]. The bone is initially templated by chondrocytes which then mature and hypertrophy. Subsequently, hypertrophic cartilage supports neovascular invasion and enables bone formation. Mechanical cues direct bone formation in development[2]. Previously, we developed a development-mimetic bone regeneration strategy to repair critical sized defects. We demonstrated that delaying mechanical cues enhanced repair[3], suggesting there is a critically mechanoresponsive cell state in the chondrocyte lineage during the endochondral program. However, which cell types are the critical mechanoresponders remains unclear. The goal of this study was to examine the effect of chondrocyte maturation on the cell and tissue response to dynamic loading. Here, we hypothesized that later stages of chondrocyte maturation and dynamic loading would increase the mechanical properties due to increased mechanosensitivity of these cells.

Materials and Methods: Human bone marrow stromal cells (hMSCs) were encapsulated in fibrin hydrogels and loaded into a bioreactor. Hydrogels were primed in chondrogenic media for 0, 2, 4, or 6 weeks before 2 weeks of dynamic compressive loading. Each hydrogel had a time-matched free-swelling control. At the end of the loading period hydrogels were analyzed for mechanical properties, biochemical content, and matrix production. Differences between groups and time points were evaluated by two-way ANOVA.

Results: Previously, we found that delayed loading *in vivo*, initiated after the onset of chondrocyte hypertrophy, accelerated endochondral ossification and enhanced neovascularization[3,4]. We used an *in vitro* model to study the effect of load timing on each tissue in isolation to determine the mechanoresponsiveness of chondrocytes during maturation. First, we determined the role of the chondrogenic priming and dynamic mechanical loading on construct mechanical properties. Following completion of the final loading cycle for each group, we tested the mechanical properties in unconfined compression, in comparison to time-matched free-swelling controls. Both equilibrium and dynamic modulus significantly increased with increasing chondrogenic priming time (Fig. 1). Dynamic loading significantly increased the equilibrium modulus under conditions of 4 weeks of priming and dynamic modulus after both 4 and 6 weeks of priming.

To determine the cause of the increased in mechanical properties, we first quantified the cellular and extracellular matrix content of the constructs at the end of their loading cycles. DNA, GAG, and collagen content all increased with increased chondrogenic priming, but there was no difference between loaded and free-swelling controls at any timepoint (data not shown). Together, these data suggested there was another reason behind the load-induced changes in construct mechanical properties.

In order to understand the increase in mechanical properties with increasing priming time we looked at matrix deposition over different stages of endochondral ossification. First, we analyzed chondrogenic matrix deposition. Alcian blue staining showed minor increases over priming time, but no appreciable differences between loaded and non-loaded groups (data not shown). Additionally, we looked at immunohistochemistry staining of Col2a1 (Fig. 2). At 0 and 2 weeks priming, Col2a1 staining was minimal regardless of loading conditions. In free-swelling constructs after 4 and 6 weeks of priming, Col2a1 staining was more prominent in the construct core compared to dynamic compression. Next, to determine the effects of loading on chondrocyte hypertrophy, we looked at immunohistochemistry staining of Col10a1 (Fig. 3). Dynamic compression exhibited lower staining under all priming conditions. The free-swelling conditions showed increased staining in the core similar to Col2a1 staining, while loaded groups had limited core staining. Lastly, we looked at osteogenic matrix composition through alizarin red staining (data not shown). Limited alizarin red staining was found only after 4 weeks priming in the FS conditions, whereas the DC group did not see any staining until 6 weeks priming.

Discussion: Together, these data demonstrate that chondrocyte lineage progression has a direct impact on the tissue mechanics of hydrogels *in vitro*. Matrix deposition results suggest that, with further chondrocyte lineage progression and dynamic loading, non-uniform staining of collagen primarily in the periphery of the hydrogels lead to stiffer matrices. This data, along with our previous data[3,5,6], suggest that delayed mechanical loading coupled with later stage chondrocyte maturation leads to an increase in mechanical properties, by altering extracellular matrix organization and distribution.

References: [1] Provot+ Osteoporosis, 2013; [2] Felsenthal & Zelzer, Development, 2017; [3] McDermott+ STM, 2019; [4] Boerckel+ PNAS, 2011; [5] Thorpe+ Ann. Biomed. Eng., 2010; [6] Luo+ Biomed. Mater., 2015

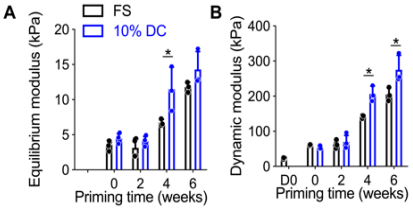

Figure 1. Mechanical properties. **(A)** Equilibrium modulus, **(B)** dynamic modulus.

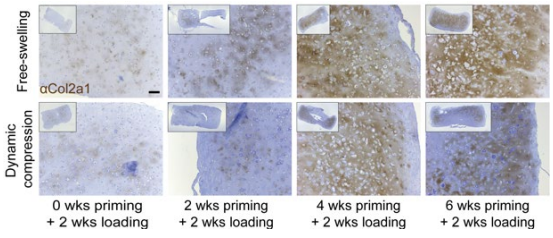

Figure 2. Immunohistochemistry for Col2a1 with hematoxylin counterstain.

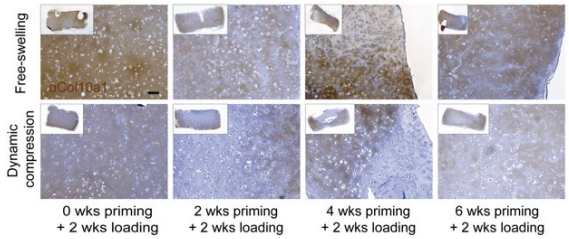

Figure 3. Immunohistochemistry for Col10a1 with hematoxylin counterstain.

Comparative Tribology: Articulation-Induced Cartilage Rehydration Across Species

Meghan E. Kupratis[1], Ahmed E. Gure[3], Jamie M. Benson[1], Kyla F. Ortved[4], David L. Burris[2], Christopher Price[1,2]
[1]Biomedical Engineering, [2]Mechanical Engineering, University of Delaware, [3]Bioengineering, University of Texas at Arlington, 4Clinical Studies, University of Pennsylvania School of Veterinary Medicine

Introduction: Osteoarthritis is a degenerative joint disease characterized by pathological degradation of cartilage extracellular matrix, leading to impaired load support and lubrication.[1] To understand the functional consequences of these changes, a variety of preclinical animal models are used in *ex vivo* biomechanical studies. Recent work from our group using the convergent stationary contact area (cSCA) configuration has demonstrated that sliding alone serves to recover interstitial pressure and lubrication lost to static compression through a mechanism we termed '*tribological rehydration.*'[2] We have characterized tribological rehydration extensively using a bovine model, demonstrating sliding-driven reversals of load-induced fluid exudation and maintenance of remarkably low friction coefficient values (μ_k < 0.02) in the absence of unloading, contact migration, or boundary lubricants.[2-4] However, direct comparisons of cartilage sliding mechanics among preclinical animal models are limited. Additionally, it is unknown how differences in geometric scaling and cartilage material properties may influence tribological rehydration in the cSCA. In this study, we demonstrate the universality of tribological rehydration across a number of mammalian species and leverage inter-species variability to define foundational relationships between cartilage's material properties and tribological performance.

Methods: Osteochondral explants were extracted from equine, bovine, porcine, ovine, and caprine femoral condyles.[4] Explant diameters were defined to generate the curved-on-flat contact necessary for the cSCA. Contact area vs. applied force calibrations were performed to enable consistent application of 0.25±0.05 MPa contact stresses.[3] Tribology tests began with a run-in period to a (species-dependent) target deformation under static load followed by four minutes of reciprocal sliding at 80 mm/s. Subsequently, a high-to-low speed sweep characterization was performed, consisting of 4 minutes of sliding at 80, 60, 40, 30, 20, and 10 mm/s, each initiated after the targeted deformation established in the run-in period was reached under static loading. Compression and strain changes during sliding, friction coefficients, and the temporal dynamics of these changes were quantified at each sliding speed. Hertz biphasic theory was used to estimate compressive and tensile moduli (E_{y-} & E_{y+}) and permeability parameters (k_0 & M) for each explant using microindentation.[5] Explants were bisected through the cSCA to measure cartilage thickness (h) and radius of curvature. Deformation (δ) and kinetic friction coefficients (μ_k) were recorded, and tissue strains ($\varepsilon = \delta/h$) calculated. Mixed effects (ME) models were used to fit tribological outcomes as functions of sliding speed and explant identity/species, and Pearson correlations were performed among all outcome parameters.

Results: Strain recovery increased significantly (p < 0.001) and similarly (no diff. in slopes, p = 0.32) with sliding speed among all species (**Fig. 1A**). End-of-sliding friction coefficients decreased significantly with sliding speed (**Fig. 1B**); however,

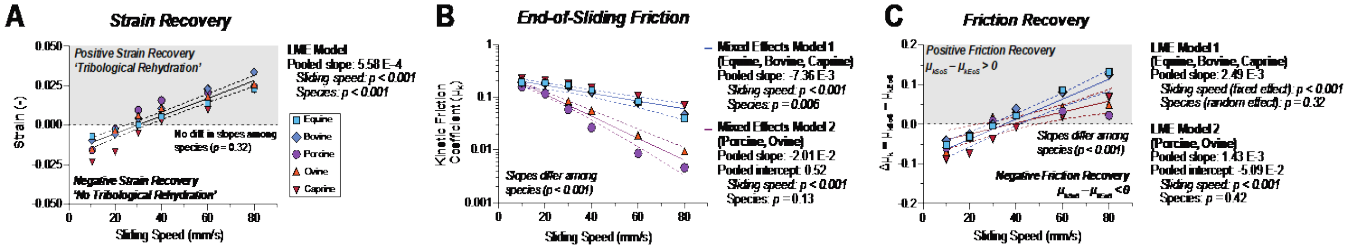

two friction responses emerged among species (equine, bovine, & caprine vs. porcine. & ovine). Friction recovery increased significantly with sliding speed, but as with other friction-based outcomes, relative friction recovery varied among species (**Fig. 1C**). In Model 1, a steeper slope of sliding speed-dependent friction recovery indicates greater proportional friction recovery with increasing speed for equine, bovine, and caprine specimens relative to porcine and ovine specimens.

Figure 1: Mixed effects models of strain recovery **(A)**, end-of-sliding friction coefficients **(B)**, and friction recovery **(C)**.

Discussion: In this comparative study, we demonstrated the universality of sliding-induced fluid recovery across five common model species. Cartilage from all species tested exhibited robust and highly consistent tribological rehydration in the cSCA, with sliding-induced strain recovery and lubrication maintained at sliding speeds ≥30 mm/s in all specimens. Sliding speed-dependent strain recovery was remarkably consistent among species, suggesting that articulation-induced fluid recovery is a universal cartilage behavior. However, the appearance of diverging friction behavior despite the consistency of tribological rehydration suggests a distinct role of the articular surface composition in the friction response. Our ongoing analyses examining correlative relationships between cartilage material properties and cSCA tribomechanics will further elucidate how variation in cartilage matrix structure influences the lubrication of both healthy and degenerated tissues.

References: [1]Bonnevie, *JOR* 2018. [2]Moore, *OA&C* 2017. [3]Farnham, *JMBBM* 2020. [4]Burris, *Trib Lett* 2019. [5]Moore, *J Biomech Eng* 2016.

Stat3 Mediates the Function of mTORC1 in Fibrovascular Scar Formation During Postnatal Tendon Development

Na Rae Park[1] and Kyu Sang Joeng[1]
[1]University of Pennsylvania, Philadelphia, PA
Email of Presenting Author: Na.Park@pennmedicine.upenn.edu

Disclosures: Na Rae Park (N), Kyu Sang Joeng (N)

INTRODUCTION: Tendon injuries are challenging clinical problems due to slow, incomplete healing with fibrovascular scar formation, which reduces tendon function and causes chronic complications such as pain and tendon ruptures. The limited understanding of the regulatory mechanisms underlying fibrovascular scar formation hinders the development of effective treatment modalities for tendon diseases. Our recent study showed that constitutive activation of mTORC1 signaling during postnatal tendon development caused fibrovascular scar-like phenotypes in tendons, including disorganized ECM, high cellularity, and neovascularization [1]. However, the downstream mechanism mediating mTORC1 function in fibrovascular scar formation is not clear. Stat3 is a transcription factor and plays a crucial role in fibrosis and inflammation via the regulation of cell proliferation and ECM organization [2]. Interestingly, a previous study showed that Stat3 can be activated by mTORC1 signaling [3]. This study aims to determine Stat3 as a mediator of mTORC1 function in fibrovascular scar formation in tendons.

METHODS: All procedures were approved by UPenn's IACUC. To genetically determine Stat3 as a mediator of mTORC1 function in fibrovascular scar formation in tendons, we performed a genetic rescue experiment by generating three types of the tendon-specific deficient mouse: 1) *Scx-Cre; Tsc1*$^{fl/fl}$ (tendon-specific mTORC1 gain-of-function mouse model), 2) *Scx-Cre; Stat3*$^{fl/fl}$ (tendon-specific Stat3 knockout mouse model), and 3) *Scx-Cre; Tsc1*$^{fl/fl}$*; Stat3*$^{fl/fl}$ (tendon-specific Tsc1 and Stat3 double knockout mouse model for rescue experiment). Histological analyses were conducted on patellar and Achilles tendons at 1 month of age. RNA sequencing analysis was used to examine gene expression changes in Achilles tendons of wildtype and *Scx-Cre; Tsc1*$^{fl/fl}$ mice. Primary tenocytes were isolated from tail tendon to perform *in vitro* molecular studies using monolayer cell culture. A western blotting experiment was performed to examine the alteration in phosphorylated protein *in vitro*. All quantitative data were analyzed using student's t-test.

RESULTS: Fibrovascular scar-like phenotypes in *Scx-Cre; Tsc1*$^{fl/fl}$ (mTORC1 gain-of-function mouse model) prompted us to examine the transcriptional changes of fibrotic markers and metalloproteinases (*Mmps*). Consistent with histological data, *Scx-Cre; Tsc1*$^{fl/fl}$ mouse exhibited the dramatically increased expression of *Col3a1*, *Fibronectin1* (*Fn1*), *Tenascin C* (*Tnc*), and *Metalloproteinases* (*Mmps*) in tendon, which are highly expressed in pathogenic tendon condition such as tendon repair and tendinopathy (Fig. 1). These data suggest the function of mTORC1 in the transcriptional gene regulation during fibrovascular scar formation. Stat3 is involved in transcriptional gene regulation, and mTORC1 can activate Stat3 via phosphorylation of serine-727 (S727). We performed western blot analysis using primary tendon cells from wildtype and *Scx-Cre; Tsc1*$^{fl/fl}$ to determine if mTORC1 can activate Stat3 in tendons. The serine-727 phosphorylation of Stat3 (Stat3 S727), which is mTOR dependent, was significantly increased in tendon cells from *Scx-Cre; Tsc1*$^{fl/fl}$ mouse. The mTORC1 independent tyrosine-705 phosphorylation of Ststs3 (Stat3 Y705) tended to increase in *Scx-Cre; Tsc1*$^{fl/fl}$ cells (Fig. 2). These results suggest that Stat3 can be a downstream target of mTORC1 in tendons. To genetically confirm that Stat3 is a downstream mediator of mTORC1 function in fibrovascular scar formation, we perform a genetic rescue experiment in which we can test if the deletion of Stat3 can rescue fibrovascular scar-like phenotypes caused by constitutive activation of mTORC1 signaling. We first generated the Stat3 loss-of-function mouse model (*Scx-Cre; Stat3*$^{fl/fl}$) to determine the function of Stat3 in tendon development. *ScxCre; Stat3*$^{f/f}$ mouse showed normal growth in tendons (Fig. 3A and 3B, second panel). We next generated a conditional double knockout mouse (*Scx-Cre; Tsc1*$^{fl/fl}$*; Stat3*$^{fl/fl}$) model to perform a genetic rescue experiment. Very interestingly, our histological analysis showed that the deletion of Stat3 noticeably rescued the fibrovascular scar-like phenotypes in the mTORC1 gain-of-function mouse (Fig. 3A and 3B, third and fourth panel). This data strongly supports our hypothesis that Stat3 mediates mTORC1 function in tendon fibrovascular scar formation.

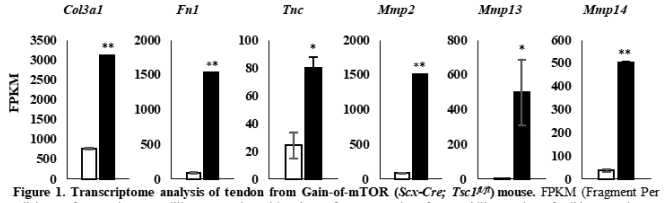

Figure 1. Transcriptome analysis of tendon from Gain-of-mTOR (*Scx-Cre; Tsc1*$^{fl/fl}$) mouse. FPKM (Fragment Per Kilobase of transcript per Million mapped reads) values of RNA-seq data from Achilles tendon of wildtype and *Scx-Cre;Tsc1*$^{fl/fl}$ mice in *Col3a1*, *Fibronectin1* (*Fn1*), *Tenascin C* (*Tnc*), and *Metalloproteinases* (*Mmps*). (White bar indicates wildtype mice, Black bar indicates *ScxCre; Tsc1*$^{fl/fl}$ mice, *indicate $P<0.05$ and **indicate $P<0.001$ between genotypes, n=3)

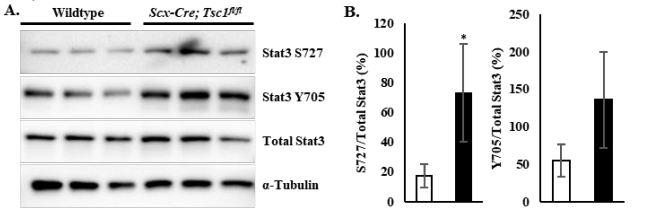

Figure 2. Gain-of-mTOR activated Stat3 signaling in primary tendon cells. Western blots to assess Stat3 signaling, phosphorylation of S727 is mTOR dependent and phosphorylation of Y705 is mTOR independent, activation in *Scx-Cre; Tsc1*$^{fl/fl}$ cells (A). Quantification of the western blot bands (B). (White bar indicates wildtype cells, Black bar indicates *ScxCre; Tsc1*$^{fl/fl}$ Cells, *indicate $P<0.05$ between genotypes, n=3)

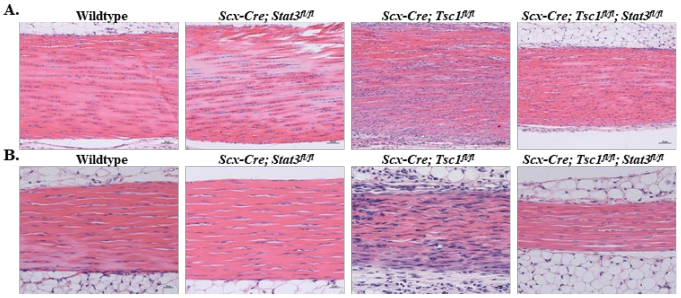

Figure 3. Tendon phenotype of wildtype, *Scx-Cre; Stat3*$^{fl/fl}$, *Scx-Cre; Tsc1*$^{fl/fl}$, and *Scx-Cre; Tsc1*$^{fl/fl}$*; Stat3*$^{fl/fl}$ mouse at 1 month old. H&E stained Achilles tendon section (A) and patellar tendon section (B).

DISCUSSION: Our study suggests that mTORC1 can be a major biological mechanism regulating fibrovascular scar formation in pathogenic tendon condition. Our cell and mouse genetic data strongly support Stat3 is a mediator of mTORC1 function in fibrovascular scar formation. The further molecular study will be required to confirm that the direct molecular interaction between mTORC1 and Stat3. We only tested our hypothesis using the developmental model. Further investigations with healing or repair models will be necessary to confirm the precise function of mTOR/Stat3 signaling in fibrovascular scar formation during tendon healing.

SIGNIFICANCE/CLINICAL RELEVANCE: This study will contribute to the understanding of regulatory mechanisms for fibrovascular scar formation, which may provide the basis and therapeutic approach for pathogenic tendon conditions such as tendon injury repair and tendinopathy.

REFERENCES: [1] Lim+, 2017 [2] Kasembeli+, 2018 [3] Saleiro+, 2015

ACKNOWLEDGEMENTS: This work is partly supported by the National Institutes of Health under award numbers K01AR069002 (KSJ). We thank to Dr. Ronen Schweitzer for providing *Scx-Cre* mouse line.

Scaffold-free 3D Tendon Cell Culture Using Mouse Tendon Cells

Yeonju Lee[1], Na Rae Park[1], Nathaniel A. Dyment[1], Kyu Sang Joeng[1]
[1]University of Pennsylvania, Philadelphia, PA
Email of Presenting Author: Yeonju.Lee@pennmedicine.upenn.edu

Disclosures: Yeonju Lee (N), Na Rae Park (N), Nathaniel A. Dyment (N), Kyu Sang Joeng (N)

INTRODUCTION: Standard two-dimensional (2D) cell culture has been widely used for in vitro studies to understand molecular mechanisms. However, tenocyte phenotype is not well-maintained in monolayer culture and it is difficult to study ECM organization and morphological maturation of cells without a 3-dimensional (3D) environment. To overcome this limitation, several 3D tendon cell cultures were developed by suture model [1] and Flexcell tissue culture plate system [2]. Based on these 3D tendon culture studies, we developed a scaffold-free 3D tendon culture system using mouse tenocytes, which can be used for genetic manipulation of specific target genes.

METHODS: All procedures were approved by UPenn's IACUC. Tendon cells were isolated from mouse tail after one hour digestion with type I collagenase. Isolated tendon cells were grown in 20% FBS and 2mM L-glutamine in a-MEM medium. We generated growth channels with 3D-printed-mold and the 2% agar in 6-well plate (Fig 1A). To enhance the attachment of the tendon cells to anchor, the anchors were surrounded by hydrophilized PCL-scaffolds. Growth area and PCL-scaffolds were coated with fibronectin. To generate the 3D tendon cell structure, tendon cells were seeded on the fibronectin-coated growth area at 2.5 x 10^6 cells/well with 20% FBS in a-MEM medium. To differentiate 3D Tendon cells, TGF-β was treated every two days after seeding. Histological analysis was conducted on 3D tendon structure at various time points (day 0, 3, 7, 14, and 21 after TGF-β treatment). qRT-PCR analysis was examined tendon related gene markers in 3D tendon structures at various time points (day 0, 3 and 7 after TGF-β treatment). To test the genetic gene manipulation by adenovirus system in 3D tendon structure, 3D tendon structures generated using cells from Rosa26-Ai9 mouse and Tsc1f/f mouse. Then, 3D tendons were infected with Ad-CMV-Cre-eGFP. All quantitative data were analyzed using student's t-test

RESULTS: We can generate six 3D tendons (7-8 mm length and 0.5-0.8 mm thickness) using tendon cells from one mouse tail (Fig. 1B). The thickness of 3D tendon structure was dramatically decreased without TGF-β 3D tendon cell (Fig. 1C). This data suggests that TGF-β treatment is essential to maintain 3D tendon structure. Interestingly, we found outer layer of 3D tendon became tendon-like structure (Fig. 1D, blue Box). This tendon-like structure also showed the similar tissue maturation process that can be found during postnatal mouse tendon development, including decreased cell density, increased thickness, and flat cells between highly aligned extracellular matrix (Fig. 1D). Consistent with histological changes, the expression of tenogenic genes are increased through the time (Fig. 2). These results suggest that our 3D tendon culture is reliable *in vitro* system to study underlying molecular and cellular mechanism regulating tendon maturation. To test the feasibility of the gene manipulation in 3D tendon culture, we infected 3D tendon with Adenovirus. We generated 3D tendon using tendon cells from R26-Ai9 mice which can express mTomato genes upon CRE recombinase expression. We used adenovirus which can express CRE recombinase and eGFP (Ad-CMV-Cre-eGFP). We confirmed the infection of virus by the expression of eGFP in outer layer of 3D tendon (Fig. 3A, Green color). We also confirmed the CRE recombinase activity by the expression of mTomato (Fig. 3A, Red color). We then used the adenovirus to activate mTORC1 signaling in 3D tendon culture by deleting Tsc1, a negative regulator of mTOC1. We generated 3D tendon using tendon cells from conditional *Tsc1* mouse line (*Tsc1$^{f/f}$*). We treated Ad-CMV-eGFP (control) or Ad-CMV-Cre-eGFP (gain-of-function) in 3D tendon generated by *Tsc1$^{f/f}$* tendon cells. Interestingly, our histology analysis showed that the activation of mTORC1 caused increased thickness and disorganized matrix with bigger and round cells in the tendon-like structure, which is similar to the tendon phenotypes of mTORC1 gain-of-function mouse model (Fig. 3B) [3].

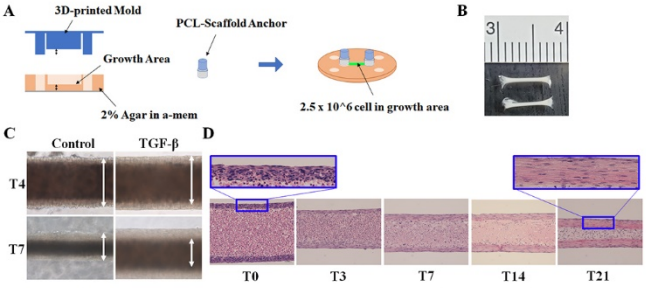

Figure 1. Method of 3D tendon cell culture system and Histology analysis of 3D tendon differentiation. The base of the 3D tendon cell culture was consisted growth area with 2% agaroses with 3D-printed-mold and hydrophilized PCL-scaffold anchor. 3D tendon cell structure was generated tendon cells at 2.5 x 10^6 in fibronectin coated growth area between PCL-scaffold anchor (A). The length of 3D tendon structure is 7 to 8 mm and the thickness is 0.5 to 1 mm (B). 3D tendon structure with or without TGF-β on days 4 and 7 (C). H&E stained 3D tendon structure during tendon cell differentiation (D).

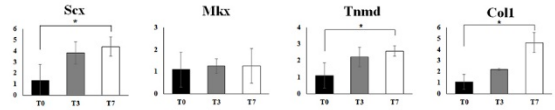

Figure 2. Transcription analysis of 3D tendon. Scleraxis, Mohawk, Tenomodulin, and Collagen type I of tendon related genes were increased in 3D tendon differentiation. (* indicate $P<0.05$ between T0 3D tendon, n=4)

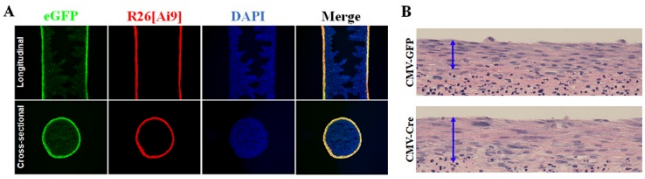

Figure 3. Infection of Adeno-virus in 3D tendon structure. CMV-eGFP and CMV-Cre-eGFP were infected 3D tendon structure from Tsc1$^{fl/fl}$;R26;Ai9 mice. Green fluorescence shows the expression of eGFP and red fluorescence shows the expression of ROSA26-tdTomato, and DAPI at T7 (A). H&E stained 3D tendon structure from Tsc1$^{fl/fl}$ mice infected CMV-GFP or CMV-Cre-eGFP at T7 (B).

DISCUSSION: Our results suggest that the 3D tendon culture system using mouse tendon cells is feasible to manipulate gene expression and effective tools to investigate the molecular mechanism underlying cell maturation and ECM organization. Although 3D tendon showed tendon-like structure, the result may not fully represent an in vivo mechanism. The thorough comparison between In vivo and in vitro result will be necessary to increase the scientific rigor of future research using our 3D tendon culture. We also expect that this system can also be used for pharmacological screening study for tendon diseases.

SIGNIFICANCE/CLINICAL RELEVANCE: This study will contribute to the understanding of cellular and molecular mechanism underlying tendon maturation in vitro using genetic manipulation.

REFERENCES: [1] R Gehwolf, 2019, 2017, [2] K Mubyana, 2018, [3] J Lim, 2017

ACKNOWLEDGEMENTS: This work is partly supported by the National Institutes of Health under award numbers K01AR069002 (KSJ). We thank to Suchin Heo for providing PCL scaffold and PCMD Biomechanics core (Snehal Shetye) for providing 3D-printed Mold.

Tendon Resident Macrophages Internalize Type 1 Collagen and Express Trophic Signaling Factors

Catherine A. Bautista[1], Mary Kate Evans[1], Tonia K. Tsinman[1], Nathaniel A. Dyment[1]
[1]University of Pennsylvania, Philadelphia, PA
cbaut@seas.upenn.edu

Disclosures: Catherine A. Bautista (N), Mary Kate Evans (N), Tonia K. Tsinman (N), Nathaniel A. Dyment (N)

INTRODUCTION: While the majority of cells within the growing tendon are tendon fibroblasts that express the common tendon reporters Scx-GFP and Col1a1-CFP, we recently identified a population of cells that are positive for the macrophage marker F4/80 and negative for the Col1a1-CFP and ScxCre;R26R-tdTomato fluorescent reporters in the mouse [1]. It is unknown at what stage these resident macrophages begin to populate the tendon and what their role is in tendon growth and development. Therefore, the objective of this study was to determine the distribution of tendon resident macrophages throughout development and elucidate potential mechanisms by which these cells may support extracellular matrix (ECM) regulation and tenogenic differentiation.

METHODS: All procedures were approved by UPenn's IACUC. Transgenic mice. Col1a1(3.6kb)CFP (Col1CFP) mice containing 3.6kb of the Col1a1 promoter driving CFP expression were used in this study [2]. Experimental design. Knees from Col1CFP mice at E15.5, P4, P28, and P56 were used for patellar tendon (PT) immunofluorescence (n=2-3/time point). Tail tendons (TTs) were isolated from 4-6-week-old Col1CFP mice for explant culture (n=4). TTs from P28 mice were used for cell sorting and gene expression analysis (2 mice per biological replicate; n=3). Immunofluorescence. Knees sections were stained with rat anti-F4/80, stained with Hoechst, and imaged. TT explant and protease substrate culture. TTs were cultured in individual channels of 6-channel slides (Ibidi µ-Slide VI) in media supplemented with 200 nM MMPSense 645 FAST MMP-activated fluorescent dye and 10 µg/ml DQ Collagen (Type 1, fluorescein conjugate) collagenase-activated fluorescent substrate (5 TTs/mouse); explants were imaged after 2 days in culture. Cell isolation and qPCR. TTs were serially digested to discard surface cells and obtain internal cells. Isolated cells were labeled with anti-F4/80 magnetic particles and sorted to obtain F4/80-enriched and F4/80-depleted populations. RNA was isolated and expression was measured via qPCR for *18S*, *Col1a1, Adgre1, Csf1, Csf1r, Tgfb1, Tgfb2, Tgfb3,* and *Tgfbr2.* Statistics. qPCR results were compared via Kruskal-Wallis followed by Mann Whitney U tests adjusted for multiple comparisons. Single-Cell Sequencing analysis. Publicly available single-cell RNA sequencing (scRNA-seq) datasets were obtained from the NCBI GEO (GSE139558 [3] and PRJNA506218 [4]). Count matrices were filtered, normalized, scaled, cell cycle regressed, reduced, and clustered using Seurat v3.1 [5].

RESULTS: Resident macrophages are present throughout tendon development. To investigate the presence of resident macrophages during tendon development, we performed immunofluorescence for the macrophage marker F4/80 on PT sections. We found that Col1CFP(-);F4/80(+) resident macrophages were present in the linear arrays of the PT at E15.5, P4, P28 and P56, ranging from 4% to 9% of total cells within the midsubstance (**Fig. 1**; magenta). Tendon resident macrophages internalize cleaved DQ Collagen and MMPSense. Because macrophages are present throughout tendon growth and development, we hypothesized that they may play a role in ECM assembly. Upon culturing P28 TT explants with media supplemented with DQ Collagen and MMPSense, we found that the unquenched cleaved fluorescent substrates were localized almost exclusively within the Col1CFP(-) cells (**Fig 2**; yellow arrows). Given this finding and the fact that virtually all Col1CFP(-);MMPSense(+) are F4/80(+) [1], we concluded that resident macrophages are capable of internalizing excess proteolytically cleaved collagen. Potential cell signaling circuit between F4/80-enriched and F4/80-depleted cell populations. Due to the observed proximity of fibroblasts and macrophages and previous studies demonstrating cell-cell communication between macrophages and stromal cells, we investigated potential signaling pathways in F4/80-sorted tendon cell populations. The F4/80-enriched (macrophage-enriched) population expressed 53.5-fold higher levels of *Csf1r* compared to the F4/80-depleted (fibroblast-enriched) population, which expressed 5.85-fold higher levels of *Csf1* (**Fig. 3**). Because TGFβ signaling plays a major role in tendon development [3] and macrophages have been shown to signal to fibroblasts via TGFβ [6], we analyzed expression levels of key TGFβ ligands and their receptor. All surveyed genes were detected in both populations. We found the macrophage-enriched population to have a 2.75-fold higher expression of *Tgfb1*, while the fibroblast-enriched population exhibited 2.38, 2.36, and 2.65-fold higher levels of *Tgfb2*, *Tgfb3,* and *Tgfbr2,* respectively. scRNA-seq datasets confirm potential cell-cell communication between fibroblasts and macrophages. Analysis of two previously published scRNA-seq data sets showed that, among clusters enriched for *Adgre1* (F4/80), 78.0% (P7 forelimb and hindlimb tendons [3]) and 64.6% (3-month-old PTs [4]) of cells express *Csf1r*; of these *Csf1r*(+) cells, 44.4% [3] and 36.5% [4] express *Tgfb1*. Furthermore, among clusters enriched for *Tnmd* (tenocyte marker), 11.0% [3] and 18.3% [4] of cells express detectable levels of *Csf1* and 12.5% [3] and 14.4% [4] express *Tgfbr2*.

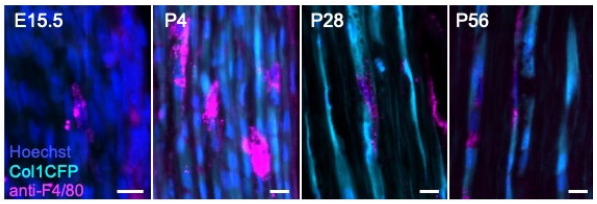

Fig 1. F4/80 immunofluorescence on Col1CFP patellar tendons (scale=10µm).

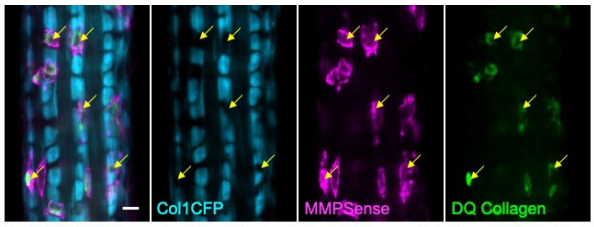

Fig 2. Col1CFP tendons cultured in medium containing MMPSense and DQ Collagen (scale=10µm).

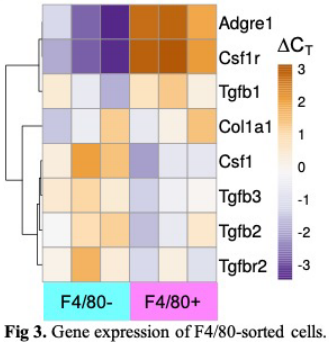

Fig 3. Gene expression of F4/80-sorted cells.

DISCUSSION: In this study, we demonstrated that resident macrophages are present alongside fibroblasts during embryonic tendon development and throughout postnatal growth (**Fig. 1**). This macrophage population is capable of internalizing proteolytically cleaved DQ Collagen and MMPSense within their native environment (**Fig. 2**), which suggests that these cells may be important in the degradation and/or clearance of ECM during development. We also established that fibroblasts express *Csf1* (**Fig. 3**), a cytokine necessary for macrophage survival and function. scRNA-seq data showed that only a subset of fibroblasts expresses detectable levels of *Csf1*, suggesting that the spatial distribution of *Csf1r*(+) macrophages is dependent on *Csf1* expression by stromal cells, as is the case in other tissues. Our data and others' showed that tendon resident macrophages express TGFβ ligands and are especially enriched for *Tgfb1*, which supports our working hypothesis that macrophages provide trophic signaling to *Tgfbr2*(+) fibroblasts. Resident macrophages in other tissues are necessary for their development and contribute to ECM regulation and cell signaling circuits with surrounding resident cells. Our future studies aim to determine if analogous phenomena occur in tendons.

SIGNIFICANCE/CLINICAL RELEVANCE: An improved understanding of the cells and signaling pathways that define and regulate the tendon lineage will be crucial to developing new therapies to attenuate the progression of pathologies and improve repair outcomes following injury. This study gives new insight into potential roles of resident macrophages during tendon development and growth and their interaction with *Col1a1*-expressing tendon fibroblasts.

REFERENCES: 1) Bautista et al., ORS 2020. 2) Kalajzic et al., *JBMR* 2001. 3) Tan et al., *eLife* 2020. 4) Harvey et al., *NCB* 2019. 5) Stuart et al., *Cell* 2019. 6) Wynn and Barron, *Semin Liv Dis* 2020.
ACKNOWLEDGEMENTS: Work supported by NIH grants T32 AR007132, R00 AR067283, P30 AR069619, UPenn URF, and UPenn startup funds.

Telomere Length Regulation of Muscle Stem Cells in Chronic Injuries

Elisia D. Tichy, Nuoying Ma, David Sidibe, Delia Chen, Jacob Kocan, and Foteini Mourkioti
McKay Orthopaedic Research Laboratory, Perelman School of Medicine, University of Pennsylvania, Philadelphia, PA 19104

Duchenne muscular dystrophy (DMD) is a muscle disease characterized by multiple rounds of skeletal muscle injury and repair. Skeletal muscle regeneration relies on the proper functioning of muscle stem cells (MuSCs), which upon injury, become activated, proliferate, differentiate, and fuse to form a repaired muscle fiber. Previous studies by the lab have shown that telomeres play a pivotal role in the severity and progression of dystrophy in mouse models, particularly in MuSCs. Recently, we have shown that telomeres are also shortened in DMD-diseased MuSCs from young patients, compared with those from healthy donors. To identify dysregulated signaling pathways in DMD that may contribute to telomere length changes, we screened dystrophic murine MuSCs, and we found that the NF-κB signaling pathway was aberrantly upregulated in the dystrophic MuSCs, as compared with controls. Using an inducible, MuSC-specific mouse model, where NF-κB signaling is upregulated in the absence of stimuli, we queried the effects of enforced NF-κB signaling in MuSCs during in both normal and chronic muscle injury conditions. We found no ill effects resulting from NF-κB activation in either MuSCs or skeletal muscle tissue, when muscles were not injured. However, upon chronic injury, we observed rapid telomere shortening of NF-κB MuSCs compared to controls, where more repetitive injuries resulted in more significant telomere shortening. This finding correlated well with increasingly poor muscle histology. We next asked whether increased activation of NF-κB signaling in mice experiencing dystrophy enhanced the phenotype of the disease. We observed a much more severe pathology, increased muscle damage, reduced muscle strength, and telomere shortening in dystrophic mice and MuSCs, when NF-κB signaling was further enhanced. To identify the mechanism by which NF-κB promotes telomere attrition in chronic injury conditions, we investigated several different aspects. We found that NF-κB MuSCs do not exhibit increased proliferation, but they do show a downregulation of Ku80 RNA. Ku80 can reside at the telomere, but its function at this location is still being elucidated. However, Ku80 is also involved in DNA damage repair by nonhomologous end joining. To assess whether more DNA damage is present at the telomere, MuSCs from injured NF-κB mice were stained with a DNA damage marker, a MuSC marker, and a telomere probe. We found increased DNA damage at the telomere, which is known mechanism for induction of telomere shortening. We observed the same phenomenon in MuSCs derived from DMD patients, as compared to healthy human MuSCs. Finally, we asked whether the NF-κB-dependent reduction of telomere length correlated with stem cell exhaustion, similar to what is observed in the DMD disease process. Using two-photon microscopy and GFP-labeled MuSCs, we observed a significant reduction in MuSC numbers in chronically injured NF-κB mice, compared to control mice. These findings are the first to identify a role for NF-κB signaling in telomere length loss and stem cell exhaustion in chronic muscle injuries and may lead to alternative avenues for the treatment of patients with DMD.

Collagen V Deficiency during Healing Mitigates the Quasi-Static Mechanical Deficits of Injured Tendons

Ryan J Leiphart[1], Stephanie N Weiss[1], David E Birk[2], Louis J Soslowsky[1]
[1]McKay Orthopedic Research Laboratory, University of Pennsylvania, Philadelphia, PA
[2]Department of Molecular Pharmacology and Physiology, University of South Florida, Tampa, FL

Disclosures: RJ Leiphart (N), SN Weiss (N), DE Birk (N), LJ Soslowsky (N)

INTRODUCTION: Classic Ehlers-Danlos Syndrome (cEDS) is characterized by genetic mutations of collagen V, a matrix protein present in tendon [1]. Two hallmarks of cEDS are connective tissue hyperelasticity and poor wound healing, and a murine model of cEDS demonstrates impaired tendon healing [2,3]. It is unknown whether this impaired healing response is due to the regulatory role of collagen V during tendon healing or due to pre-existing differences in collagen V-deficient tendons. Therefore, the objective of this study was to determine the isolated role of collagen V on healing tendon mechanics. Due to its role in fibrillogenesis, we hypothesized that acute knockout of collagen V following injury would result in decreased tendon mechanical properties at both intermediate and late healing time points.

METHODS: *Animals*: Male wild-type (WT) (n=45) and bitransgenic *Col5a1*$^{flox/+}$ (n=30) and *Col5a1*$^{flox/flox}$ (n=30) mice with a tamoxifen (TM)-inducible Cre were used in this study (IACUC approved). At 120 days old, mice received bilateral, full thickness, partial width patellar tendon injuries under sterile conditions [4]. For Cre-mediated excision of the *Col5a1* gene, mice received two consecutive daily doses of TM (2mg/40g body weight) beginning on the day of injury. Mice were sacrificed at 3 or 6 weeks post-injury. Healthy WT control mice received TM doses (3 days of 4mg/40g body weight) at 120 days old and were sacrificed 30 days later. Tibia-patellar tendon-patella complexes were harvested and prepared for mechanical testing as previously described [5]. *Mechanical Testing*: Uniaxial, viscoelastic testing was performed with an Instron 5848. The testing protocol consisted of 10 cycles of preconditioning, followed by stress relaxations at 3%, 4%, and 5% strain. Following each stress relaxation, frequency sweeps of 10 cycles at 0.1, 1, 5, and 10Hz were performed. A ramp-to-failure followed the 5% stress relaxation. Percent relaxation, dynamic modulus (E*), and phase shift (δ) were quantified for each stress relaxation and frequency sweep. Stiffness, modulus, maximum load, and maximum stress were quantified from the ramp-to-failure data. *Statistics*: For all mechanical properties, one-way ANOVAs with Bonferroni post-hoc tests were used to compare across genotypes and uninjured controls at each healing time point. Significance was set at $p \leq 0.05$, and trends were set at $p \leq 0.1$.

RESULTS: ***Injury effects:*** Compared to uninjured tendons, injured WT tendons had increased cross-sectional area (CSA) (Fig 1). *Quasi-Static Mechanics*: Compared to uninjured tendons, injured WT tendons were less stiff (Fig 2A), had no differences in max load (data not shown), had decreased modulus (data not shown), and lower max stress (Fig 2B). *Stress Relaxation*: Compared to uninjured tendons, injured WT tendons had greater stress relaxation at 3%, 4%, and 5% strains (data not shown). *Dynamic Mechanics*: Compared to uninjured tendons, injured WT tendons had decreased dynamic moduli at all strains and frequencies, larger tan(δ) values at 3 and 4% strain and for most frequencies at 5% strain for 6-week WT tendons (data not shown). ***Genotype effects:*** Injured *Col5a1*$^{+/-}$ (HET) and *Col5a1*$^{-/-}$ (NULL) tendons had increased CSA relative to uninjured (Fig 1). At 3 weeks post-injury, NULL tendons had decreased CSA relative to WT and a trend towards smaller CSA relative to HET. *Quasi-Static Mechanics*: No differences in stiffness were observed between HET and uninjured tendons (Fig 2A). HET tendons trended towards higher stiffness relative to injured WT tendons at both healing time points. 3-week NULL tendons were less stiff than uninjured tendons, but this decrease did not persist at 6-weeks. 3-week HET tendons had lower max stress than uninjured tendons, but this decrease did not persist at 6-weeks (Fig 2B). 3-week NULL tendons had lower max stress than uninjured tendons, and this difference persisted as a trend at 6-weeks. 3-week NULL tendons had higher max stress than 3-week WT tendons and trended towards higher max stress relative to 3-week HET tendons. HET and NULL tendons had decreased modulus compared to uninjured. No differences in max load were observed between knockout and uninjured tendons. No differences in max load or modulus were observed between injured genotypes. *Stress Relaxation*: HET and NULL tendons had increased stress relaxation at 3% and 4% strain relative to uninjured. 3-week HET and NULL tendons exhibited increased stress relaxation at 5% strain relative to uninjured, which persisted for 6-weeks HET but not for 6-week NULL tendons. No differences in stress relaxation were observed between injured genotypes at any strain. *Dynamic Mechanics*: HET and NULL tendons had decreased dynamic moduli relative to uninjured. For most frequencies at 3% and 4% strain, HET and NULL tendons had larger tan(δ) values than uninjured, while at 5% strain, 6-week HET tendons had larger tan(δ) values than uninjured. No differences in tan(δ) values were observed between 6-week NULL and uninjured tendons. No differences in dynamic modulus or tan(δ) values were observed between injured genotypes at any strain or frequency.

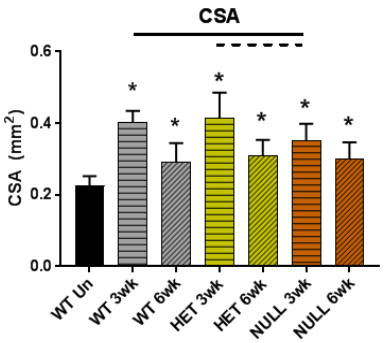

Fig 1. Cross-sectional area. Injured tendons across all genotypes and healing time points had larger CSA than uninjured tendons. * indicates $p \leq 0.05$ compared to uninjured tendons. Solid bars indicate $p \leq 0.05$, and dashed bars indicate $p \leq 0.1$.

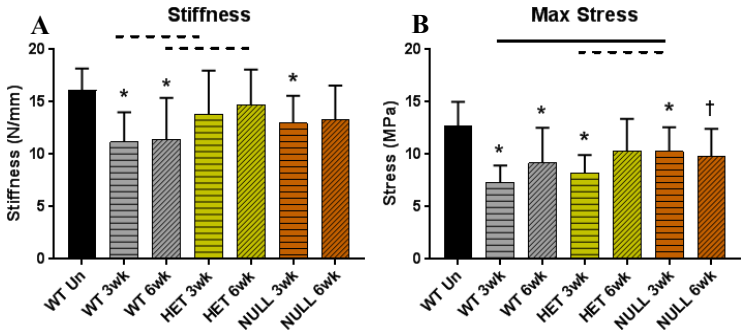

Fig 2. Quasi-static properties. (A) HET tendons had no differences in stiffness compared to uninjured tendons but trended towards higher stiffness compared to WT at both healing time points. (B) 6-week HET tendons had no differences in max stress compared to uninjured tendons. * indicates $p \leq 0.05$, and † indicates $p \leq 0.1$, compared to uninjured tendons. Solid bars indicate $p \leq 0.05$ and dashed bars indicate $p \leq 0.1$.

DISCUSSION: Injured tendons exhibited substantial deficits in mechanical properties relative to uninjured tendons. Contrary to our hypothesis, however, acute knockout of collagen V did not further impair the mechanical properties of these healing tendons. Instead, stiffness did not decrease through healing in HET tendons. Injured HET tendons were stiffer than WT tendons at each healing time point. No decreases in max stress were seen with 6-week HET tendons. These results demonstrate that while healing tendons have impaired mechanical properties, collagen V deficiency during healing does not further diminish these properties. Instead, collagen V haploinsufficiency during healing mitigated the decreases in stiffness and max stress seen in WT injured tendons. Impaired tendon healing in cEDS patients may not be due to the regulatory role of collagen V during healing and may instead be due to pre-existing deficiencies of the tissue. A previous study found that fibroblasts from a murine model of cEDS demonstrated decreased proliferation, migration, and wound healing relative to WT fibroblasts [6]. Results of the present study support the notion that poor wound healing in cEDS patients is due to differences in tissue properties that existed prior to injury. A limitation of this study is the global nature of the collagen V knockouts, which could cause confounding effects on neighboring tissues. The inducible knockout models used here lessen these effects due to the short period of knockout. Future studies will analyze the composition and gene expression of these tendons to identify other differences in healing, collagen V-deficient tendons. Overall, this study demonstrates that collagen V deficiency does not impair the mechanical properties of injured tendons beyond the normal healing response, and instead mitigates some of these mechanical deficits.

SIGNIFICANCE: This study reveals that the quasi-static mechanical deficits of injured tendons are not worsened, and are instead mitigated, by collagen V deficiency. These results provide a further understanding of the role of collagen V in tendon healing.

REFERENCES: [1] Symoens S et al. *Hum Mutat*. 2012. [2] Malfait F & De Paepe A. *AEMB*. 2014. [3] Johnston JM et al. *JOR*. 2017. [4] Beason DP et al. *J Biomech*. 2012. [5] Dunkman AA et al. *Matrix Biol*. 2013. [6] DeNigris J et al. *Connect Tissue Res*. 2016.

ACKNOWLEDGEMENTS: This work was supported by the NIH (R01AR065995, P30AR069619) and the NSF GRFP.

Delineating the Effects of Pregnancy and Lactation on Rat Maternal Bone Responses to Future Estrogen Deficiency

Rebecca Chung[1], Yihan Li[1], Chantal de Bakker[1], Carlos Osuna[1], Justin Leggin[1], Zachary Davis[1], Liyun Wang[2], X. Sherry Liu[1]
[1] Department of Orthopaedic Surgery, University of Pennsylvania, Philadelphia, PA; rebecca.chung@pennmedicine.upenn.edu
[2] Department of Mechanical Engineering, University of Delaware, Newark, DE.

Disclosures: All authors have nothing to disclose.

INTRODUCTION: Lactation and menopause are physiological events where significant changes in skeletal metabolism are triggered by rapid estrogen decline, resulting in bone loss and bone microarchitecture deterioration [1,2]. Our previous study demonstrated that rat maternal bone actively adapts to multiple cycles of reproduction and lactation, resulting in a unique structural phenotype that is resistant to estrogen deficiency-induced bone loss [3]. However, to date nearly 60% of mothers do not breastfeed for as long as they intend to [4]. Therefore, an investigation of how reproduction without lactation influences post-menopausal bone health is necessary, as we hypothesize that the absence of lactation will differentially alter the skeletal response to estrogen deficiency. Furthermore, we hypothesize that peri-lacunar/canalicular remodeling (PLR) induced by reproduction and lactation may alter the responsiveness of osteocytes against estrogen deficiency post-menopause, which in turn could lead to changes in skeletal mechano-sensitivity. In our continued efforts to further elucidate the role of lactation, the goal of the current study is to investigate changes in bone structure, mechano-responsiveness, and osteocyte activities in response to estrogen deficiency in virgin and reproductive rats that underwent three cycles of reproduction with and without lactation.

METHODS: *Animals:* Female, SD rats were assigned to 3 groups: Virgin, reproductive without lactation (Preg-NL), and with lactation (Lactation). Beginning at age 3-4 months, reproductive rats underwent 3 consecutive cycles of pregnancy, lactation, with a 6-wk post-weaning recovery. At age 12 months, virgin and reproductive rats underwent bilateral ovariectomy (OVX) surgery to induce estrogen deficiency. *Microstructural Analysis:* 56 rats (n=20 Virgin, n=17 Preg-NL, and n=19 Lactation) underwent *in vivo* μCT imaging of the proximal tibia during the first reproductive cycle (baseline, parturition, end of 3-wk lactation, and 3- and 6-wk post-weaning recovery), prior to OVX, as well as 4, 8, and 12 weeks post-OVX (10.5um, vivaCT40, Scanco Medical). *In vivo loading and osteocyte analysis:* 21 rats (n=8 Virgin, n=6 Preg-NL, and n=7 Lactation) were subjected to 2-week dynamic, compressive loading protocol at 6 weeks post-OVX [5] before euthanasia. A peak load of 45N, corresponding to ~1500 με at the tibial shaft determined by strain gauges, was applied to the left tibia at 2 Hz (*i.e.*, 0.15s ramp up, 0.15s ramp down, and 0.2s dwell time), for 5 min/day over 2 weeks (5 days/week), while the right tibia served as non-loaded control. *In vivo* μCT scans were performed on both tibiae at day 0 and day 14. Paraffin embedded non-loaded tibial cortices were immunostained for MMP13 to assess PLR enzyme expression and Ploton silver stained to examine lacunar size. *Statistics:* Longitudinal comparisons were made using 2-way, repeated-measures ANOVA, adjusted for baseline values, and cross-sectional comparisons were made using 1-way ANOVA. Bonferroni corrections were applied to all post hoc tests. Significant differences were considered when $p<0.05$.

RESULTS: Trabecular bone changes were minimal for Virgins during the first reproductive cycle, whereas Preg-NL and Lactation rats experienced BV/TV reductions of 39% and 42% respectively at parturition (Fig 1A). During lactation, Tb.Th (-34%) and Tb.N (-54%) continued to deteriorate for Lactation rats while Preg-NL rats began to recover (Fig 1BC). By the end of the post-weaning recovery, Tb.Th recovered entirely for both reproductive groups and was not different compared to Virgins (Fig 1B). After three cycles of reproduction, Preg-NL rats had 35% and 35% greater BV/TV and Tb.N compared to Lactation rats, but 27% less BV/TV and 31% less Tb.N compared with Virgins. In the 12-week post-OVX period, Preg-NL and Lactation rats underwent a 62% and 53% decrease in BV/TV at a relatively lower rate compared to Virgins (77%, Fig 2AB). Similar post-OVX changes were found in Tb.N while no change in Tb.Th was found in any group (Fig 2C). Interestingly, differences in trabecular microstructure among 3 groups prior to OVX no longer existed at 12weeks post-OVX (Fig 2D). Significant loading responses were observed in tibial Ct.Area and pMOI in all 3 post-OVX groups (Fig 3AB). Additionally, there was a trend toward a two-fold greater response in pMOI for Lactation rats compared with Virgins ($p=0.06$), but no differences were detected between Preg-NL and Lactation rats (Fig 3C). Investigation of PLR enzymatic expression revealed that Preg-NL rats had 17% greater percentage of MMP13+ osteocytes than Virgins but 25% less percentage compared to Lactation rats (Fig 3D). Furthermore, Lactation rats had 8% greater lacunar size compared to Virgins, while a trend of 4% greater was found compared to Preg-NL rats ($p=0.08$, Fig 3E).

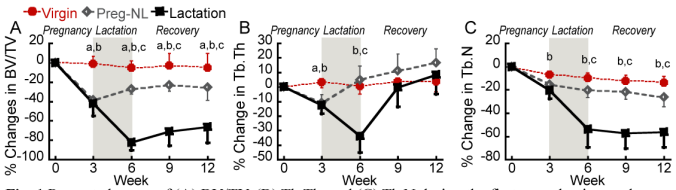

Fig. 1 Percent changes of (A) BV/TV, (B) Tb.Th, and (C) Tb.N during the first reproductive cycle. $p<0.05$: a: Virgin ≠ Preg-NL; b: Virgin ≠ Lactation; c: Preg-NL ≠ Lactation.

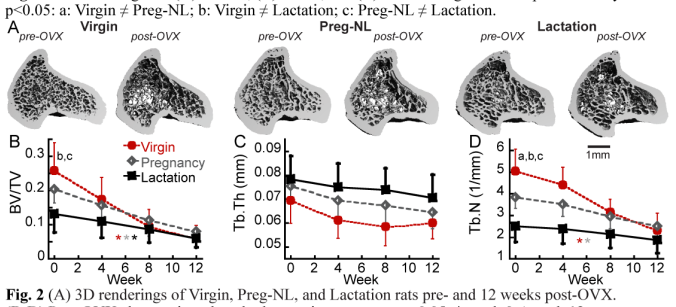

Fig. 2 (A) 3D renderings of Virgin, Preg-NL, and Lactation rats pre- and 12 weeks post-OVX. (B-D) Post-OVX changes in trabecular bone microstructure. $p<0.05$: * week 0 ≠ week 12; a: Virgin ≠ Preg-NL; b: Virgin ≠ Lactation; c: Preg-NL ≠ Lactation.

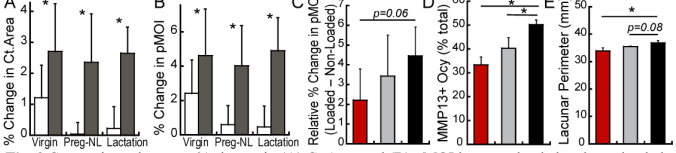

Fig. 3 Comparisons between % change in (A) Ct.Area and (B) pMOI between loaded and non-loaded tibia. (C-E) Comparisons in (C) % change in pMOI in loaded relative to non-loaded tibia, (D) % of MMP13+ osteocytes, and (E) lacunar perimeter between Virgin, Preg-NL, and Lactation rats. *$p<0.05$.

DISCUSSION: Similar to post-lactation recovery, we discovered an anabolic response in rat trabecular bone immediately after parturition without lactation. However, pregnancy with and without following lactation still resulted in different degree of trabecular bone deterioration in rat maternal bone after a single or multiple reproductive cycles. Interestingly, despite these deficits, reproductive rats with and without lactation had attenuated bone loss by 12 weeks following OVX, suggesting that a structural phenotype with thicker and greater number of trabeculae may be protective against future estrogen deficiency, and demonstrates the ability of maternal bone to compensate for reproductive bone loss and incomplete recovery post-weaning to maintain skeletal mechanical integrity. This was also evident upon discovery that reproduction with lactation history leads toward greater mechano-responsiveness of the tibial midshaft at 6 weeks post-OVX. Furthermore, as osteocytes undergo PLR and partake in the liberation of skeletal calcium during reproductive cycles [6], the changes in the osteocytic microenvironment in response to reproduction and lactation may condition the osteocytes to functionally adapt and enhance their mechano-sensitivity through PLR [7]. Hence, our findings revealed differences in osteocyte activities between reproductive groups when subjected to estrogen deficiency, where Preg-NL rats endured relatively less dramatic alterations in trabecular bone microstructure, PLR, and lacunar size as compared to Lactation rats, which experience more dynamic hormonal changes such as hypoestrogenic levels during lactation. This suggests that reproduction, especially if followed by lactation, may exert a protective effect throughout the maternal lifespan.

SIGNIFICANCE: A deeper understanding of the differential effects of reproduction and lactation on postmenopausal bone health can contribute to new insights for the development of strategies to engage mothers to breastfeed longer and identify targets for novel treatments to enhance the skeletal mechano-responsiveness post menopause.

REFERENCES: [1] Kovacs CS, *Physiol Rev.,* 2015; [2] de Bakker CM *et al.*, *JBMR.*, 2017; [3] de Bakker CM *et al.*, *JBMR*, 2018; [4] Odom EC *et al., Pediatrics.*, 2013; [5] Fritton *et al.,* Bone, 2005; [6] Qing H *et al.*, *JBMR,* 2012; [7] Li Y *et al.*, SB3C, 2019.

ACKNOWLEDGEMENTS: NIH/NIAMS R01-AR071718, NSF #1653216, and Penn Center for Musculoskeletal Disorders (P30-AR069619).

Tendon Pathology Alters Chromatin Organization and Mechano-sensitivity in Human Tenocytes

Su Chin Heo[1], Shreyasi Thakur[1], Claudia Loebel[1], Boao Xia[1], Rowena McBeath[2], Jason Burdick[1], Melike Lakadamyali[1], Robert Mauck[1]
[1]University of Pennsylvania, Philadelphia, PA; [2]Thomas Jefferson University Hospital, Philadelphia, PA

Disclosures: Su-Jin Heo (N), Shreyasi Thakur (N), Claudia Loebel (N), Boao Xia (N), Rowena Mcbeath (N), Jason Burdick (N), Melike Lakadamyali (N), Robert Mauck (N)

INTRODUCTION: Fibrous connective tissue injury or degeneration (e.g. tendinosis) is prevalent, with few treatments that restore function. Pathological changes in tendon alter the tissue chemo-physical environment, impacting endogenous cell behavior [**1, 2**]. For instance, degeneration alters collagen orientation and changes tissue stiffness [1, **2**], and lower local oxygen levels present in damaged tissues may promote early tendinopathy [**2**]. Further, in the early phase of the injury/disease process, pro-inflammatory cytokines in the local milieu promote tendon cell catabolic response. These pathological changes in tissues impact cells across length scales, including at the level of chromatin organization. In a previous study, using super-resolution imaging, we found that tendinosis results in nano-scale chromatin reorganization in human tenocytes, with chromatin increasingly localized to the nuclear periphery, compared to healthy age matched controls [**3**]. Moreover, when healthy human tenocytes were cultured on a soft microenvironment (~3 kPa), we observed similar chromatin reorganization as seen in degenerative tenocytes [**3**]. Based on these findings, here we extended these studies to further investigate how cues from pathological chemo-physical environment (e.g. dynamic changes in stiffness, induction of hypoxia, and presence of inflammatory factors) impact chromatin remodeling in tenocytes.

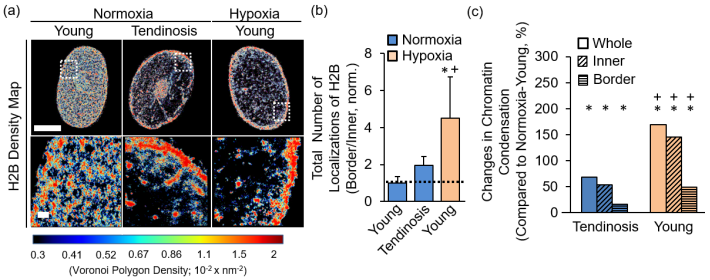

Figure 1: (a) Heat maps showing H2B localization density in young or tendinosis under normoxia or hypoxia culture condition (scale bars: top = 5μm, bottom = 500 nm). Quantification of the ratio of the total number of H2B localizations in the border to the inner (b) and changes in chromatin condensation (compared to young tenocyte in the normoxia culture condition). n = 5 cells, *:p<0.05 vs. Young-normoxia, +:p<0.05 vs. Tendinosis-normoxia.

METHODS: Human tenocytes were isolated from young [Young (y), 42 years] or degenerative [Tendinosis (t), 35 years] tendons according to established protocols [2]. To investigate how changes in oxygen tension affect nanoscale chromatin organization, young healthy tenocytes were seeded on chambered-coverglass (500 cells/mm^2) for 1 day, followed by 4-days of culture under normoxic (21% O_2) or hypoxic (1% O_2) conditions. Next, to investigate how pro-inflammatory cytokines impact chromatin, young tenocytes were cultured on chambered-cover glasses for 1 day followed by additional culture for 24-hours with/without exposure to IL-1β (0.1-1ng/ml) or TNFα (1-10 ng/ml). Finally, to investigate how degeneration impacts mechano-sensitivity of tenocytes, young or tendinosis tenocytes were seeded onto a "stiffening" hydrogel system that provides rapid dynamic changes in substrate stiffness (for example, ~3→30 kPa) in the presence of cells [**5**]. For this, cells were pre-cultured for 24 hours followed by additional 24 hours of culture after stiffening. For all studies, fixed cells were immunostained for histone-H2B (H2B, Proteintech), and then incubated with secondary antibodies custom labeled with activator-reporter dye pairs (Alexa Fluor 405-Alexa Fluor 647, Invitrogen) for super-resolution stochastic optical reconstruction microscopy (STORM) imaging (Nanoimager, ONI) [**3, 4**]. Obtained STORM images were analyzed by dividing the inner border of the nucleus (border: 15-20% determined from the image intensity profile across the diameter of the nucleus) from the rest of the nucleus and rendered these segments using custom MATLAB code and the Nanoimager software (ONI) respectively. For quantitative analysis, in MATLAB, Voronoi tessellation of the H2B localizations was adapted to segment super-resolution images [**3, 4**].

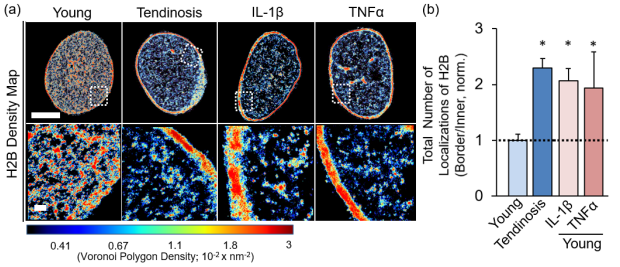

Figure 2: (a) Heat maps showing H2B localization density in young, tendinosis, or young human tenocytes with IL-1β (1 ng/ml) or TNFα (10 ng/ml) treatment. (b) Quantification of the ratio of the total number of H2B localizations in the border to the inner. n = 5 cells, *:p<0.05 vs. Young human tenocyte (normalized). (scale bars: top = 5μm, bottom = 500 nm).

RESULTS: Consistent with our previous findings [**3**], super-resolution imaging H2B heat maps showed that, while dense chromatin was distributed through the nucleus in young healthy tenocytes (Young), H2B was more condensed and primary localized to the nuclear periphery in young degenerative nuclei (Tendinosis) (**Fig. 1a-c**). Strikingly, when healthy tenocytes were cultured under the hypoxic conditions, chromatin relocalized to the nuclear periphery and became more condensed (**Fig. 1a-c**). This suggests that altered oxygen tension in tendon after injury or during degeneration may promote aberrant chromatin remodeling. Given that injury and degeneration increase inflammation, we next investigated how pro-inflammatory cytokines impact nanoscale chromatin organization in young healthy tenocytes. These studies showed that exposure to pro-inflammatory cytokines (IL-1β or TNFα) for one day resulted in rapid led chromatin reorganization to the nuclear periphery (**Fig. 2a-b)** and increased chromatin condensation (not shown). This suggests that pro-inflammatory present in the wound environment impact chromatin organization in tenocytes during repair. Finally, we next examined how a change in tissue stiffness impacts chromatin mechano-response in tendons. As was seen in soft substrates [**3**], H2B in young or tendinosis tenocytes was primarily localized to the nuclear periphery within 4 hours after stiffening (**Fig. 3a-b)**. With 24 hours of stiffening, however, H2B became more uniformly dispersed and de-compacted in young healthy tenocyte nuclei. Conversely, in tendinopathic cells, no change in the spatial organization of chromatin and less de-compaction was observed (**Fig. 3a-c)**. This may suggest that prolonged changes in chromatin organization in diseased tenocytes may be associated with a loss of mechanical sensitivity and chromatin reorganization capacity with tissue degeneration.

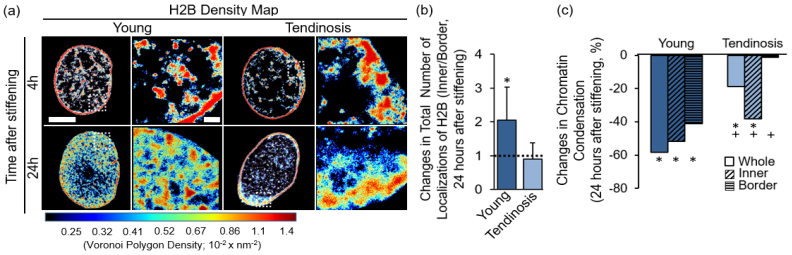

Figure 3: (a) Heat maps showing H2B localization density in young or tendinosis cultured on stiffening hydrogel system (4 hours or 24 hours after stiffening, scale bars: left = 5μm, right = 500 nm). Quantification of the ratio of the total number of H2B localizations in the inner to the border (b) or changes in chromatin condensation at 24 hours after stiffening (c). n = 5 cells, *:p<0.05 vs. before the stiffening, +:p<0.05 vs. Young tenocyte.

DISCUSSION: In this study, we show that tendon degeneration alters nanoscale chromatin organization in tenocytes and impacts their mechanical sensitivity. These data indicate that alterations in the chemo-physical environment that arise with tendon injury or degeneration induces phenotypic and chromatin alterations that are apparent at the nanoscale. Chromatin reorganization to the nuclear periphery has been described as silent chromatin (heterochromatin) suppressing transitional activation [**6**]. Current work is identifying specific genetic loci that move to the periphery and the transcriptional activity of these loci in diseased tenocytes.

SIGNIFICANCE: Our data show that degeneration alters the nanoscale chromatin organization of tenocytes and changes their mechano-sensitivity. This study may inform new directions to identify novel therapeutic targets for the treatment of connective tissue pathologies.

REFERENCES: [1] Han+, Nat Mater 2016; [2] McBeath+, Aging Cell 2019; [3] Heo+, ORS 2020; [4] Ricci+, Cell 2015; [5] Guvendiren+, Nat Commun 2012; [6] Shevelyov+, Cells 2019. **ACKNOWLEDGEMENTS:** This work was supported by the NIH (R01 AR056624, K01 AR077087) and NSF (CMMI-1548571).

Microtubule tyrosination-state and Rho signaling regulate chondrogenic differentiation in ATDC5 cells

Ryan Daniels[1] and Robert L. Mauck, PhD[1,2]
[1]McKay Orthopaedic Research Laboratory, University of Pennsylvania, Philadelphia, PA
[2]Department of Bioengineering, University of Pennsylvania, Philadelphia, PA

DISCLOSURES: RLM (8, *JOR Spine*), no other disclosures.

INTRODUCTION: Articular cartilage is an integral load bearing tissue that lines diarthrodial joints, secretes a specialized extracellular matrix (ECM), and organizes that ECM to provide compressive resistance and near-frictionless movement. Articular cartilage is made up a single cell type, the articular chondrocyte (AC), which is responsible for responding to physiologic load by producing ECM and inhibiting inflammation. The cytoskeletal architecture of ACs is critical for maintenance of identity and appropriate response to load. In healthy ACs, microtubules (MTs) engage and form a mesh-like cage around the nucleus, while the actin is cortical and spatially separated from the nucleus [1]. Damaged or diseased ACs lose this MT mesh-like nuclear cage, and instead form actin stress fibers that engage the nucleus as ACs dedifferentiate [1]. Cytoskeletal engagement of the nucleus relays mechanotransductive signals to influence cell behavior, such as differentiation, through the Linker of Nucleoskeleton and Cytoskeleton complex. We hypothesize that MT-based mechanotransduction promotes chondrogenesis while actin-based mechanotransduction inhibits chondrogenesis and is a potential factor that initiates dedifferentiation of chondrocytes in diseased environments.

METHODS: To study the effects of cytoskeletal dynamics on chondrogenic gene expression, we used a chondrogenic progenitor cell line, ATDC5 cells. Inhibitors were added 2 hours post-seeding in chondrogenic media [2] and media was replaced daily with or without inhibitors for 3 days. Expression of chondrogenic markers was measured by quantitative polymerase chain reaction (qPCR), using 18srRNA as a housekeeping gene. Immunofluorescence (IF) was used to evaluate cytoskeletal architecture and to semi-quantitatively measure Sox9 nuclear intensity in Fiji. MT-nuclear association was measured by using the nucleus as a mask and calculating mean overlay intensity in Fiji. Statistical significance (for gene expression) was determined by one-way ANOVA with a Brown Forscythe and Welch test, and significance was accepted if $p<0.05$.

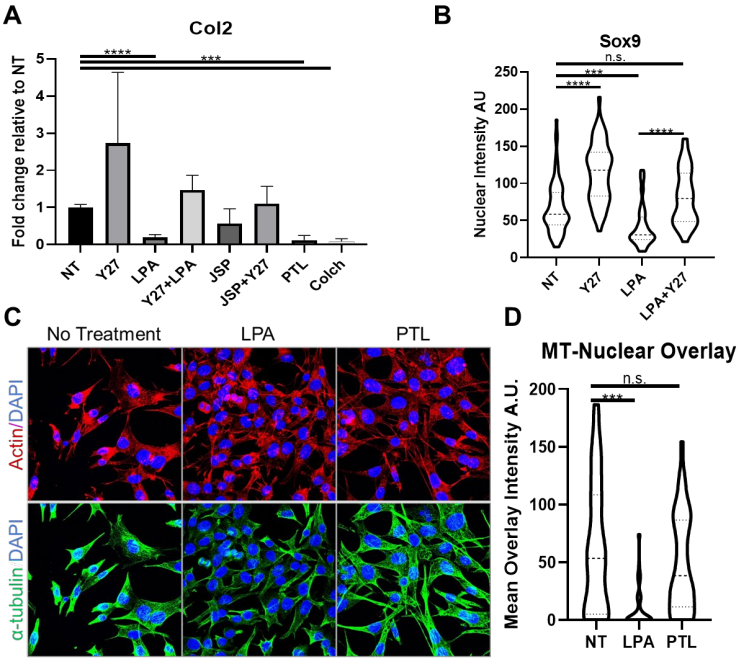

Figure 1. Cytoskeletal regulation of chondrogenesis in ATDC5 cells. **A.** ATDC5 cells were seeded in chondrogenic media for 3 days with or without Y27 (ROCK inhibitor, 20uM), LPA (Rho Agonist 30uM), both LPA and Y27, Jasplakinolide (actin stress fiber initiator, 20nM), both JSP and Y27, Colchicine (MT destabilizer), and Parthenolide (MT detyrosination inhibitor 10uM) and assed by qPCR n=4. **B.** ATDC5 cells treated as in A were assessed for Sox9 nuclear intensity via IF in the Y27, LPA, and LPA+Y27 groups n=1 50-60 cells per group. **C.** Cytoskeletal architecture was visualized via IF for qualitative assessment. **D.** MT-nuclear overlay was quantified in cells from **C.** n=150-60 cells per group ***p<0.01, ****p<0.0001, n.s.= not significant

RESULTS: Three days of culture in chondrogenic media with ROCK inhibition (Y27, Figure 1A) to decrease actin stress fiber formation, resulted in a trend towards increased Col2 expression and a significant increase in Sox9 nuclear intensity (Figure 1B). Conversely, promoting Rho activity through LPA (and an increase actin stress fiber formation, Figure 1C top middle panel) resulted in a significant decrease in Col2 expression and Sox9 nuclear localization (Figure 1A,B). These inhibitory effects on chondrogenesis could be reversed when Y27 to LPA were added to cultures simultaneously (Figure 1A,B). The cytoskeletal architecture of these cells supported these finds. In control cells, actin as visualized by Phalloidin (Figure 1C top left panel) showed few stress fibers and little actin-nuclear overlay. Conversely, MTs that were visualized by staining for alpha-tubulin (Figure 1C bottom left panel) were abundant and had high levels of nuclear overlay. With LPA treatment, actin stress fibers became more organized (Figure 1C middle top panel) while the MT network was almost completely abrogated (Figure 1C, middle bottom panel, Figure 1D). We also asked whether the effects of LPA were specific to increased actin stress fiber formation or were due to Rho signaling in general. For this, we applied Jasplakinolide (JSP) to directly promote and stabilize actin stress fibers. JSP treatment resulted in a trend towards decreased Col2 expression and a partial rescue when combined with Y27 (Figure 1A). Lastly, to determine the role of the MT network in chondrogenesis of ATDC5 cells, MTs were destabilized with Colchicine. This resulted in a significant decrease in Col2 expression (Figure 1A). To evaluate the effects of MT modification on chondrogenesis, parthenolide (PTL) was added to inhibit MT detyrosination. Treatment of ATDC5 cells with PTL led to a significant reduction in Col2 expression (Figure 1A). The cytoskeletal architecture of PTL-treated cells showed that the actin network overall was reduced while the MT network showed no significant changes in MT-nuclear overlay (Figure 1C right panels, Figure 1D).

DISCUSSION: These data demonstrate that the Rho signaling plays a key role in chondrogenesis of ATDC5 cells. Increased Rho signaling decreases chondrogenesis, in part due to increased actin stress fiber formation. The negative effects of increased Rho signaling with LPA could be rescued by inhibiting the down-stream molecule ROCK with Y27. From these data, it also appeared that solely increasing actin stress fiber formation (with JSP) leads to a moderate decrease in Col2 expression, but to a lesser extent as when combined with increased Rho signaling. This would suggest that increased Rho signaling decreases chondrogenesis not solely through increased actin stress fiber formation [2]. It may be that both increasing actin stress fiber formation and decreasing MT network density is required for decreased chondrogenesis, as is seen in LPA treated cells. The role of MTs in general and the impact of their tyrosinated state on chondrogenesis is poorly understood. Inhibiting microtubule detyrosination with PTL, which decreases MT stiffness, decreases chondrogenesis even though it also decreased the amount of actin stress fibers. PTL treatment has been shown to be pro-osteogenic [2] but promotes endochondral ossification and decreases Sox9 expression [4]. This supports that for chondrogenesis to occur, a lack of actin stress fibers and a detyrosinated microtubule network may be essential. It is also possible that chondrocytes require a stiff MT network that is tyrosinated to mechanosense, in contrast to other cell types that require a stiff and contractile actin network. Future experiments are will assess the role of tyrosinated MTs on chondrogenic differentiation and resistance to degenerative stimuli.

SIGNIFICANCE: In osteoarthritic (OA) joints, articular cartilage erosion results in changes in matrix properties and is characterized by dedifferentiated cells that mechano-sense through actin-based connections to the nucleus as well as a decreased microtubule network [1]. These results highlight that not only the presence of microtubules but also their biochemical modification may play a compounding role in chondrogenic dedifferentiation. Future experiments will explore how we can modulate these cytoskeletal networks to generate chondrocytes that can resist the degenerative environments seen in OA.

REFERENCES: 1. Blain, EJ (2009) Exp Path. 2. Woods, A (2005) J. Biochem. 3. Mao, W (2018) Mol Med Rept. 4. Caron M (2012) PlosOne.

ACKNOWLEDGEMENTS: This work was supported by HHMI, the NIH (R01 AR077362), and the NSF (CMMI-1548571).

Alterations in Fibrous Network Topography Regulates Onset of Fibrotic Phenotypes in Annulus Fibrosus Cells

Edward Bonnevie[1], Sarah Gullbrand[1], Beth Ashinsky[1,2], Tonia Tsinman[1], Dawn Elliott[3], Harvey Smith[1], Robert Mauck[1]
[1]University of Pennsylvania and CMC VA Medical Center, Philadelphia, PA, [2]Drexel University, Philadelphia, PA, [3]University of Delaware, Newark, DE
edbon@pennmedicine.upenn.edu

Disclosures: Bonnevie (2, Fidia Pharma USA), Mauck (8, JOR Spine), no other disclosures.

INTRODUCTION: Cells respond to local mechanical and topographic cues to regulate their phenotype[1,2], with 'stiff' environments driving a fibrotic phenotype[3]. In the context of disc degeneration, loss of nucleus pulposus swelling and residual strains in the annulus fibrosus likely alter the mechanics and organization of the cellular microenvironment[4]. Here, we used in vivo and in vitro models to test the hypothesis that altered fiber organization in the annulus fibrosus regulates the emergence of fibrotic phenotypes seen in the context of intervertebral disc injury and subsequent degeneration.

METHODS: New Zealand White rabbits were subjected to annulus puncture[5] with a 16-gauge needle to 5 mm depth, with 2-, 4-, and 8-week survival. The annulus fibrosus was assessed via second harmonic generation imaging and staining for alpha smooth muscle actin (αSMA). In vitro, bovine annulus cells were seeded onto electrospun PCL scaffolds, and a tensile stretching device was use to apply pre-strain to scaffolds prior to cell seeding (9% prestrain) for 24 hours. Both aligned and nonaligned prestrained and free swelling scaffolds (NE, NF, AE, AF) were assessed for fiber organization (angular spread), focal adhesions, YAP/TAZ nuclear localization, and αSMA+ stress fibers. Angular spread is reported as the standard deviation of the fiber angle distribution.

RESULTS: In the in vivo model, release of residual strains via needle puncture resulted in progressive disorganization of the AF (**Fig 1ab**) and the emergence of fibrotic phenotypes (i.e., αSMA expressing cells) after 2 weeks; these fibrotic signatures remained elevated through 8 weeks (**Fig 1ac**). In the in vitro model, both baseline organization and prestrain dictated fiber organization at the cellular length scale (**Fig 1f**). This organization had a significant effect on cell spreading (aspect ratio and spread area, **Fig 1gh**), with aligned microenvironments promoting elongation and minimizing spread area. These organized, pre-strained fiber environments limited focal adhesion area and maintained nuclear levels of YAP/TAZ at a low level (**Fig 1de,ij**), outcomes representative of cells interpreting the environmental cues as 'soft'[2]. Likewise, incorporation of αSMA into stress fibers was dependent on the organizational and prestrained state of fibrous environments, with aligned prestrained scaffolds reducing the fibrotic phenotype compared to nonaligned free swelling scaffolds (**Fig 1kl**). Thus, the contact-guidance provided by fiber organization inhibited the fibrotic phenotypes expected in stiff environments[3].

DISCUSSION: Our findings suggest that fibrotic phenotypes emerge with the release of residual strains in the annulus of injured discs. This patho-mechanobiologic event was replicated by an in vitro scaffold system, where cellular perception of the local environment was dictated by both baseline and strain-mediated fiber organization. Fiber organization provided cues (contact guidance) in aligned environments to modulate cell shape and size such that YAP/TAZ remained largely cytosolic, which in turn, suppressed incorporation of αSMA into stress fibers and the development of a fibrotic phenotype[3]. Continuing work is focused on using this scaffold-based system to evaluate pharmacologics that might inhibit this fibrotic remodeling response after injury.

SIGNIFICANCE: This study shows that the emergence of fibrotic phenotypes in annulus fibrosus cells is governed by local fiber organization, providing new directions for the development of therapeutics that can attenuate disease progression after fibrous tissue injury.

REFERENCES: [1] Engler+ 2005, [2] Dupont+ 2011, [3] Li+ 2017, [4] Michalek+ 2012, [5] Masuda+ 2005

ACKNOWLEDGEMENTS: This study was supported by NIH F32AR072478, R01EB02425, T32AR53461, P30AR050950, and VA I01RX002274.

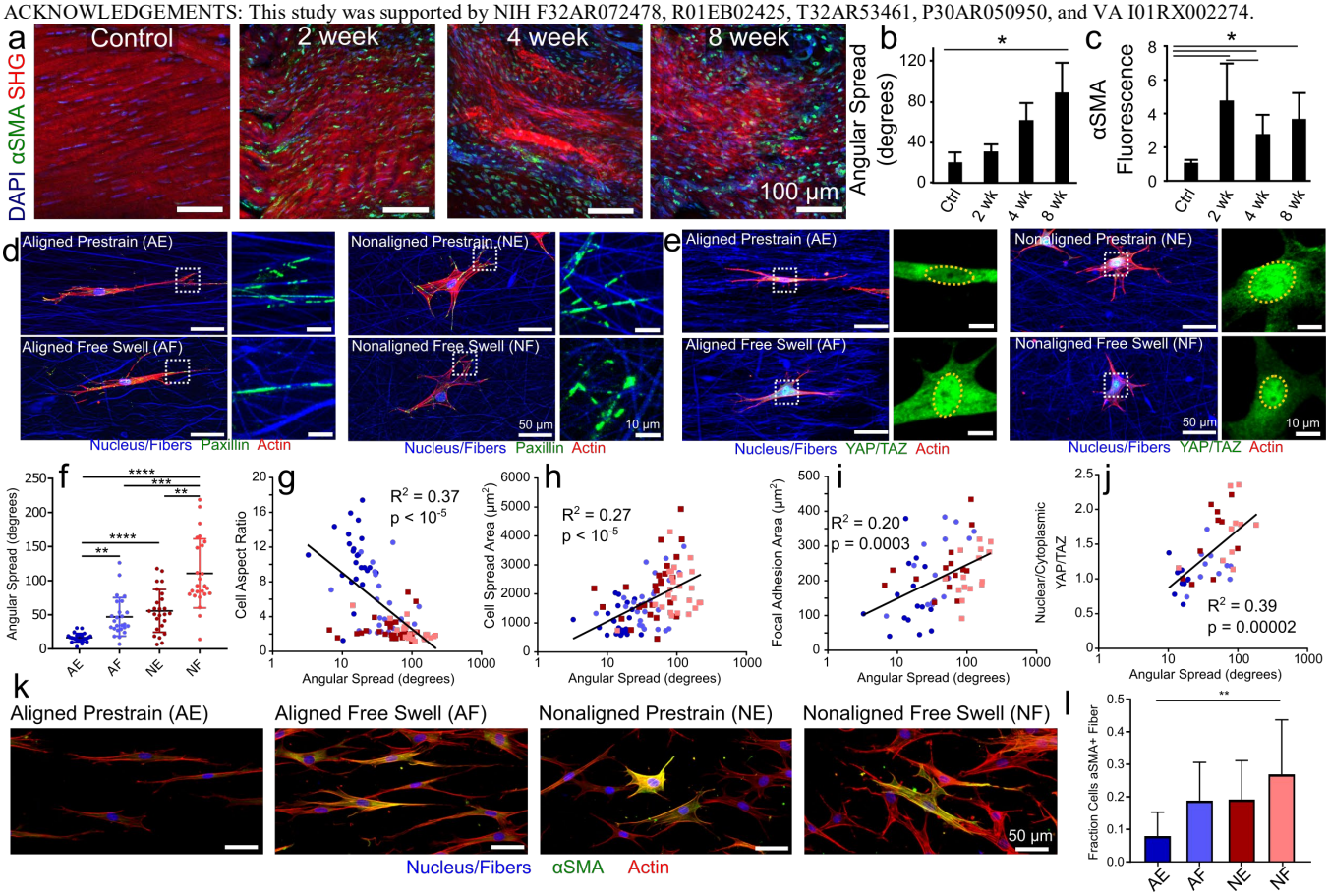

Figure 1: (a) SHG imaging coupled with αSMA localization and DAPI of injured native annulus fibrosus tissue. (b) Angular spread (standard deviation of fiber angle distribution) and (c) αSMA increased following puncture injury (n = 3 rabbits/group). (d) angular spread on scaffolds predicted (e) cellular morphology and spread area (f) (n = 100 cells/correlation), as well as (g, i) focal adhesion (i.e., paxillin) area per cell and (h. j) YAP/TAZ localization (n = 60 and 40 cells/correlation, respectively). (k, l) Fiber organization modulated αSMA+ expression and localization to stress fibers (n = 6 scaffolds/group) (*p<0.05, **p<0.01, ***p<0.001, ****p<0.0001).

Inflammatory Challenge Alters Cytoskeletal Networks and Transiently Inhibits Meniscus Cell Migration

Elisabeth A. Lemmon[1,2], Liane M. Miller[1,2], Jay M. Patel[1,2], Robert L. Mauck[1,2]

[1]Corporal Michael Crescenz VA Medical Center, Philadelphia, PA, [2]McKay Orthopaedic Research Laboratory, University of Pennsylvania, Philadelphia, PA

Meniscus injuries are common, accounting for 20% of orthopaedic surgical interventions each year to restore pain-free function of the knee. Pro-inflammatory cytokines IL1β and TNFα are found at higher levels post-injury and promote catabolic meniscal remodeling, inhibiting tissue repair. We evaluated the effects of IL1β and TNFα on meniscus fibrochondrocytes (MFC) migration in 2D and 3D. Further, we tested whether these factors impact cell spreading and adhesion through focal adhesion (FA) analysis. MFCs exposed to pro-inflammatory cytokines showed a dose dependent decrease in 2D migration. To assess duration of migratory inhibition after cytokine exposure, cells were exposed to cytokines for 24 hours and were evaluated over the following 7 days. Cytokine exposure resulted in persistent attenuation of 2D migration through day 3. By day 7, MFCs returned to control levels. Cell morphological analysis revealed that MFCs treated with IL1β were larger and had an increased number of FAs compared to controls. Interestingly, the average area of each FA was lower with IL1β treatment, suggesting that meniscus cells exposed to inflammatory conditions may be more firmly attached to the substrate than control cells. TNFα resulted in fewer marked changes in cell shape and adhesion, suggesting that this factor may attenuate migration through other mechanisms. Results from the 3D migration study showed that neither TNFα nor IL1β altered infiltration depth of cells from a meniscus explant; however, both factors reduced the number of cells migrating from the explant to the substrate. These findings support the concept that exposure to pro-inflammatory cytokines inhibits the migratory capacity of MFCs. Our data also provide new insight into the persistence of this migratory deficit, suggesting that cells remain compromised for at least 3 days after exposure to pro-inflammatory cytokines. These findings may improve clinical decision making by identifying the best timing for surgical repair of the meniscus as well as direct the development of new therapeutics to address inflammation during repair.

Adult muscle stem cells are morphologically heterogeneous *in vivo* with dynamically regulated cellular extensions

Nuoying Ma [1, 2], Paola Kuri [3], Edward Blake Hernandez [1], Jacob Kocan [1], Delia Chen [1], Elisia D. Tichy [1], Panteleimon Rompolas [3, 4] and Foteini Mourkioti [1, 4, 5, *]

[1]Department of Orthopaedic Surgery, [2]Bioengineering Graduate Program, [3]Department of Dermatology, [4]Department of Cell and Developmental Biology, and [5]Penn Institute for Regenerative Medicine, Musculoskeletal Program, Perelman School of Medicine, University of Pennsylvania, Philadelphia, PA 19104, USA.

Abstract

Muscle stem cells (MuSCs) are essential for tissue homeostasis and regeneration, but the potential contribution of MuSCs morphology to *in vivo* function remains unknown. Pax7 is a marker of adult MuSCs and we recently generated a Pax7EGFP reporter mouse to track MuSCs. Utilizing this model, we demonstrate that quiescent MuSCs in unperturbed muscles exhibit long protrusions that are morphologically heterogeneous. Adult MuSCs could be classified into three morphologically and functionally distinct subtypes, responsive, intermediate, and sensory. Upon injury, protrusion length was dynamically re-adjusted, with responsive cells responding first, followed by responses from sensory cells. As regeneration progressed and stem cell self-renewal returned, MuSC protrusions reappeared coincident with quiescence. The functional significance of our findings was reinforced by the aberrant regulation of MuSC protrusions in response to aging and dystrophy. Given the emerging interest of stem cell protrusions in other systems, our findings on the fundamental regulatory aspects of MuSC morphology may greatly inform the field.

Roles of TNFAIP8 family in intervertebral disc degeneration

Yejia Zhang [1,2], Zuozhen Tian [1], Lutian Yao [1], Honghong Sun [1], Ling Qin [1], Youhai H. Chen [1]

[1]Perelman School of Medicine, University of Pennsylvania; [2]Corporal Michael J. Crescenz Veterans Affairs Medical Center, Philadelphia, PA

Disclosures: This work was supported, in part, by research grants to YZ from the Department of Veterans Affairs Healthcare Network. histology core facilities have been supported by a grant to the Penn Center for Musculoskeletal Disorders (PCMD; P30AR069619).

INTRODUCTION: The TNF-α-induced protein-8 (TNFAIP8, also known as TIPE) family of molecules comprises four members: TNFAIP8 and TIPEs1-3. Since the first description of these proteins, their roles in fine-tuning inflammation and in directing leukocyte migration have been described in several organ systems. However, their relationship to intervertebral disc degeneration (IVD) is unknown.

METHODS: TIPE2 has been shown to direct leukocyte migration (Fayngerts, Wang et al. 2017) and we have preliminary evidence that TNFAIP8 participates in this process as well. Here, we studied tail IVDs in TNFAIP8 and TIPE2 double knockout (dko) mice and their wild type littermates (age 20-33 weeks), with the adjacent intact discs as controls. Macrophages were identified by immunostaining of the F4/80 antigen (EMR1), a known marker for cells of monocyte-macrophage lineage (antibody: Cell Signaling Rabbit mAb #70076). CXCL1 (known to attract leukocytes) gene expression was examined by Real Time PCR.

RESULTS. In the injured annulus fibrosus (AF) of wild type (WT) mice, macrophages were easily detectable by F4/80 staining (n=8 mice). In comparison, there was only faint staining in the outer edge of the AF, near the needle entry site (Figure 1, red arrow; n=10 mice). There was minimal staining at the outer edge of the AF, in the intact IVDs of both WT and TNFAIP8/TIPE2 dko mice (Figure 1). Cxcl1 gene expression was upregulated in the injured discs of the WT mice and dko mice compared with adjacent intact controls (n=8 and 10 mice, respectively; $p<0.05$), but there were no significant differences between the injured discs of the mutant mice and WT mice, with regard to gene expression ($p>0.05$).

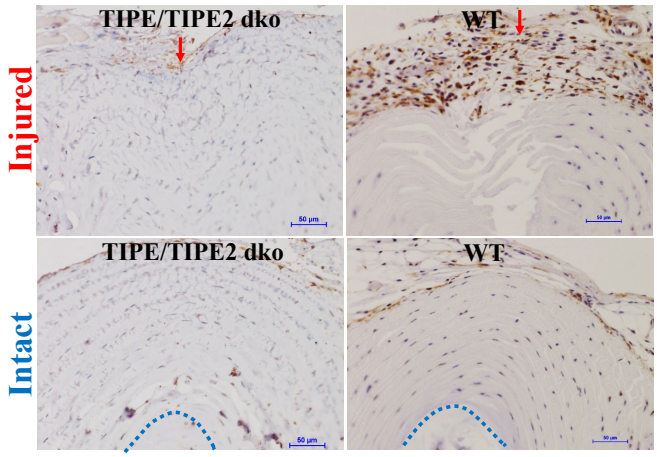

Figure 1. TIPE/TIPE2 double knock out (dko) mouse shows reduced macrophage recruitment compared with wild type (WT) mouse. Red arrow: direction of injury to the annulus fibrosus (AF). **Bar:** 50 μm. **Blue dotted line in intact discs** outlines the border of AF and nucleus pulposus (NP).

DISCUSSION: We found elevated gene expression of chemokines in the injured discs in both WT and mutant mice, but fewer F4/80 stained cells in the injured AF of the mutant mice, suggesting that the leukocyte is a primary 'target' of the mutation. Future studies include quantifying macrophages in the AF tissues, and correlating IVD morphology and mouse behavior, to further delineate the roles of TIPE molecules in IVD inflammation and degeneration. Discussion, including limitations and conclusions within the framework of stated question, hypothesis, or objective.

SIGNIFICANCE/CLINICAL RELEVANCE: Macrophages, found in diseased human IVDs (Nakazawa, Walter et al. 2018, Shamji, Setton et al. 2010) may be of pathophysiological significance.

REFERENCES:

1. Fayngerts SA, et al. Direction of leukocyte polarization and migration by the phosphoinositide-transfer protein TIPE2. Nat Immunol. 2017 Dec;18(12):1353-60. PMCID: PMC5690821.

2. Nakazawa KR et al. Accumulation and localization of macrophage phenotypes with human intervertebral disc degeneration. Spine J. 2018 Feb;18(2):343-56. PMCID: PMC5815908.

3. Shamji MF, et al. Proinflammatory cytokine expression profile in degenerated and herniated human intervertebral disc tissues. Arthritis Rheum. 2010 Jul;62(7):1974-82. PMCID: PMC2917579.

Role of Energy Metabolism in Bone Mass Accrual

Mohd Parvez Khan[1], Wen-Chih Lee[2,1], Fanxin Long[2,1] and Ernestina Schipani[1]

[1]McKay Laboratory, Department of Orthopedic Surgery, Perelman School of Medicine, University of Pennsylvania, Pennsylvania, USA. [2]CHOP, Philadelphia, Pennsylvania, USA

Once thought to be a mere consequence of the cell state, metabolism is now known to play a critical role in dictating the cell fate. Glycolysis and oxidative phosphorylation (OxPhos) are the two main sources of intracellular ATP. Factors that promote osteoblast activity, such as the Hypoxia-Inducible Factor 1 (HIF1), activate glycolysis. Notably, during *in vitro* osteogenic differentiation of mesenchymal progenitors, both glycolysis and OxPhos increase. The role of OxPhos in osteoblast biology *in vivo* is still mostly unexplored. To fill this gap of knowledge, we generated a mutant mouse lacking Mitochondrial Transcription Factor A (TFAM) in uncommitted mesenchymal progenitors and their descendants using PRX1-Cre (PRX;TFAM$^{f/f}$). TFAM regulates transcription of mitochondrial genes that encode thirteen subunits of the electron transport chain and thus controls OxPhos. Three-week-old PRX;TFAM$^{f/f}$ mice displayed a low bone mass phenotype with multiple spontaneous. Our data indicate that mesenchymal TFAM is necessary for bone mass accrual. Impairment of OxPhos is the most powerful, consistent, and best characterized biological consequence of loss of TFAM across numerous cell types. However, TFAM also regulates duplication of mitochondrial DNA, and mitochondria have a variety of functions beyond OxPhos and ATP production. Therefore, to establish if the impairment of OxPhos, and thus the decreased intracellular ATP, is the primary cause of the PRX;TFAM$^{f/f}$ bone phenotype, we asked whether forced upregulation of glycolysis would prevent the low bone mass of PRX;TFAM$^{f/f}$ mice. For this purpose, we generated a double mutant mouse, lacking TFAM and overexpressing a constitutively stabilized HIF1 in the same cells, PRX;TFAM$^{f/f}$;HIF1dPA$^{f/f}$. Analysis of PRX;TFAM$^{f/f}$;HIF1dPA$^{f/f}$ bones revealed that increased HIF1 activity prevented the bone fractures occurring in PRX;TFAM$^{f/f}$ mutants. Building on those findings, we are currently testing the hypothesis that TFAM in cells of the osteoblast lineage is crucial for bone mass accrual by promoting OxPhos, and thus ensuring the proper levels of intracellular ATP. The successful accomplishment of these experiments will expand and deepen our knowledge of the role of energy metabolism, particularly OxPhos, in the regulation of osteoblast differentiation and bone mass accrual.

Macrophage Regulator of G-protein signaling 12 Contributes to Inflammatory Pain Hypersensitivity

Gongsheng Yuan[1], Shuting Yang[1], Wenqin Lou[2], Mayank Gautam[2], Shuying Yang[1,3,4*]

[1]Department of Basic and Translational Sciences, School of Dental Medicine, University of Pennsylvania, Philadelphia, PA 19104, USA
[2]Department of Neuroscience, Perelman School of Medicine, University of Pennsylvania, Philadelphia, PA 19104, USA
[3]Center for Innovation & Precision Dentistry, School of Dental Medicine, School of Engineering and Applied Sciences, University of Pennsylvania, Philadelphia, PA 19104, USA
[4]The Penn Center for Musculoskeletal Disorders, School of Medicine, University of Pennsylvania, Philadelphia, PA 19104, USA

Background: Pain is a predominant symptom in rheumatoid arthritis (RA) patients which results from joint inflammation and is augmented by central sensitization. Regulator of G-protein signaling 12 (RGS12) is the largest protein in RGS protein family which plays a key role in the development of inflammation. This study aims to investigate the regulation of RGS12 in inflammatory pain and explore underlying mechanisms and the potential RA pain targets.

Methods: Macrophage RGS12 deficient (LysM-Cre^{+};RGS12$^{fl/fl}$) mice were generated by mating RGS12$^{fl/fl}$ mice with LysM-Cre^{+} transgenic mice. Collagen Antibody-Induced Arthritis (CAIA) models were induced in LysM-Cre^{+};RGS12$^{fl/fl}$ mice by administration of a cocktail of five monoclonal antibodies and LPS. Mouse nociception was examined using the von Frey and heat plate test. Primary macrophages and RAW264.7 cells were used to analyze the regulation function and mechanism of RGS12 in vitro. The expression and function of RGS12 and COX2 were determined by the real-time PCR, ELISA assay, and luciferase assay.

Results: Ablation of RGS12 in macrophages decreased pain-related phenotypes, such as paw swelling, clinical score, and inflammatory score in CAIA model. LysM-Cre^{+};RGS12$^{fl/fl}$ mice displayed an increase of the resistance to thermal and mechanical stimulation from day 3 to day 9 during the CAIA, demonstrating inhibition of the inflammatory pain. Overexpression of COX2 and PGE2 in macrophages enhances RGS12 expression, and PGE2 regulates RGS12 expression through the G-protein-coupled receptors EP2 and EP4. Furthermore, RGS12 or RGS12 PTB domain strengthens the transcriptional regulation of COX2 by NF-κB, whereas inhibition of NF-κB suppressed the regulation of RGS12 on COX2 in macrophages.

Conclusions: Our results demonstrate that deletion of RGS12 in macrophages attenuates the inflammatory pain, which is likely due to the impaired regulation in the COX2/PGE2 signaling pathway.

Single-cell transcriptomics reveals key roles for SOXC transcription factors in proliferation and migration of cranial progenitor cells

Marco Angelozzi[1], Fernanda Mafra[2], Michael Gonzalez[2], Renata Pellegrino[2], Pallavi Bhattaram[3], Véronique Lefebvre[1]

[1]Division of Orthopaedics Surgery, Children's Hospital of Philadelphia, Pennsylvania, USA
[2]Center for Applied Genomics, Children's Hospital of Philadelphia, Pennsylvania, USA
[3] Department of Orthopaedics, Emory University School of Medicine, Atlanta, Georgia, USA
E-mail contacts: angelozzim@email.chop.edu; lefebvrev1@email.chop.edu

The skull is essential in vertebrates, as it protects the brain from potential injuries. Its development is complex, as it involves the establishment of several bones and intervening sutures in a spatially and temporally tightly regulated manner. It relies on bipotent progenitor cells that originate in the early embryo in a supraorbital ridge. While some of these cells coalesce and start forming bone and dermis in the basolateral region, others ensure expansion of the two tissue primordia by proliferating and migrating towards the apex and lateral sides of the head. Perturbations in the cellular and molecular mechanisms controlling these phenomena cause defects of the skull, often associated with neurological abnormalities and impairing disabilities. For this reason, it is essential to investigate molecular pathways involved in skull development. SOXC proteins (i.e., SOX4, SOX11 and SOX12) are key transcription factors in the formation of several systems, including the skeleton. However, their role in craniogenesis has never been investigated. Thus, we generated mice in which we conditionally inactivated the SOXC genes using a *Prx1Cre* transgene active in skeletal progenitor cells (*SOXC$^{fl/fl}$ Prx1Cre* mice). Skeletal preparations of fetuses near birth showed an abnormal cranial vault. The interparietal and occipital bones and the apex of the frontal and parietal bones appeared to be either lacking or not mineralized. Single-cell RNA-sequencing (scRNA-seq) analysis of cranial tissues at different developmental stages and in situ hybridization (ISH) assays showed strong expression of *Sox4* and *Sox11* in proliferating and migrating osteodermal progenitor cells. These cell populations were undersized in mutant calvarium, and an EdU incorporation assay showed a reduced rate of proliferation of mutant cranial progenitor cells. Furthermore, scRNA-seq analysis revealed downregulation of a specific set of cytoskeleton genes in mutant cells. ISH assays validated this finding and showed that osteoprogenitors were scarse and disseminated rather than abundant and spatially organized in the apical layers of the mutant cranial mesenchyme. Overall, our data demonstrate key roles for the SOXC genes in skull development. By enhancing the expression of cytoskeletal genes in progenitor cells, they ensure the proliferation and migration of these cells, and thereby the formation of the multiple bones that compose the cranium. Our findings provide novel mechanistic insights into syndromic craniofacial dysmorphism caused by *SOX4* and *SOX11* heterozygous variants in humans and into various other normal and pathological processes dependent on the SOXC genes and progenitor cell proliferation and migration.

Dependence of Tendon Multiscale Mechanics on Sample Length is Consistent with Discontinuous Fibrils

Authors: Benjamin E. Peterson[1], Spencer E. Szczesny[1,2]

[1] *Department of Biomedical Engineering, Pennsylvania State University, University Park, PA*

[2] *Department of Orthopaedics and Rehabilitation, Pennsylvania State University, Hershey, PA*

Introduction: Tendons transmit forces from muscle to bone and are critical for proper musculoskeletal function. Despite this, the structure-function relationships governing physiological tendon function and the changes underlying tendon pathology are unclear. Specifically, it is unclear how collagen fibrils transmit load across length scales within the tendon hierarchical structure. Previous studies tracking collagen fibril lengths concluded that they are likely functionally continuous[1,2]. However, multiscale mechanical testing has contested this, showing that fibril strains are significantly less than the bulk tissue strains, suggesting that the fibrils are discontinuous and transmit load via interfibrillar sliding[3,4]. In order to address the question of collagen fibril continuity, the **objective** of this study was to assess whether tendon multiscale mechanics is dependent on the sample gauge length. We hypothesized that as the gauge length decreases and approaches the fibril length, the tendon mechanics will transition to a continuous fibril response with a fibril:tissue strain ratio of one and an increase in modulus.

Materials and Methods: Twenty-two tail tendons were harvested from one-year old Long Evan rats. Samples were stained with DTAF at 5 µg/ml and secured into a tensile testing device mounted atop a confocal microscope. The samples were gripped at four varying gauge lengths (GLs) of 30 mm (n=6), 20 mm (n=6), 10mm (n=5) and 5 mm (n=5). Sets of photobleached lines (PBL) (4 lines, 100 µm apart) were bleached at the sample center and at ± 1.25 mm. Samples were loaded to onset of failure in 2 % strain increments at 10 %/s followed by a 15-minute stress relaxation and imaging at each PBL site. Tissue macrostrains were quantified by the displacement of the peripheral ± 1.25 mm PBL sites and fibril macrostrains were quantified by the relative displacements between the local PBL lines at each location. The macroscale modulus was calculated by a linear fit through the origin and first two quasi-static points on the stress-strain curve. A one-way ANOVA was conducted to test significance of gauge length on the tendon samples modulus. Statistical significance was set to $p < 0.05$.

Results and Discussion: Analysis of the fibril:tissue strain ratio (Fig. 1A) at the last increment preceding failure shows that the 30 mm and 20 mm GL show significant deviation from one ($p < 0.0001$ and $p < .05$, respectively), while the 10 mm and 5 mm GL were not shown to be different than one ($p = .1529$ and $p = .7721$, respectively). A linear regression of the fibril:tissue behavior across all strain increments demonstrated a negative correlation with tissue strain for the 30mm and 10mm samples ($p < 0.0001$ and $p < .05$, respectively), while the 20mm and 5mm samples exhibited no change with increasing strain ($p = .091$ and $p = .2722$, respectively). The 5mm GL condition was the only sample which showed both a fibril:tissue strain ratio response that was equivalent to one and was independent of increasing tissue strain. Analysis of the macroscale mechanical behavior showed a significant increase in tissue stiffness for the 5 and 10 mm gauge lengths (Fig. 1B & 1C).

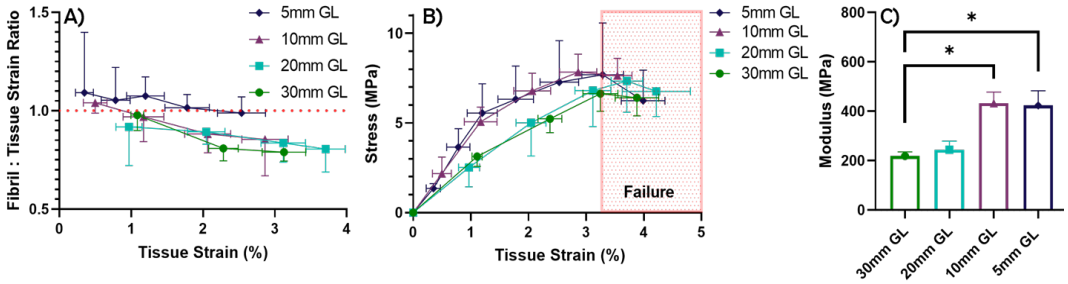

Figure 1. **A)** The fibril:tissue strain ratio response across various gauge lengths **B)** Stress vs. strain response. **C)**. Sample modulus across various gauge length conditions. Significance (*) shown at p<.0001.

Conclusions: In conclusion, this study demonstrates that gauge length has a significant effect on the multiscale mechanical properties of tendons. Specifically, when the gauge length is reduced to 5mm, the fibril strains were equal to the macroscale tissue strains, suggesting that at this gauge length the fibril are continuous. The lack of interfibrillar sliding between continuous fibrils is further supported by the significantly elevated tissue stiffness with the reduced gauge lengths. Together, this supports our hypothesis that collagen fibrils in tendons are discontinuous and suggests that they have a "functional length" of about 5-10 mm in rat tail tendon fascicles. This information is essential to understanding basic physiological loading behavior of tendons and can provide critical insight into how structural changes can lead to pathological disease states.

References: 1. Almutairi, et al. *IEEE Comput. Soc. Conf. Comput. Vis. Pattern Recognit. Work.* 2016; 1342-1349
2. Svensson, et al. *Acta Biomater.* 2017; **50**,293-301 3. Szczesny, et al. *Acta Biomater*. 2014;**10**,2582-2590
4. Screen. et al. *Proc. Inst. Mech. Eng.* 2014;**218**,109-119

RGS12 is required for the maintenance of mitochondrial function during skeletal development

Gongsheng Yuan[1], Shuting Yang[1], Min Liu[1], Shuying Yang[1,2,3*]

[1]Department of Basic and Translational Sciences, School of Dental Medicine, University of Pennsylvania, Philadelphia, PA 19104, USA

[2]Center for Innovation & Precision Dentistry, School of Dental Medicine, School of Engineering and Applied Sciences, University of Pennsylvania, Philadelphia, PA 19104, USA

[3]The Penn Center for Musculoskeletal Disorders, School of Medicine, University of Pennsylvania, Philadelphia, PA 19104, USA

Mitochondrial morphology and function are crucial for tissue homeostasis, such as for skeletal development, but the cellular and molecular mechanisms remain unclear. Here, we provide evidence that regulator of G-protein signaling 12 (RGS12) is present in the mitochondria of primary chondrocytes and cartilage tissues. Deletion of RGS12 in type II collagen-positive cells led to a significant decrease in mitochondrial number, membrane potential, and oxidative phosphorylation function. Mechanistically, RGS12 promoted the function of ATP5A as an enhancer of tyrosine phosphorylation. Mice with RGS12 deficiency in the chondrocyte lineage showed serious body retardation, decreased bone mass, and chondrocyte apoptosis due to the defective activity of ATP synthase. To our knowledge, this is the first report that RGS12 is required for maintaining the function of mitochondria, which may allow it to orchestrate responses to cellular homeostasis.

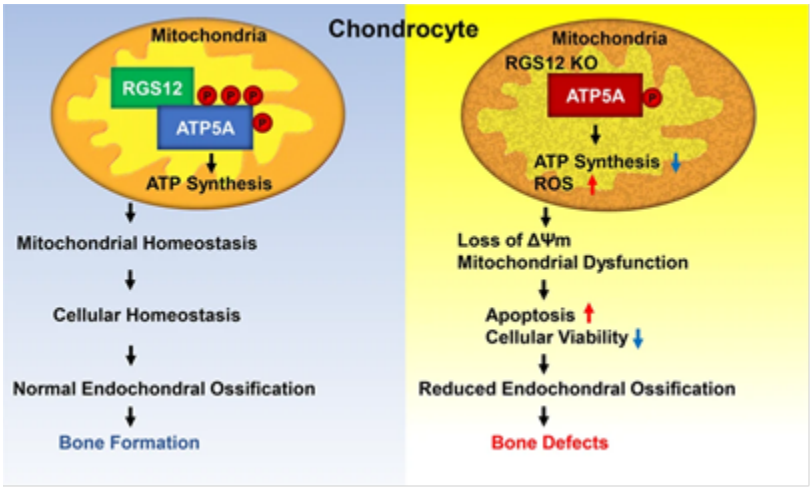

Viability of Cells within Anterior Cruciate Ligament Explants during Mechanical Stimulation

Lauren Paschall, Sabrina Carrozzi, and Spencer Szczesny
The Pennsylvania State University, University Park, PA

Introduction: The anterior cruciate ligament (ACL) is one of the most damaged or torn ligaments in the human body.[1] ACL reconstructions are common surgical procedures, where the native ACL is replaced by a tendon allograft or autograft.[2] However, allografts are not recommended in active or young patients due to high failure rates.[1] Data suggest that differences in clinical outcomes between graft types is due to increased mechanical loading.[3] Therefore, we hypothesize that poor allograft performance in young individuals is because of an altered response to mechanical loading leading to impaired post-surgical remodeling. To investigate a potential mechanobiological deficit in allograft reconstructions, we intend to use a bioreactor to apply stress to ACL reconstructions within a controlled environment. However, it is first necessary to demonstrate that the cells remain viable in the explanted tissue during loading. Therefore, the goal of this project was to study the cell viability of cyclically loaded ACL explants in a tensile bioreactor.

Methods: ACLs were harvested from both knees of five New Zealand white rabbits and placed in a tensile bioreactor with culture media kept at 37°C. After 10 h of acclimating the ACLs to explant culture, the bioreactor cyclically loaded the samples to 2 MPa at 0.25 Hz for 8 h. The specific choice of 2 MPa is based on estimates of *in situ* ACL graft loading.[4] Since unloading is detrimental to tendon homeostasis,[5] control samples will be placed in the bioreactor for the same duration but under a minimal (0.1 MPa) static load. After loading, the ACLs were stained in PBS with fluorescein diacetate (FDA) at 2 µL/mL and propidium iodide (PI) at 5 µL/mL for 5 min. Volumetric image stacks were acquired at multiple locations using an inverted confocal microscope. The image stacks were segmented into three different regions based on imaging depth into the tissue (surface: 0 µm depth; middle: 32-39 µm depth; deep: 55-62µm depth). The images were thresholded to determine regions of positive labeling, and cell viability was determined by dividing the area of FDA signal by the total (FDA + PI) signal. Wilcoxon signed rank tests were used to determine differences in cell viability between loading conditions. Kruskal-Wallis tests were used to compare cell viability across imaging depth.

Results: In the statically loaded samples, the median cell viability values for the surface, middle, and deep regions are 57%, 84%, and 77%, respectively **(Fig. 1)**. In the cyclically loaded samples, the median cell viability values for the surface, middle, and deep regions are 66%, 79%, and 88%, respectively. Our results showed no significant difference in cell viability across depth for each loading condition ($p = 0.25, 0.26$). In addition, there was no significant difference observed between loading conditions at each depth ($p = 0.63, 0.88, 0.63$).

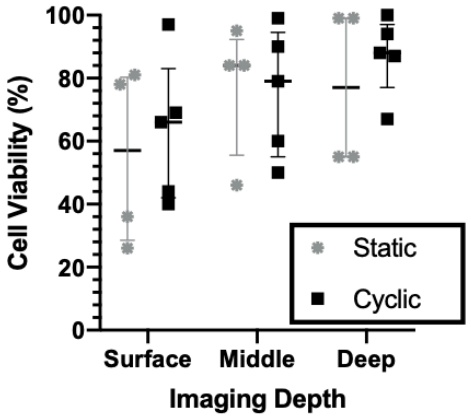

Figure 1. While not statistically significant, cell viability appeared to increase with increasing tissue depth. No statistically significant differences in viability were observed between static and cyclic loading conditions. (n=4-5). Data presented as median with interquartile range.

Conclusions: The purpose of this study was to determine whether ACL explants remain viable during cyclic loading in a tensile bioreactor. While not statistically significant, it did appear that cell viability was dependent on tissue depth. Specifically, significant cell death was observed in the surface and middle sections, while the deep sections exhibited approximately 80% viability. This increase in cell viability occurred over a total imaging depth of about 55-62 µm into the tissue. Since the average thickness of an ACL is approximately 3 mm, this suggests that the innermost portion of the tissue has a cell viability of 80% or greater. The higher cell death near the surface of the tissue is expected because this layer is susceptible to damage by external factors (like harsh surfaces). In addition, dissection of the ACL into an *ex vivo* environment may cause desiccation of the outermost cell layer. While a greater sample size is necessary to confirm this depth dependent cell viability, the high cell viability in the sample interior suggests that this loading protocol is appropriate for mechanically stimulating native ACLs and potentially ACL reconstructions. In the future, we will use this protocol to determine the discrepancies between allograft and autograft mechanical properties. Future research is expected to reveal differences in the mechanosensing and mechanotransduction pathways between each graft type.

References:

1. Barret GR+ Arth - J Arth Rela Surg 2010 26:1593–601; 2. Zeng C+ Arth - J Arth Rela Surg 2016 32:153-163; 3. Borchers Am J Sprts Med 2009 37:2362-7; 4. Wang T+ Biotechnol Bioeng 2013 110(5):1495-507; 5. Galloway+ J Bone Joint Surg Am 2013 95(17):1620-8

Acknowledgements: We would like to thank Krishna Pedaprolu for his assistance on this project. Funding was provided by internal Penn State grants

Elastic Modulus Mapping for Bovine Cortical Bone from Submillimeter- to Submicron-scales using PeakForce Tapping Atomic Force Microscopy

Yuxiao Zhou[a], Markus J. Kastner[b], Timothy B. Tighe[b], Jing Du[a*]
[a] Department of Mechanical Engineering, Pennsylvania State University, University Park, PA
[b] Materials Research Institute, Pennsylvania State University, University Park, PA

Abstract

Bone is a composite material consisting of organic and inorganic components that organized into hierarchical structures to provide load-bearing functions. This paper presents the results of PeakForce Tapping atomic force microscopy (AFM) scans on cut and polished bovine cortical bone specimens that were submerged in water.

The elastic modulus map and surface morphology were obtained for various bone hierarchical structures from submillimeter- to submicron-scales. The elastic modulus of osteons (20.51 ± 6.85 GPa) was slightly lower than the interstitial bone (21.87 ± 5.48 GPa); they were both much greater than that of the cement lines (7.49 ± 4.23 GPa). The elastic modulus in the lamella structures varied periodically from higher values in thick sub-lamellae (21.49 ± 6.58 GPa) to the lower values in thin sub-lamellae (9.67 ± 2.69 GPa). The results also show relatively softer mineralized collagen fibril bundle arrays (12.94 ± 2.71GPa) embedded in harder matrix materials (28.39 ± 5.75 GPa).

The variations in the elastic modulus suggest different degrees of mineralization or different fibril orientations. Cement lines are considered to play an important role in the fracture and fatigue behaviors of bone, as they arrest crack growth and absorb energy. To the best of our knowledge, current work is the first direct measurement of the elastic modulus of cement lines. The higher modulus of interstitial bone can be attributed to the fact that interstitial bone was osteons that formed earlier and is more mineralized than the recently-formed osteons. The MCF bundles were measured to be softer than the matrix in the current work. It indicates that the MCF bundles have less mineral content than the matrix, and the intrafibrillar space is smaller than extrafibrillar space. The histograms of elastic modulus indicate the dominating compositions or dominating fibril orientations.

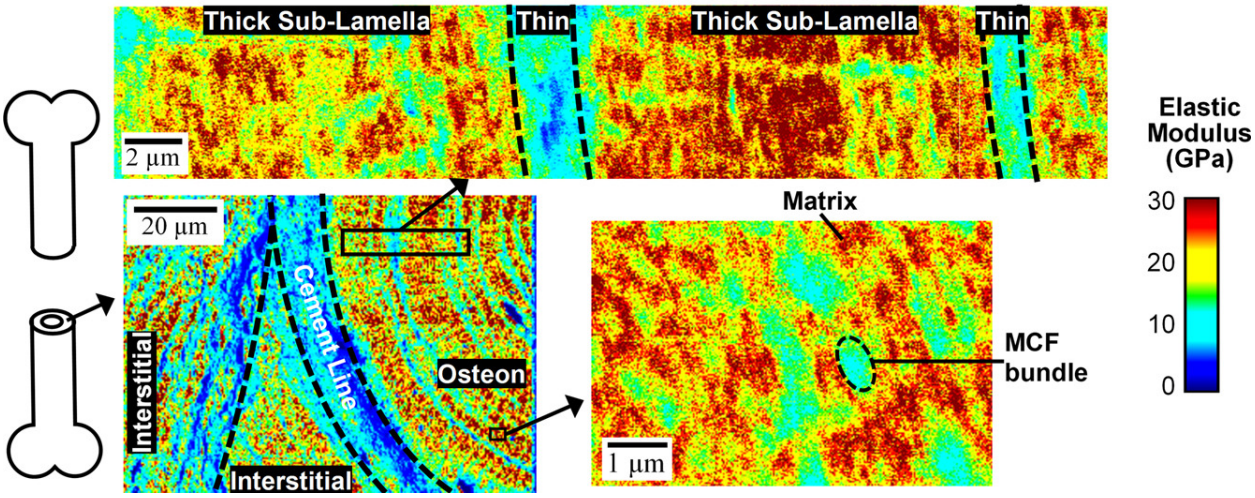

Keywords: Cortical bone, atomic force microscopy, elastic modulus, PeakForce Tapping

SOX9 maintains growth plate and articular cartilage throughout life by promoting the chondrocyte differentiation program and repressing the osteoblast program

Abdul Haseeb*, Ranjan Kc*, Marco Angelozzi, Charles de Charleroy, Danielle Rux, Maurizio Pacifici and Véronique Lefebvre

Translational Research Program in Pediatric Orthopaedics, Division of Orthopaedic Surgery, The Children's Hospital of Philadelphia, Philadelphia, PA 19104

*These authors contributed equally to this work

Cartilage is essential throughout vertebrate life. It arises during development when osteochondroprogenitor cells commit to chondrogenesis, activate a pancartilaginous program to form cartilaginous skeletal primordia, and then embrace either a growth-plate program to ensure skeletal growth or an articular program to build permanent joint cartilage. Various diseases characterized by malformation or degeneration of cartilage afflict a large number of humans. Incomplete knowledge of the mechanisms underlying these diseases currently limits the development of effective preventive and therapeutic treatments. The transcription factor SOX9 is known to be required for embryonic chondrogenesis, but its postnatal roles remain unclear, despite evidence that it is downregulated in osteoarthritis and heterozygously inactivated in campomelic dysplasia, a severe skeletal dysplasia characterized postnatally by small stature and kyphoscoliosis. Using conditional knockout mice and high-throughput sequencing assays, we show here that SOX9 is required postnatally to prevent growth plate closure and pre-osteoarthritic deterioration of articular cartilage. Its deficiency prompts growth-plate chondrocytes at all stages to downregulate most pancartilaginous (e.g., *Acan* and *Col2a1*) and growth plate-specific genes (*Fgfr3*, *Ihh*, and *Col10a1*) and to reach a post-hypertrophic chondrocyte terminal stage (namely marked by high-level expression of *Mgp* and *Nt5e*). Upregulation of osteogenic genes (*Runx2* and *Sp7*) quickly ensues, followed by upregulation of osteoblast differentiation genes (*Col1a1* and *Bglap*). SOX9 deficiency does not perturb the articular chondrocyte-specific program, except in load-bearing regions, where it also provokes chondrocyte conversion to osteoblastogenesis. Pathway analyses support roles for SOX9 in controlling TGF□ and BMP signaling activities during this chondrocyte-to-osteoblast transition. These findings deepen current understanding of the cellular and molecular mechanisms that specifically ensure lifelong growth-plate and articular cartilage vigor by identifying osteogenic plasticity of growth-plate and articular chondrocytes and a SOX9-countered chondrocyte dedifferentiation/osteoblast differentiation process.

Elevated Inflammatory Gene Expression in Intervertebral Disc Tissues in Mice with ADAM8 Inactivated

Yejia Zhang, MD, PhD, Zuozhen Tian, MS, David Gerard, MS, Lutian Yao, MD, Frances S. Shofer, PhD, Gabriella Cs-Szabo, PhD, Ling Qin, PhD, Maurizio Pacifici, PhD, Motomi Enomoto-Iwamoto, DDS, PhD

Departments of Physical Medicine & Rehabilitation, Orthopedic Surgery, and Emergency Medicine, Perelman School of Medicine, University of Pennsylvania

We previously found ADAM8 enzymatic activity elevated in degenerative human intervertebral disc (IVD).[1] Here, we examined the discs of an ADAM8-inactivation mouse that carries a mutation preventing self-activation of the enzyme.[2] Surprisingly, elevated gene expression for inflammatory markers (*Cxcl1*, *IL6*; Figure 1) was observed in the injured discs of ADAM8 mutant mice, along with elevated expression of type 2 collagen gene (*Col2a1*), compared with that of wild type controls. The injured annulus fibrosus of mutant and wild type mice contained a larger proportion of large collagen fibers compared with intact discs, as documented by microscopic examination under circular polarized light. There may be fewer small collagen fibers in the annulus fibrosus of mutant mice than in control animals. This suggests that ADAM8 may regulate inflammation and collagen fiber size. The seemingly contradictory findings of elevated inflammatory markers in the mutant mice and excessive ADAM8 activity in the human degenerative discs suggest that ADAM8 may follow the "Goldilocks principle", in that an optimal level of enzymatic activity is needed for tissue maintenance and repair. As a future therapeutic intervention to retard intervertebral disc degeneration, partial inhibition of ADAM8 proteolysis may be more desirable than complete inactivation of this enzyme.

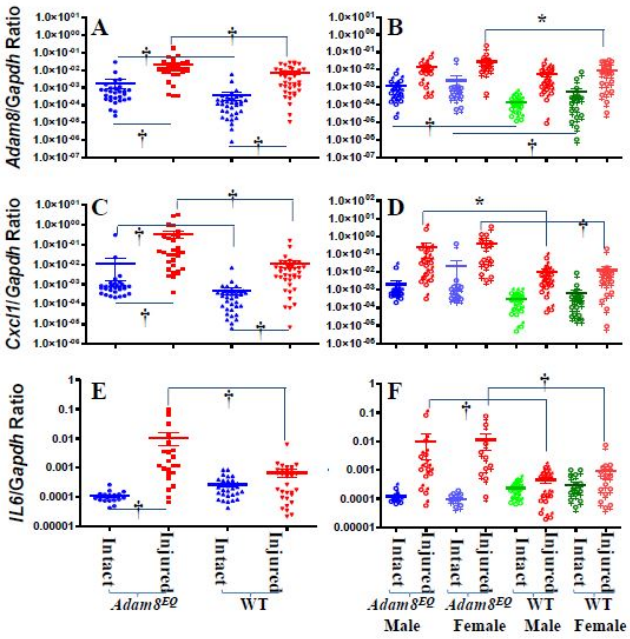

Figure 1. *Adam8* and Pro-inflammatory Gene Expression in the Injured Mouse Tail Intervertebral.

References

1. Ruel, N. *et al*. Fibronectin Fragments and the Cleaving Enzyme ADAM-8 in the Degenerative Human Intervertebral Disc. *Spine (Phila Pa. 1976)* **39**, 1274-1279 (2014).

2. Zack, M. D. *et al*. Reduced incidence and severity of experimental autoimmune arthritis in mice expressing catalytically inactive A disintegrin and metalloproteinase 8 (ADAM8). *Clin. Exp. Immunol.* **158**, 246-256 (2009).

Targeting Cartilage EGFR Pathway for Osteoarthritis Treatment

Tao Gui[1](Tao.Gui@pennmedicine.upenn.edu), Yulong Wei[1,2,3], Lijun Luo[2], Feifan Yu[4], Lesan Yan[2], Lutian Yao[1], Leilei Zhong[1], Wei Yu[1,3], Biao Han[5], Jay M. Patel[1,6], Frank Beier[7], Zengwu Shao[3], Lin Han[5], Robert L. Mauck[1,2,6], Andrew Tsourkas[2], Jaimo Ahn[1], Zhiliang Cheng[2*], and Ling Qin[1*]

[1]Department of Orthopaedic Surgery, [2]Department of Bioengineering, University of Pennsylvania, Philadelphia, USA; [3]Department of Orthopaedics, Huazhong University of Science and Technology, Wuhan, China; [4]Alphathera, Inc. Philadelphia, USA; [5]School of Biomedical Engineering, Drexel University, Philadelphia, USA; [6]Corporal Michael J Crescenz VA Medical Center, Philadelphia, USA; [7]University of Western Ontario, London, Canada.

Disclosures: A.T. is a founder and owns equity in AlphaThera.

INTRODUCTION: Osteoarthritis (OA) is a widespread chronic joint disease characterized by cartilage degeneration. We previously discovered that EGFR signaling is critical for maintaining the superficial layer of articular cartilage and found that mice with cartilage-specific (*Col2-Cre*) EGFR deficiency develop spontaneous OA (1). Here, we designed a two-pronged approach to investigate the effects of positively targeting the EGFR pathway on articular cartilage. First, we genetically enhanced EGFR activity by adopting a *Rosa-DTR* model. Originally identified as a receptor for bacterial diphtheria toxin (DT), DTR was later discovered to be human full-length HBEGF (2), a ligand for EGFR. Thus, it allows us to study the effect of cartilage-specific EGFR over-activation on OA progression. Second, we synthesized and characterized nanoparticles (NPs) conjugated with TGFα, another EGFR ligand, and tested their therapeutic efficacy in OA mice.

METHODS: *Animals*- All animal work was approved by the Institutional Animal Care and Use Committee (IACUC) at the University of Pennsylvania. *Col2-Cre Rosa-DTR* (*HBEGF Over^{Col2}*) and *Aggrecan-CreER Rosa-DTR* (*HBEGF Over^{AgcER}*) mice, and their *WT* (*DTR* or *Cre* only) siblings were generated. *HBEGF Over^{AgcER}* mice and *WT* received Tamoxifen (Tam, 75 mg/kg/day) injections for 5 days before surgery. Male mice at 3 months of age were subjected to destabilization of medial meniscus (DMM) or sham surgery at right knee. For treatment, *WT* mice received 10 µl of PBS, TGFα-DBCO (10 µM TGFα content), Ctrl-NP (no TGFα) and TGFα-NPs (10 µM TGFα content) intra-articularly once every 3 weeks starting from right after DMM surgery for 3 months. *TGFα-NP synthesis*- Bacteria-expressed human TGFα were labeled at the C-terminus with a constrained alkyne, dibenzocyclooctyne (DBCO), via sortase-tag expressed protein ligation (STEPL). TGFα-NPs were then prepared via copper-free click chemistry, by mixing TGFα-DBCO with azide-functionalized NPs made from 55mol% poly(ethylene glycol)-polycaprolactone (PEG-PCL)/20mol% poly(L-lysine-block-poly(ε-caprolactone) (PLL-PCL)/25mol% 1,2-distearoyl-sn-glycero-3-phosphoethanolamine-N-[azido(polyethylene glycol)-5000] (DSPE-PEG5K-N3) using the film hydration method. *Histology*- Knee joints were processed for paraffin sections followed by HE, Safranin-O/fast green (SO/FG), p-EGFR, Ki67, TUNEL, and PRG4 staining. *MicroCT*- Femurs were scanned from the epiphyseal end at a 6-µm resolution by microCT 35. The 3D images of the femoral distal end were reconstructed to generate a 3-D color map of thickness for the entire subchondral bone plate (SBP). *Cell culture*- Chondroprogenitors were harvested from articular cartilage of 5-month-old mouse knee joints by enzymatic digestion. Cells were then used for Western blots and CFU-F assays. *Statistics*- Data are expressed as means±SEM and analyzed by one- or two-way ANOVA and unpaired, two-tailed Student's t-test.

RESULTS: *HBEGF Over^{Col2}* mice displayed normal knee joints. No gross abnormality was detected. Long bone structure, including subchondral trabecular bone, subchondral bone plate (SBP), and metaphyseal trabecular bone, was also not affected. The most obvious change was cartilage. *HBEGF Over^{Col2}* mice displayed expanded growth plate and articular cartilage at 1 and 5 months of age (23.27% and 34.28% thicker than *WT* cartilage, respectively) (Fig. 1A). The superficial layer contains chondroprogenitors for articular cartilage. *HBEGF Over^{Col2}* articular cartilage had 1.79-fold more superficial chondrocytes (Fig. 1B, D) and formed 1.96-fold more CFU-F colonies than *WT* mice at 5 months of age, which was accompanied by enhanced Ki67 and Prg4 staining and reduced TUNEL staining (Fig. 1C). Interestingly, after DMM injury, articular cartilage degeneration was remarkably attenuated in *HBEGF Over^{Col2}* mice (Fig. 2A, D) and *Over^{AgcER}* mice (with Tam injections before the surgery, Fig. 2D, E). This cartilage protective action is mediated by EGFR signaling because it was completely abolished by co-treatment of EGFR inhibitor, Gefinitib (Fig. 2C, F). TGFα-NPs (Fig. 3A) were approximately spherical in shape with a hydrodynamic diameter of 25.93 nm. They activated EGFR signaling in primary chondrocytes as potent as free TGFα (Fig. 3B). Due to a positive charge, TGFα-NPs had superior cartilage uptake, penetration, and joint retention abilities compared to free TGFα. Strikingly, intra-articular delivery of TGFα-NPs effectively maintained EGFR activity (p-EGFR) in cartilage (Fig. 3C) and attenuated DMM-induced OA cartilage degeneration (Fig. 3D), SBP sclerosis (Fig 3E) and joint pain measured by von Frey assay. Free TGFα or NPs alone did not alter OA progression.

DISCUSSION: Our study provides genetic evidence demonstrating that overactivation of EGFR signaling modestly thickens the articular cartilage and completely blocks OA progression after DMM surgery. Other joint tissues, such as bone, synovium, and meniscus, as well as major vital organs, appeared normal in mice up to 12 months of age, suggesting that EGFR signaling could be precisely regulated in vivo to fulfill its anabolic actions without inciting catabolic, damaging effects. We also provided proof-of-principle evidence that administration of TGFα into mouse joints using an advanced nanoparticle delivery system is effective in preventing DMM-induced OA initiation and development.

SIGNIFICANCE: Our studies uncover the critical role of EGFR signaling in cartilage homeostasis and demonstrate the feasibility of targeting EGFR signaling for OA treatment as a novel therapeutic approach using nanotechnology.

REFERENCES: (1) Jia H. et al. PNAS. 2016;113(50):14360-14365; (2) Iwamoto R. et al. EMBO J. 1994;13(10):2322-2330.

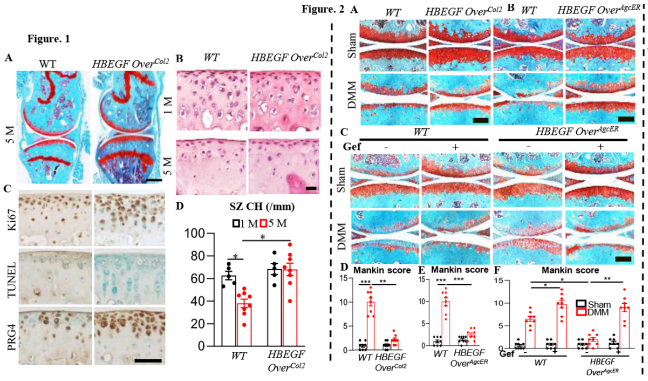

Figure 1. HBEGF overexpression in chondrocytes enlarges cartilage thickness and expands the chondroprogenitor pool. A: SO/FG staining of *WT* and *HBEGF Over^{Col2}* knee joints at 5 months of age. Scale bar, 1 mm. **B:** HE staining of *WT* and *HBEGF Over^{Col2}* knee joints at 1- and 5-month-old mice. Scale bar, 50 µm. **C:** Ki67, TUNEL, and Prg4 staining in articular cartilage. Scale bar, 100 µm. D Quantification of superficial layer chondrocytes of (B). n=8 mice/group. *: p<0.05

Figure 2. Cartilage-specific EGFR overactivation attenuates OA progression. A: *WT* and *HBEGF Over^{Col2}* joints at 4 months post sham or DMM surgery were stained with SO/FG. **B:** *WT* and *HBEGF Over^{AgcER}* mice received Tam injections right before DMM and their joints were harvest at 4 months post-surgery for SO/FG staining. **C:** *WT* and *HBEGF Over^{AgcER}* mice were subjected to sham or DMM surgery followed by vehicle or Gefinitib (100 mg/kg, once every other day) treatment for 3 months. Joints were harvested for histology analysis. Scale bars, 200 µm. **D:** The OA severity of (A) was measured by Mankin score, n=8 mice/group. **E:** Mankin score of (B). n=8 mice/group. **F:** Mankin score of (C). n=8 mice/group. *: p<0.05; **: p<0.01; ***: p<0.001. **Figure 3. TGFα-NPs maintain EGFR signaling in chondrocyte and prevents cartilage damage after DMM surgery. A:** Schematic diagram of TGFα-NPs. **B:** Western blots of EGFR activity (p-ERK) in primary chondrocytes with indicated treatment. **C:** EGFR activity (p-EGFR) staining in the articular cartilage of mice received intra-articular injections of PBS, free TGFα, Ctrl-NPs, and TGFα-NPs for 3 months after sham or DMM surgery. Scale bar, 100 µm. **D:** SO/FG staining. Scale bar, 200 µm. Mankin score: 0.63 ± 0.26 (Sham); 8.88 ± 0.74 (DMM PBS); 8.13 ± 0.81 (DMM TGFα-DBCO); 8.38 ± 0.82 (DMM Ctrl-NP); 3.25 ± 0.59 (DMM TGFα-NP). (TGFa-NP vs PBS: p<0.001) **E:** Representative 3D color maps showing SBP thickness. Color ranges from 0 (blue) to 320 µm (red).

Acute Reduction in Collagen V Expression Increases Viscoelasticity in Mature Tendons

Ryan J Leiphart[1], Stephanie N Weiss[1], David E Birk[2], Louis J Soslowsky[1]
[1]McKay Orthopedic Research Laboratory, University of Pennsylvania, Philadelphia, PA
[2]Department of Molecular Pharmacology and Physiology, University of South Florida, Tampa, FL

Disclosures: RJ Leiphart (N), SN Weiss (N), DE Birk (N), LJ Soslowsky (N)

INTRODUCTION: Classic Ehlers-Danlos Syndrome (cEDS) is a disease caused by mutations in the gene encoding collagen V, a fibrillogenic protein present in tendon [1]. cEDS patients experience joint hypermobility, which is likely caused by connective tissue dysregulation in the absence of collagen V [2]. Tendon-specific knockout of collagen V decreases tendon mechanical properties due to an aberrant development of tissue fibrils [3]. However, the regulatory role of collagen V in tendon homeostasis has not been distinguished from its role in development. Understanding this homeostatic role is critical for establishing the baseline effect of collagen V knockdown in both healthy and injured mature tendons. Therefore, the objective of this study was to determine the effect of acute knockdown of collagen V on the mechanical properties of mature tendons. Since the tendon fibril network is well-established by tissue maturity, we hypothesized that acute knockdown of collagen V in mature tendons would result in minimal changes to tendon mechanical properties.

METHODS: *Animals*: Male wild-type (WT) (n=15) and bitransgenic *Col5a1*$^{flox/+}$ (n=15) and *Col5a1*$^{flox/flox}$ (n=15) mice with a tamoxifen (TM)-inducible Cre were used in this study (IACUC approved). At 120 days old, mice received 3 consecutive daily TM doses (4mg/40g body weight) for Cre-mediated excision of the *Col5a1* gene. Mice were sacrificed 30 days later. Tibia-patellar tendon-patella complexes were harvested and prepared for mechanical testing as previously described [4]. *Mechanical Testing*: Uniaxial, viscoelastic testing was performed with an Instron 5848. The testing protocol consisted of 10 cycles of preconditioning, followed by stress relaxations at 3%, 4%, and 5% strain. Following each stress relaxation, frequency sweeps of 10 cycles at 0.1, 1, 5, and 10Hz were performed. A ramp-to-failure followed the 5% stress relaxation. Percent relaxation, dynamic modulus (E*), and phase shift (δ) were quantified for each stress relaxation and frequency sweep. Stiffness, modulus, maximum load, and maximum stress were quantified from the ramp-to-failure data. *Statistics*: For all mechanical properties, one-way ANOVAs with Bonferroni post-hoc tests were used to compare across genotypes. Significance was set at $p \leq 0.05$, and trends were set at $p \leq 0.10$.

RESULTS: No differences in cross-sectional area (CSA) were observed between genotypes (data not shown). *Quasi-Static Mechanics*: *Col5a1*$^{-/-}$ (NULL) tendons had a decreased modulus relative to WT tendons (Fig 1). No differences in stiffness, max load, or max stress were observed between genotypes (data not shown). *Stress Relaxation*: *Col5a1*$^{+/-}$ (HET) tendons exhibited increased stress relaxation compared to WT tendons at 4% strain (Fig 2). NULL tendons trended towards increased stress relaxation compared to WT tendons at 4% strain. No differences were observed in stress relaxation between genotypes at 3% and 5% strain. *Dynamic Mechanics*: At 3% strain, NULL tendons had increased tan(δ) values compared to WT tendons at 0.1Hz (trend), 1Hz, and 5Hz and had increased tan(δ) values compared to HET tendons at 0.1Hz (data not shown). HET tendons had increased tan(δ) values compared to WT tendons at 1Hz and 5Hz (trend). At 4% strain, NULL tendons had increased tan(δ) values compared to WT tendons at all frequencies and trended towards higher tan(δ) values relative to HET tendons at 0.1Hz and 1Hz (Fig 3A). HET tendons had increased tan(δ) values compared to WT tendons at all frequencies (trend at 0.1Hz). At 5% strain, NULL tendons had increased tan(δ) values compared to WT tendons at all frequencies (Fig 3B). NULL tendons had increased tan(δ) values compared to HET tendons at 1Hz and 5Hz, with trending increases at 0.1Hz and 10Hz. No differences in dynamic moduli were observed between genotypes across strain levels and frequencies (data not shown).

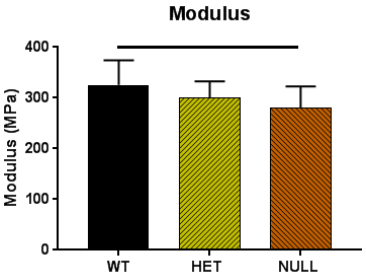

Fig 1. Elastic modulus. NULL tendons exhibited a decreased modulus relative to WT tendons. Solid bars indicate $p \leq 0.05$.

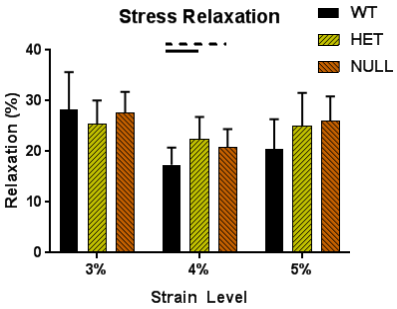

Fig 2. Stress relaxation. HET and NULL tendons displayed increased stress relaxation compared to WT tendons at 4% strain. Solid bars indicate $p \leq 0.05$, and dashed bars indicate $p \leq 0.1$.

DISCUSSION: Surprisingly, acute reduction in collagen V expression in mature tendons led to numerous changes in tendon viscoelastic properties. NULL tendons exhibited increased stress relaxation at 4% strain and increased tan(δ) values at nearly every strain and frequency. HET tendons exhibited increased stress relaxation at 4% strain and displayed intermediate tan(δ) values between those of WT and NULL tendons. These results are in direct contrast to our hypothesis, as knockdown of collagen V increased tendon viscoelasticity in an allele dosage-dependent manner. While mature tendons were generally believed to be quiescent tissues, there is growing evidence that tendon fibril networks are dynamic and remodel on shorter time scales than previously thought [5]. Results of this study strongly support the notion of these dynamic networks, with collagen V playing a large role in regulating fibril properties beyond the developmental time frame. While this study is limited by global knockout models and potential confounding effects on neighboring tissue, the induced and short period of knockdown minimizes these effects. Future studies will analyze the composition and gene expression of these collagen V-knockdown tendons to further elucidate the surprising regulatory role of collagen V in mature tendons. Overall, this study demonstrates that acute reduction of collagen V expression in mature tendons leads to an increase in their viscoelastic properties.

A machine learning approach to identify the primary features of *in vivo* disc degeneration

Beth G. Ashinsky[1,2,3], Chao Wang[2], Sai A. Mandalapu[1,3], Edward D. Bonnevie[1,3], Stephen Pickup[1], Lin Han[2], Robert L. Mauck[1,3], Harvey E. Smith[1,3], Sarah E. Gullbrand[1,3]

[1]University of Pennsylvania, Philadelphia, PA; [2]Drexel University, Philadelphia, PA; [3]Corporal Michael J. Crescenz VA Medical Center, Philadelphia, PA

Disclosures: Beth G. Ashinsky (N) Beth.ashinsky@gmail.com, Chao Wang (N), Sai A. Mandalapu (N), Edward Bonnevie (N), Stephen Pickup (N), Lin Han (N), Robert L. Mauck (JOR Spine), Harvey E. Smith (N), Sarah E. Gullbrand (N)

INTRODUCTION: Intervertebral disc (IVD) degeneration is a causative factor in back pain. Despite the immense clinical burden of back pain, the etiology and pathogenesis of disc degeneration remain poorly understood [1]. Genetic factors, disc cell catabolism, aberrant mechanical loading, and reduced nutritional transport into the avascular disc have all been suggested as contributors to end stage disease [3]. Further, IVD degeneration is a multifactorial process that can be described using a spectrum of cellular, compositional, structural and functional changes to the nucleus pulposus (NP), annulus fibrosus (AF), and boney and cartilage endplates (EP) [2]. These attributes are rarely studied in concert, and therefore, their relative contributions to degeneration remain unknown. The purpose of this study was to use an animal model to quantify the structure-function properties of the degenerating spinal motion segment, and use a machine learning model to identify which of these quantitative measurements would be the most informative features of disease status.

METHODS: Following IACUC approval, 29 male New Zealand white rabbits underwent a surgical procedure to puncture 4 lumbar spine levels per animal [4,5]. The adjacent, non-punctured levels were utilized as healthy controls. Animals were euthanized 2, 4, 8, and 12 weeks post puncture and motion segments were harvested for analysis. At each time point, motion segments underwent T2 MRI to quantify disc composition [4], and post-contrast enhanced T1 mapping to assess disc nutrition [2]. Following MRI, motion segments were subjected to tension-compression and creep mechanical testing [4]. Motion segments (n=4-6 per group) underwent μCT scanning to quantify bone volume (BV) fraction and trabecular (Tb.) morphometry parameters in the vertebral EP. Following μCT, atomic force microscopy (AFM)-nanoindentation (n=3-5 per group) was performed on fresh, 20μm thick cryosections at the inner AF, outer AF, AF-EP and NP-EP interfaces, using microspherical tips ($R \approx 12.5$ μm), to calculate the effective indentation modulus, E_{ind} [6]. Motion segments were dissected into AF and NP components to assess biochemical composition via the hydroxyproline (collagen) and dimethylmethylene Blue (glycosoaminoglycan, GAG) assays [4]. A subset of animals (n=1-3 per time point), were reserved to quantify perfusion fraction of the EP via μCT scanning following perfusion of the spinal vasculature with microFil. Additional motion segments (n=3-5 per group) were processed for paraffin histology, sectioned to 10μm thickness, and stained with alcian blue/picrosirius red (GAG/collagen), hematoxylin and eosin (H&E, cellular morphology), or Mallory-Heidenhain trichrome (vascularity). The erythrocyte staining of the Mallory-Heidenhain stained sections was thresholded in ImageJ, and used to calculate vessel area and number for each sample. Slides stained with alcian blue/picrosirius red and H&E were used for histology grading (total 0-500) of AF organization (0-100), AF-NP border acuity (0-100), NP matrix (0-100) and cellularity (0-100), and EP structure (0-100), by two blinded, independent observers [7]. The above assays yielded total of 23 quantitative input parameters that are listed in **Fig. 1A**. These parameters were used as inputs (predictors) into a neural network model (**Fig. 1B**), using the multilayer perceptron (MLP) algorithm, for classification of total histology score (SPSS Modeler). Training of the MLP was performed on iterations of 75% of the dataset using backpropagation, and testing was performed on the remaining 25% of the samples. The algorithm was optimized by minimizing the cross-entropy loss function, and the resulting error values were propagated through each layer of the network, such that each neuron was assigned an error value (bias term) that reflects its contribution to the output.

RESULTS: Progressive degeneration of the disc occurred with time post-puncture, and was accompanied by substantial remodeling of the vertebral bone, vasculature, and cartilage endplate [4]. Mean (+/- standard deviation) of total histology scores for the control, 2, 4, 8 and 12 week groups were 16.8 (17.3), 155.8 (68.5). 210.7 (202.6), 308.2 (31.2), and 258.6 (77.0), respectively (**Fig.1C**). Using 6 hidden layer neurons, the neural network model (**Fig. 1B**) predicted the target variable (histology score) with 95% accuracy. The model identified %T1 reduction in the NP (indicating small molecule diffusion into the NP), outer AF and EP-AF indentation modulus, NP collagen content, and NZ ROM, as parameters with the highest weighted contributions (**Fig 1A-B**).

DISCUSSION: Machine learning is a tool that has been previously utilized to assess various diseases, including the pathological state of articular cartilage in knee and hip osteoarthritis [8-9]. In this study, we utilized a neural network model, and found that small molecule diffusion into NP, as measured by contrast enhanced MRI, was most informative feature to predict degeneration grade. Disc nutritional status has long been postulated to be a primary contributor to degeneration [2,3], however, this is the first experimental evidence in an *in vivo* animal model of degeneration to verify this concept. We also identified the micromechanical parameters of the AF and EP as the second most important predictors of degeneration, highlighting the relevance of EP structure and function in disease. These findings have important implications in not only understanding degeneration, but also in developing strategies for disc regeneration, as therapies that do not address deficiencies in disc nutrition or micromechanical alterations to the disc may ultimately be unsuccessful.

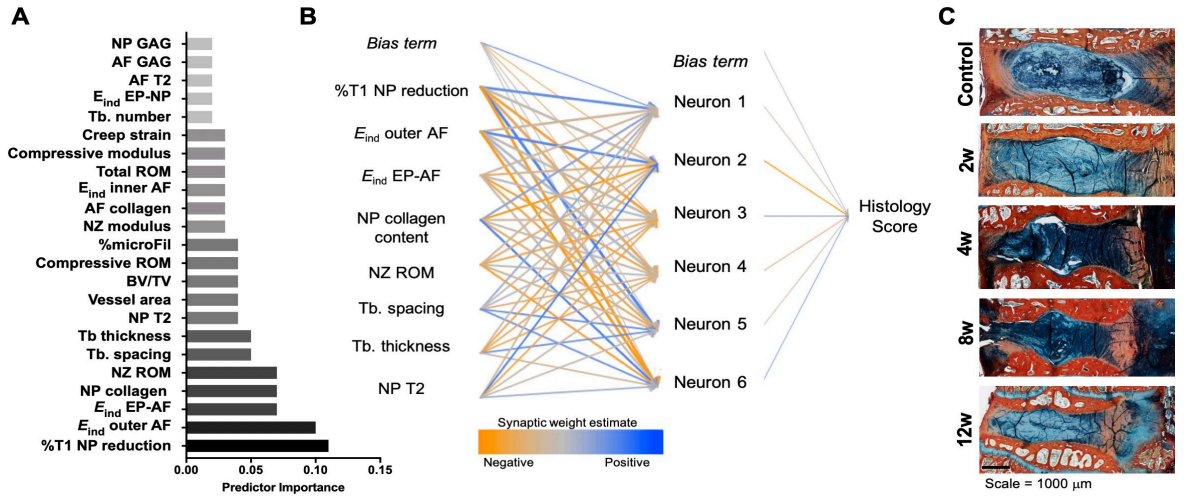

Figure 1. A) Predictor importance, B) representation of the neural network model for the 8 input parameters with the highest weights, C) representative alcian blue/picrosirius red histology for the control, 2, 4, 8, and 12 week groups.

SIGNIFICANCE: This work furthers our understanding the primary factors contributing to disc degeneration, and identifies key quantitative experimental outcomes that should be utilized when evaluating both degeneration and regeneration.

REFERENCES: [1] Mokdad et al., *JAMA*, 319:1444, 2018. [2] Gullbrand et al., *Spine*, 40:1158, 2015. [3] Ohshima, Urban, *Spine*, 17: 1992. [4] Ashinsky, Gullbrand et al., *Osteoarthritis Cartilage*, *in press* 2019. [5] Masuda, et al. *Spine*, 30, 2004. [6] Han et al. *Biophysical J*, 100:1846, 2011. [7] Gullbrand et al., *Osteoarthritis Cartilage* 1:146, 2017. [8] Ashinsky et al., *Osteoarthritis Cartilage* 10:1704, 2015. [9] Ashinsky et al. *J Orthop Res* 10:2243, 2017.

ACKNOWLEDGEMENTS: This work was supported by the NIH, the Dept. of Veterans' Affairs, and the Penn Center for Musculoskeletal Disorders.